DOKUZ EYLÜL UNIVERSITY

GRADUATE SCHOOL OF NATURAL AND APPLIED SCIENCES

FABRICATION AND CHARACTERIZATION OF IONIC POLYMER-METAL COMPOSITES

by

Okan ÖZDEMİR

December, 2015

İZMİR

FABRICATION AND CHARACTERIZATION OF IONIC POLYMER-METAL COMPOSITES

A Thesis Submitted to the
Graduate School of Natural and Applied Sciences of Dokuz Eylül University
In Partial Fulfillment of the Requirements for the Degree of Doctor of Philosophy in Mechanical Engineering, Mechanics Program

by
Okan ÖZDEMİR

December, 2015
İZMİR

Ph.D. THESIS EXAMINATION RESULT FORM

We have read the thesis entitled **"FABRICATION AND CHARACTERIZATION OF IONIC POLYMER-METAL COMPOSITES"** completed by **OKAN ÖZDEMİR** under supervision of **PROF. DR. RAMAZAN KARAKUZU** and **ASSIST. PROF. DR. MEHMET SARIKANAT** and we certify that in our opinion it is fully adequate, in scope and in quality, as a thesis for the degree of Doctor of Philosophy.

Prof. Dr. Ramazan KARAKUZU

Supervisor

Assoc. Prof. Dr. Bülent Murat İÇTEN

Thesis Committee Member

Assoc. Prof. Dr. Yoldaş SEKİ

Thesis Committee Member

Prof. Dr. İsmail ÖZDEMİR

Examining Committee Member

Prof. Dr. Hakan ÇETİNEL

Examining Committee Member

Prof. Dr. Ayşe OKUR

Director

Graduate School of Natural and Applied Sciences

ACKNOWLEDGMENTS

First and foremost, I would like to thank my supervisor, Prof. Dr. Ramazan KARAKUZU, for his help, excellent guidance and continuous encouragement throughout my student life at Dokuz Eylül University. I would also like to thank my second supervisor, Assist. Prof. Dr. Mehmet SARIKANAT, for the useful discussions and technical information during production and experimental procedure.

I want to acknowledge my thesis committee members, Assoc. Prof. Dr. Yoldaş SEKİ and Assoc. Prof. Dr. Bülent Murat İÇTEN, for the helpful comments and encouragements.

I want to express my gratitude to Assoc. Prof. Dr. Kutlay SEVER, Assist. Prof. Dr. Levent ÇETİN, Emine AKAR, İbrahim ŞEN, Özgün Cem YILMAZ and Barış Oğuz GÜRSES for their endless patience and support during experimental stages of this study.

This thesis is financially supported by The Scientific and Technological Research Council of Turkey (TÜBİTAK) under grant number 111M643. I also want to thank TÜBİTAK – BİDEB for their *2211 Yurt içi Doktora Burs Programı* which allowed me to concentrate totally on my Ph. D. education with monetary support.

Finally, I would like to thank my family for their great support. Very special thanks to my wife for her understanding and encouragement during my Ph.D. education.

Okan ÖZDEMİR

FABRICATION AND CHARACTERIZATION OF IONIC POLYMER-METAL COMPOSITES

ABSTRACT

The objective of this thesis is to investigate the electroactive behavior of carboxymethylcellulose (CMC)-based actuators. CMC-based films were synthesized by using 1-butyl-3-methylimidazolium bromide (BMIMBr) ionic liquid. Thereafter, both sides of the films were coated with gold-leaf to produce CMC-based ionic polymer metal composite (IPMC) actuators. In the first part of the study, polyethylene glycol (PEG) at different ratios (1, 1.5 and 2 g) was used to improve the electroactive behavior of CMC-based actuators. The synthesized CMC-based films were characterized by Fourier transform infrared spectroscopy analysis (FTIR), X-ray diffraction analysis (XRD), thermogravimetric analysis (TGA), scanning electron microscopy (SEM), and tensile tests. Under DC excitation voltages of 1, 3, 5, and 7V, maximum tip displacements of actuators were determined with a laser displacement sensor. According to obtained results, CMC-based actuator including 1.5 g PEG exhibited the largest tip displacement for each excitation voltage.

In the second part of the study, since the optimal amount of PEG was obtained to be 1.5 g in terms of maximum tip displacement, graphene nanoplatelets (Gr) at different loadings (0.1, 0.2 and 0.3 wt. percent) were added in order to improve the actuation characteristic of CMC-based film including 1.5 g PEG. The fabricated Gr-loaded CMC-based films were then characterized by similar analysis techniques. The experimental results showed that the Gr loading into CMC-based films improved the actuator performance.

Keywords: Carboxymethylcellulose (CMC), electromechanical properties, ionic liquid, smart materials, graphene

İYONİK POLİMER - METAL KOMPOZİTLERİN ÜRETİMİ VE KAREKTERİZASYONU

ÖZ

Bu tez çalışmasının amacı, karboksimetil selüloz (CMC) tabanlı aktüatörlerin elektro aktif davranışını incelemektir. CMC tabanlı filmler, 1-butyl-3-methylimidazolium bromide (BMIMBr) iyonik sıvısı kullanılarak sentezlenmiştir. Daha sonra, filmlerin her iki tarafı altın folyo ile kaplanarak CMC tabanlı iyonik polimer metal kompozit (İPMK) aktüatörler elde edilmiştir. Çalışmanın birinci kısmında, CMC tabanlı aktüatörlerin elektro aktif davranışlarını artırabilmek amacıyla farklı oranlarda (1, 1,5, ve 2 gr) polyethylene glycol (PEG) kullanılmıştır. Sentezlenen CMC tabanlı filmler, Fourier Dönüşümlü Kızılötesi Spektroskopi (FTIR) analizi, X-Işını kırınımı analizi (XRD), Termogravimetrik analizi (TGA), taramalı elektron mikroskobu (SEM) ve çekme testleri ile karakterize edilmiştir. Aktüatörlerin maksimum uç noktasının yer değiştirmeleri, 1, 3, 5 ve 7V'luk DC voltaj çıkışları altında lazer deplasman sensör ile belirlenmiştir. Elde edilen sonuçlara göre, 1,5 gr PEG içeren CMC tabanlı aktüatör, uygulanan her çıkış voltajında en büyük yer değiştirme sergilemiştir.

Aktüatörlerin maksimum yer değiştirmesi açısından en uygun PEG miktarı 1,5 gr olarak elde edildiği için, çalışmanın ikinci kısmında, 1,5 gr PEG içeren CMC tabanlı filmin aktüatör karakteristiğini geliştirebilmek amacıyla farklı yüklemelerdeki (ağırlıkça yüzde 0,1, 0,2 ve 0,3) grafen nano plateletler eklenmiştir. Üretilen Gr yüklü CMC tabanlı filmler daha sonra benzer analiz teknikleriyle karakterize edilmiştir. Deneysel sonuçlar, CMC tabanlı filmlere grafen yüklemesinin aktüatör performansını artırdığını göstermektedir.

Anahtar kelimeler: Karboksimetil selüloz (CMC), elektromekanik özellikler, iyonik sıvı, akıllı malzemeler, grafen

CONTENTS

Pages

LIST OF FIGURES

Pages

LIST OF TABLES

Pages

CHAPTER ONE
INTRODUCTION

1.1 Active Polymers

Owing to rapid technological development and increased competition in industry, conventional materials such as metals and alloys are being replaced by polymers. Polymers have some important properties such as lightweight, inexpensive, fracture tolerant, pliable and easily processed when compared to inorganic materials. When polymers are subjected to external stimuli, they change their shape and size. Electrical field, pH, light and magnetic field are some examples of these external stimuli. These intelligent polymers can be called *active polymers* and they are heavily studied by researchers for recent decades (Gurunathan, Murugan, Marimuthu, Mulik, & Amalnerkar, 1999; Bar-Cohen, 2001; Kim & Tadokoro, 2007).

According to activation mechanism of active polymers, active polymers are categorized into the two main categories. These are:

- ✓ Noneelectrically deformable polymers
- ✓ Electroactive polymers

None electrically deformable polymers are actuated by nonelectric stimuli such as pH, light and temperature. Chemically activated polymers, shape-memory polymers, magnetically activated polymers and thermally activated gels are some examples of none electroactive polymers (Kim & Tadokoro, 2007).

Electroactive polymers (EAPs) have been widely developed for many applications such as biomimetic robots and biomedical devices owing to their unique sensing and actuation advantages. Electroactive polymers (EAPs), which are actuated by Coulumb forces or electric field, can be classified depending on the activation mechanism as below (Kim & Tadokoro, 2007; Bar-Cohen, 2001);

- ✓ Electronic electroactive polymers

    - Dielectric EAP
    - Electrostrictive graft elastomers
    - Electro-viscoelastic elastomers
    - Ferroelectric polymers
    - Liguid crystal elastomers (LCE)

- ✓ Ionic electroactive polymers

    - Ionic polymers gels (IPG)
    - *Ionic polymer metal composite (IPMC)*
    - Conducting polymers (CP)
    - Carbon nanotubes (CNT)

In the following subchapter, the essential overview about ionic polymer metal composite (IPMC) is given in the context of the thesis study.

1.1.1 Ionic Polymer Metal Composite (IPMC)

One of the most important types of ionic electroactive polymers is ionic polymer metal composites (IPMCs) which are driven by external electric inputs. They have some invaluable properties such as large bending deformations under applied low voltages of 1 – 5V, easy fabrication process, flexibility, and working in air and water (Shahinpoor & Kim, 2001). They are one of the candidate materials for application in artificial muscles and robotic systems due to these invaluable properties (Bar-Cohen, 2001; Shahinpoor & Kim, 2001; Kikuchi & Tsuchitani, 2009; Bar-Cohen, 2012).

Typically, an IPMC composes of an ionic polymer membrane (ion exchange polymer) and electrodes. Both surfaces of ionic polymer membrane are coated with electrodes. There are several ionic polymer membranes to fabricate IPMC. But, the most commonly used ionic polymer membrane is Nafion^{TM} from Dupont and

Flemion^{TM} from Asahi. Au, Ag and Pt can be used as electrode material (Kim & Tadokoro, 2007).

When the voltage is applied to the electrodes, hydrated cations migrate to the cathode. As a result, bending of IPMC takes places toward to the anode owing to the symmetrical swelling of the proton exchange membrane (PEM) induced by the cations (Fang, Lin, & Ju, 2010). A schematic representation of the actuation principle of the IPMC is given in Figure 1.1.

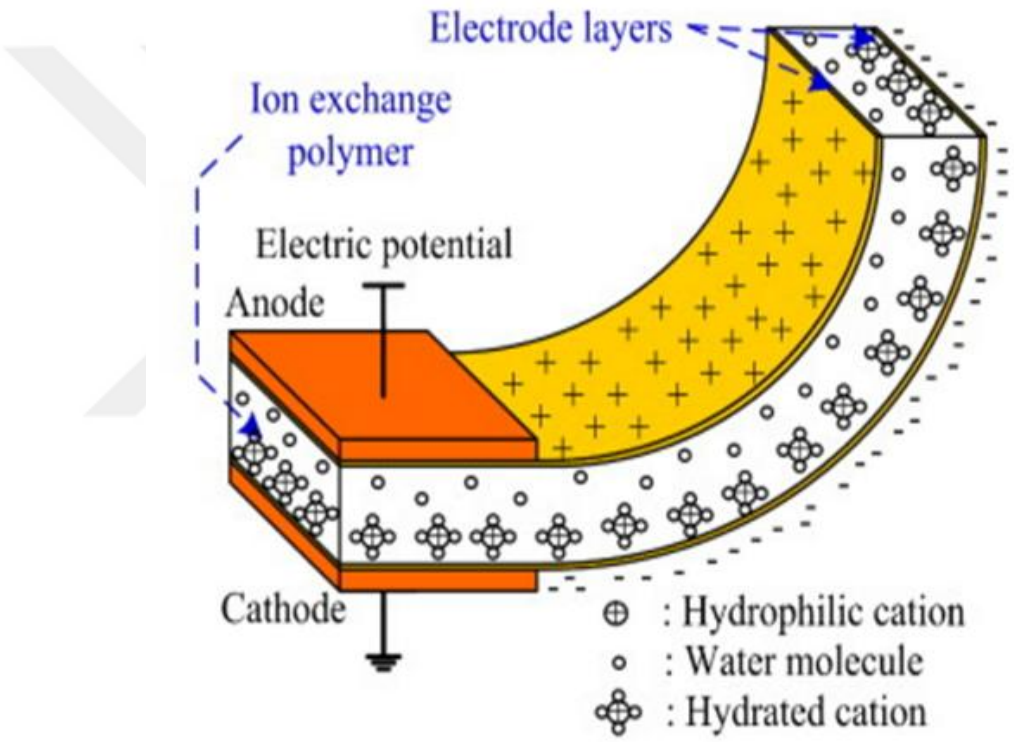

Figure 1.1 The actuation principle of the IPMC (Fang, Lin, & Ju, 2010)

1.2 Cellulose

Cellulose, which is the most abundant molecule on the Earth, can be commonly used to manufacture ionic polymer metal composite (IPMC) actuators due to mechanical endurance, hydrophilicity, biocompatibility, and capability of broad chemical modification (Murphy & Wudl, 2010; Qiu & Hu, 2013). The molecular structure of cellulose is given in Figure 1.2.

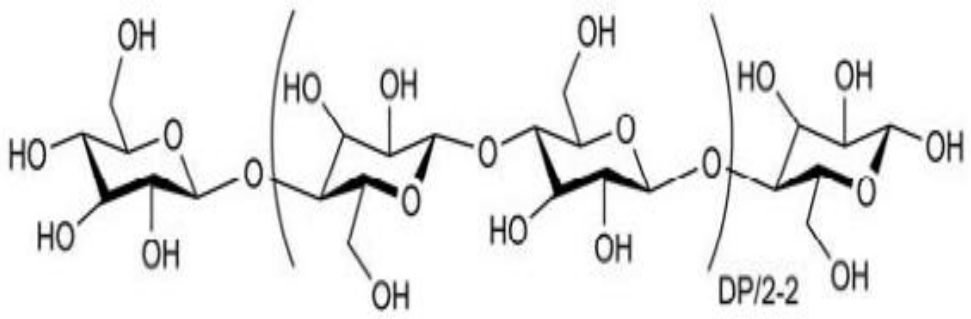

Figure 1.2 The molecular structure of cellulose (Qiu & Hu, 2013)

Moreover, it drew considerable interest and encouraged researchers to developed smart materials based on cellulose in the last two decades. Among these studies, an important paper related to cellulose-paper was performed by Kim, Yun & Ounaies (2006). They produced the bending actuator based cellulose paper and revealed the actuation phenomenon of the actuator. Also, they concluded that cellulose-based electroactive paper (EAPap) can be used as biosensors due to its invaluable properties such as biodegrable, biocompatible and sustainable.

However, dissolution of cellulose is difficult in water due to its crystalline structure. Cellulose can be dissolved by some solvents; however, they are toxic, volatile, and unstable during dissolution processing (Cao et al., 2009; Kim, K. B., & Kim, J., 2013).

Cellulose esters and cellulose ethers are two main categories of cellulose derivatives with different physicochemical and mechanical properties (Shokri & Adibkia, 2013).

Some example of cellulose ester derivatives are cellulose acetate (CA), cellulose acetate phthalate (CAP), cellulose acetate butyrate (CAB), cellulose acetate trimelitate (CAT), hydroxupropylmethyl cellulose phthalate (HPMCP) (Heinämäki, Iraizoz, Nordström, & Yliruusi, 1994; Shokri & Adibkia, 2013).

Some example of cellulose ether derivatives are methyl cellulose (MC), ethyl cellulose (EC), hydroxyethyl cellulose (HEC), hydroxypropyl cellulose (HPC), hydroxypropylmethyl cellulose (HPMC), carboxymethyl cellulose (CMC) and sodium carboxymethyl cellulose (NaCMC) (Shokri & Adibkia, 2013).

1.2.1 Sodium carboxymethyl cellulose (NaCMC)

Sodium carboxymethyl cellulose (NaCMC), which has been used commercially, is one of the cellulose derivatives that can be dissolved in water because of the presence of the polar carboxy and hydroxyl groups in its structure. The molecular structure of NaCMC is given in Figure 1.3. These polar groups also provide the chemical reactivity and strong chelating capability (Heinze & Pfeiffer, 1999; Haldorai & Shim, 2014). NaCMC has been widely used in many fields such as responsive polymers or hydrogels by researchers (Qiu & Hu, 2013).

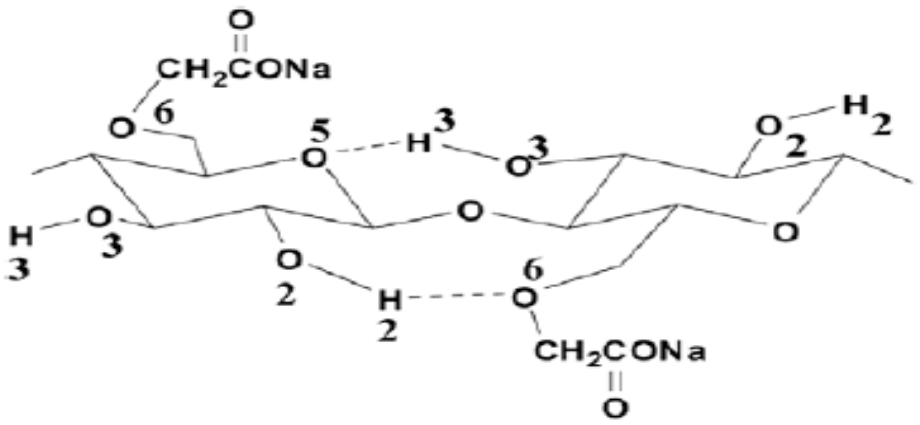

Figure 1.3 The molecular structure of sodium carboxymethyl cellulose (Wei, Bingjie, & Peiyi, 2013)

Using ionic liquid (IL) is another alternative method to overcome the problem regarding dissolution of cellulose and its derivatives (Muzart, 2006; Patil & Sasi, 2008). In the next subchapter, essential information about ionic liquid (IL) is given.

1.3 Ionic Liquid (IL)

Ionic liquids are salts which have some invaluable properties such as nonvolatility, high stability, suitable polarity, and especially high ionic conductivity (Plechkova & Seddon, 2008). Besides, ILs have been suggested as green solvents and used as alternatives to dissolve cellulose and its derivatives (Kim K. B., & Kim, J., 2013).

According to recent studies, ILs have been used for biopolymers, molecular self-assemblies and actuators (Edgar et al., 2001; Swatloski, Spear, Holbrey, & Rogers, 2002). In this study, 1-butyl-3-methylimidazolium bromide (BMIMBr) which is one of the ILs that melts at low temperature (76°C), is used as ionic liquid. BMIMBr, which is inexpensive and versatile, has been widely used in research areas (Akbari & Heydari, 2012). The molecular structure of BMIMBr ionic liquid is given in Figure 1.4.

Figure 1.4. The molecular structure of BMIMBr ionic liquid (Ramenskaya, Grishina, Pimenova, & Gruzdev, 2008)

1.4 Graphene (Gr)

Graphene, which is a stable 2D one atom layer material, shows excellent properties as below:

- ✓ Good electrical conductivity
- ✓ Mechanical strength
- ✓ High surface area
- ✓ Superior performance (Huang, Liang, & Chen, 2012).

Feng, Y. Y., Zhang, Shen, Yoshino & Feng, W. (2012), emphasized that graphene loading enhanced the electrical and mechanical properties. Zhao, Song, Zhang & Qu (2013), also investigated the effects of graphene loading into the smart materials and found that graphene loaded actuators can be used as sensors, switches and artificial muscles. For these reasons, the graphene nanaplatelets were used in order to improve the both mechanical and electroactive behaviors of CMC-based actuators, in this thesis.

1.5 Poly(ethylene glycol) (PEG)

Besides the challenges of dissolution of cellulose in water, the brittle characteristic of CMC-based films is a very important problem. This problem restricts the use of these films as actuators. Plasticization can be used to improve both chemical and physical properties of the films (Pang, Liu, Zhang, Wu, & Sun, 2013). Poly(ethylene glycol) (PEG) is one of the plasticizers which can be used to improve the mechanical properties of films and actuators. The molecular structure of poly(ethylene glycol) (PEG) (Barron, 2012) is given in Figure 1.5. It can be also dissolved in water and various organic solvents (Cai & Kim, 2010). Hence, it can be used for improving tensile properties and bending displacement of actuators.

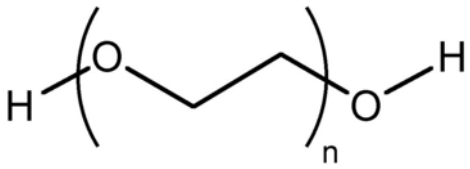

Figure 1.5. The molecular structure of poly(ethylene glycol) (Barron, 2012)

1.6 Previous Studies on IPMC

In this subchapter, the literature review regarding the Nafion based ionic polymer metal composite (IPMC) and different types of hydro-carbon ion-exchangeable actuators is presented. Besides, the literature review regarding the physics based models of IPMCs is given.

Lee & Yoo (2009), used four ionic liquids as inner solvent in order to fabricate a Nafion based actuators. The imidazolium salts were consisted of 1-ethyl-3-methylimidazolium [EMIm] cation and anions including bromide [Br], nitrate [NO_3], acetate [AcO], and trifluoroacetate [TA]. They obtained that [EMIm][Br]- and [EMIm][NO_3]-based IPMCs showed a superior performance in terms of maximum tip displacement.

An electro-active artificial muscle based on the fullerene-reinforced ionic polymer membrane was developed by Jung, Vadahanambi, & Oh, (2010). They found that tensile strength and Young's modulus more than doubled with addition of minute quantities of fullerenes. Also, they showed that the harmonic responses of the fullerene reinforced ionic polymer actuators almost doubled and the frequency responses improved in the low frequency region. Jung, Jeon, Vadahanambi, & Oh (2011), were developed an electro-active actuators based on graphene reinforced Nafion composite electrolytes and determined their electro-chemo-mechanical properties and actuation performances (Figure 1.6). They performed some characterization techniques and concluded that a minute loading of graphene improves the harmonic responses, the blocking force and the energy efficiency of Nafion-based ionic polymer-metal composite actuators.

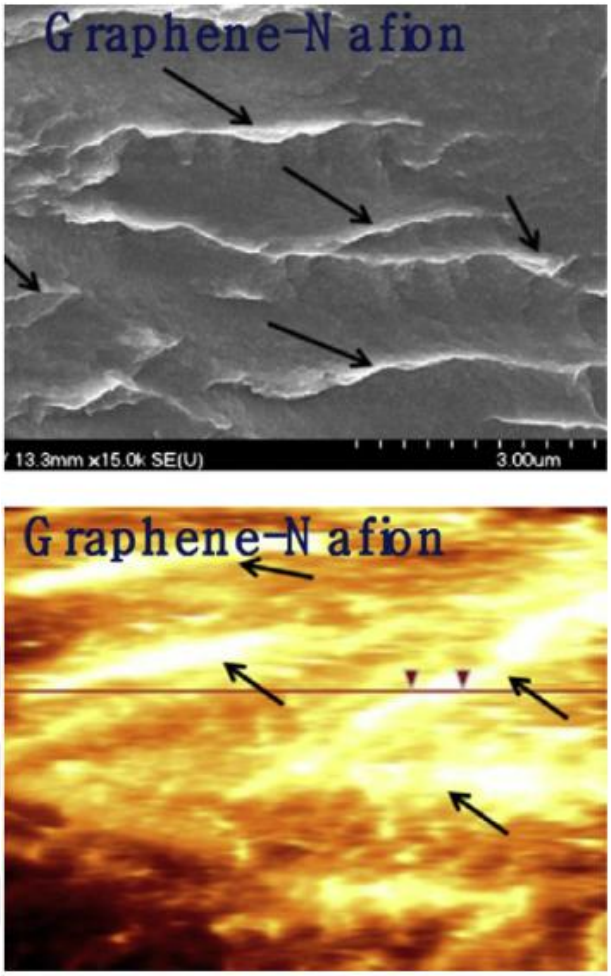

Figure 1.6. SEM and AFM morphologies of graphene-Nafion composites (Jung, Jeon, Vadahanambi, & Oh, 2011)

Yang, Choi, H., Choi, S., Jeon, & Lee (2012) developed a new ionic polymer-metal composite (IPMC) by replacing a typical platinum or gold electrode with a multi-walled carbon nanotube (MWNT)-graphene based electrode. They fabricated four kinds of IPMC samples with different MWNT-graphene ratios with the same solid Nafion film. According to their results, the IPMC with a pure MWNT based electrode exhibits higher maximum tip displacement compared to the conventional IPMC with a platinum electrode.

Jung & Oh (2007), fabricated a ionic polymer metal composite (IPMC) actuators with multi-carbon nanotubes (MWNT) and sulfonated poly(styrene-b-ethylene-co-

butylene-b-styrene) (SSEBS) ionic polymers. They found that the addition of MWNTs in SSEBS-based IPMC actuator increases the maximum tip displacement.

Lu, Kim, Lee, & Oh (2008), developed a novel electro-active polymer actuator employing the ionic networking membrane of poly(styrene-*alt*-maleimide) (PSMI)-incorporated poly(vinylidene fluoride) (PVDF) in order to improve the electrical and mechanical performance of artificial muscles. They found that their actuator overcomes the back relaxation of the ionic polymer-metal composite actuator under the constant voltage and also shows much larger maximum tip displacement compared to Nafion-based actuator. Panwar, Cha, Park, J. O., & Park, S. H. (2012) tested the tip displacement of polyvinylidene fluoride (PVDF)/polyvinyl pyrrolidone (PVP)/polystyrene sulfonic acid (PSSA) based ionic polymer metal composites (IPMCs) actuators at DC and AC voltages of 1–2V. PVDF/PVP/PSSA actuator exhibited large actuation displacement under the low DC and AC voltages of 1–2V.

Mahadeva & Kim (2010), studied the effect of humidity and polyethylene oxide (PEO)-polyethylene glycol (PEG) content on the actuator performance of cellulose/PEO-PEG microcomposites. They obtained that the maximum blending displacement of the 5% PEO-PEG actuator increases nearly twice compared to that of cellulose based actuators. Ozdemir et al. (2015a) investigated the electroactive behavior of carboxymethyl-cellulose (CMC) based actuators. They fabricated the CMC-based actuators by using 1-butyl-3-methylimidazolium bromide (BMIMBr) ionic liquid. They found that CMC-based actuator loaded with 1.5 g PEG exhibits the largest maximum tip displacement compared to other actuators. The effects of graphene loading (0.1, 0.2 and 0.3 wt.%) on both electromechanical and mechanical properties of CMC-based actuators were studied by Ozdemir et al. (2015b). According to their results, the maximum tip displacement of 0.2 wt.% graphene loaded actuators increased by about 15% compared to unloaded actuators.

Fleming, Hubbard, Kim, & Leang (2011), proposed a new method to mitigate back relaxation of IPMC. Their method involves proper control of isolated electrodes to compensate for the back relaxation and does not require sensor feedback. Chen,

Tan, & Shahinpoor (2005) presented the hysteresis during quasi-static IPMC actuation. They used the Preisach operator to model the hysteresis. An open-loop positioning scheme was studied based on the inversion of the Preisach operator. They concluded that using IPMC for quasi-static applications is feasible.

Some applications of IPMC actuators were presented below. A gripper was fabricated by (Shahinpoor, Bar-Cohen, Simpson & Smith, 1998) that uses ionic polymer metal composite fingers in the form of an end-effector of a miniature low-mass robotic arm, as shown in Figure 1.7. When the electrical input is applied, this wiring configuration allows the fingers to bend either inward or outward similar to the operation of a hand.

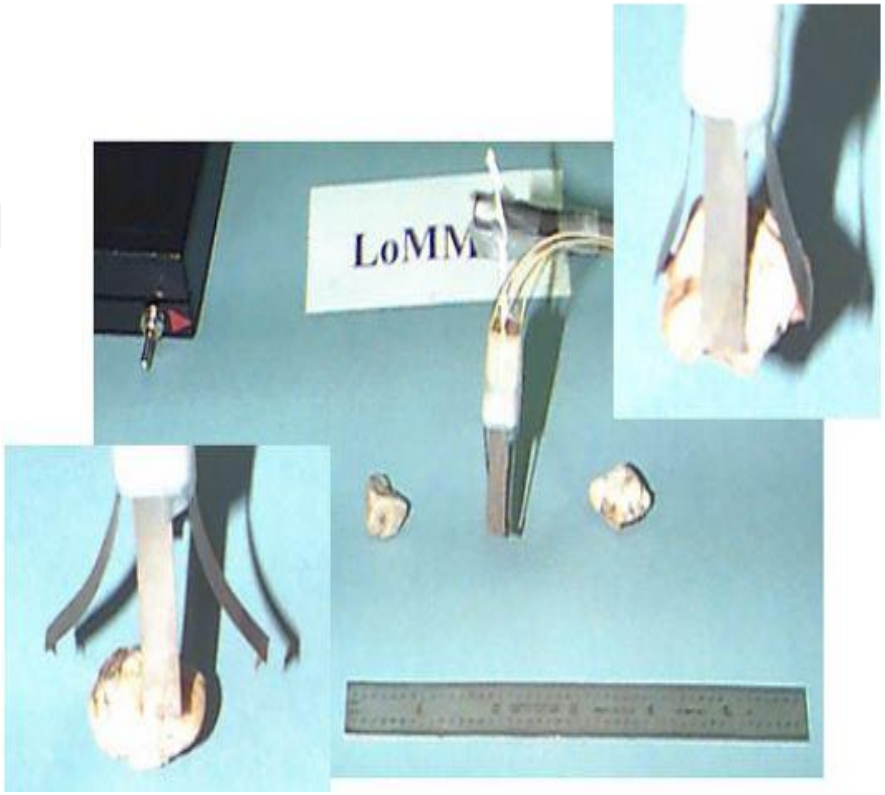

Figure 1.7 An end-effector gripper (Shahinpoor, Bar-Cohen, Simpson & Smith, 1998)

In Figure 1.8, electrically controllable caudal actuator fins and pectoral actuator fins and remotely controllable stealthy, noiseless, biomimetic swimming robotic fish made with IPMCs were investigated by (Shahinpoor & Kim, 2005).

Figure 1.8 A designed and fabricated undulating caudal fin actuator and two robotic fish equipped with IPMC fin actuator (Shahinpoor & Kim, 2005)

Shahinpoor & Kim (2005), developed a double-diaphragm mini-pump and determined pumping characteristics (Figure 1.9).

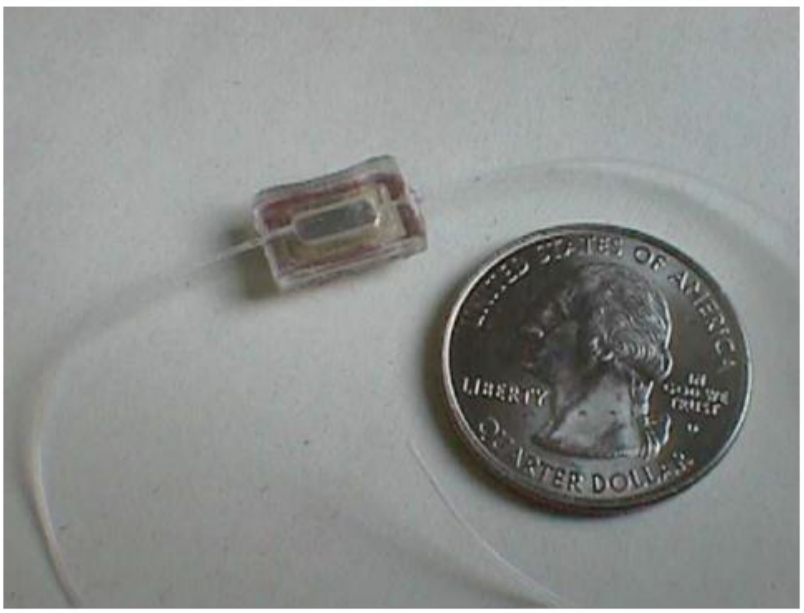

Figure 1.9 A fabricated double-diaphragm mini-pump (Shahinpoor & Kim, 2005)

He et al. (2012), investigated the effect of tetraethyl orthosilicate (TEOS) loading on the corresponding electro-mechanical actuation performance of IPMCs. They obtained that their fabricated IPMC can be used to actuate the artificial eye as shown in Figure 1.10.

(a) (b) (c)

Figure 1.10 Motions of the artificial eye (a) Left-motion, (b) Initial state and (c) Right-motion (He et al., 2012)

1.7 Objectives of This Study

Although many studies have been reported to improve the electromechanical behavior of the cellulose- and modified cellulose-based films, the fabrication of electroactive actuators and films of CMC-based films with BMIMBr ionic liquid and PEG has not been previously reported. Hence, this thesis aims to produce and characterize a CMC/BMIMBr/PEG based films and actuators.

In the first part of the study, to determine the optimal amount of PEG in terms of maximum tip displacement, three different PEG contents (1, 1.5 and 2g) were added to films in order to improve the both electromechanical and mechanical performance. In the second part of the study, the actuation performance of CMC-based films was improved by graphene loading (0.1, 0.2 and 0.3wt.%).

The films were then characterized by thermogravimetric analysis (TGA), X-ray diffraction analysis (XRD), Fourier transform infrared analysis (FTIR), scanning

electron microscopy (SEM) and tensile tests. Also, the electromechanical performances and blocking force values of the actuators were determined under DC excitation voltages of 1, 3, 5 and 7V. Besides, the blocking force values and maximum tip displacements of actuators were determined with ANSYS 14.5 packet program. Obtained results were compared with experimental results.

CHAPTER TWO
MATERIALS AND METHODS

2.1 Materials

Carboxymethylcellulose sodium salt (CMC) with low viscosity (C5678-500G, DS: 0.65 – 090 and molecular weight: 90 kDA), 1-butyl-3-methylimidazolium bromide (BMIMBr) and Polyethylene glycol (PEG) (P5402-500G; average mol wt 1450 g/mol) were provided from Sigma – Aldrich (Steinheim, Germany). Graphene nanoplatelets (Gr) were supplied by Grafen Kimya Sanayi A.Ş (Ankara, Turkey). Thickness and average particle diameter of Gr have approximately 5 – 10 μm and 50 – 100 nm, respectively. Gold leaf, having thickness of 0.14 μm, was obtained from L.A. Gold Leaf (Azuza, ABD).

2.2 Fabrication of CMC-based Films and Actuators

1.44 g Carboxymethylcellulose sodium salt (CMC) was firstly dissolved in 14.4 mL distilled water at room temperature. Thereafter, 3.21 g BMIMBr was added to this solution. The prepared solution in beaker was placed into the water bath (approximately, 90 – 95˚C) and stirred until a homogeneous mixture was obtained. Afterwards, PEG at three different amounts (1, 1.5 and 2 g) were added to this mixture. Prepared these samples were used in the first part of the thesis.

In the second part of the thesis, films were again prepared with same amount of CMC and BMIMBr. Since the optimal amount of PEG was found to be 1.5 g, after dissolution of BMIMBr, 1.5 g PEG were added to this mixture. Then, Gr with fractions of 0.1, 0.2 and 0.3 wt.% of total mass was well dispersed in the solution by using ultrasonic homogenizer. Finally, the mixture was cast into a petri dish and dried for 1 day at room temperature.

After the film formation, the IPMC actuators were obtained by coating both sides of the films with gold leaf. The IPMC actuator samples were cut into the shape as shown in Figure 2.1 with dimension of 5x50x1 mm.

Figure 2.1 Gold leaf coated IPMC actuator

In this thesis, CMC-based films and actuators with 1, 1.5 and 2 g PEG were coded as CMC-Br-1PEG, CMC-Br-1.5PEG and CMC-Br-2PEG, respectively. Also, CMC-based films and actuators including 1.5 g PEG and Gr with fractions of 0.1, 0.2 and 0.3 wt.% of total mass were termed as CMC-Br-0.1Gr, CMC-Br-0.2Gr and CMC-Br-0.3, respectively.

2.3 Fourier Transform Infrared Spectroscopy (FTIR) Analysis

FTIR analyses of the all CMC-based films were carried out via Perkin Elmer Spectrum BX-II with pellets of 1 g samples. FTIR spectra of the samples were recorded with the sum of 25 scans at a resolution of 4cm^{-1} in the range of 400-4000 cm^{-1}.

2.4 Thermogravimetric Analysis (TGA)

Perkin Elmer model Thermogravimetric analyzer was used to determine the thermal behavior of the all CMC-based films. The samples were heated at a rate of 10˚C/min under nitrogen atmosphere in the temperature range 25 – 600˚C.

2.5 X-ray Diffraction (XRD) Analysis

X-ray diffraction (XRD) curves of the all CMC-based films were determined by using a Philips X-Pert Pro Diffractometer system with Ni-filtered Cu Kα radiation (λ=1.54 Å). The machine was operated at a voltage of 45 kV and current of 40 mA. Besides, the scan step size and time per step were arranged to 0.03˚ and 10 s, respectively. The curves were analyzed in the 2θ angle range of 5˚ - 90˚ at room temperature.

2.6 Scanning Electron Microscope (SEM) Analysis

Scanning electron microscope (SEM) observations of the all CMC-based films were investigated by means of high resolution scanning electron microscope (FEI Quanta FEG 250). The micro images were obtained at an accelerating voltage of 5 kV. Before the SEM analysis, gold sputtering of the samples was conducted through the plasma sputtering technique.

2.7 Mechanical Properties

The mechanical properties of the all CMC-based films and actuators, such as tensile strength and tensile modulus, were determined via a Shimadzu universal testing machine having load cell capacity of 100 N. The crosshead speed of the machine was set to 0.1 mm/min. The samples size was approximately 10x40x1 mm.

2.8 Electroactive Properties

The electromechanical behavior of the all CMC-based actuators was studied under DC voltages of 1, 3, 5 and 7V. As the signal source, buffer circuit and data acquisition hardware (NI-PXI 7854R) were utilized. The maximum tip displacements of the actuators were recorded with a KEYENCE LK-51 laser displacement sensor with a sampling frequency of 100 Hz.

Photo of the experimental setup is given in Figure 2.2. Selected DC voltages were applied to actuator samples with dimension of 5x50x1 mm.

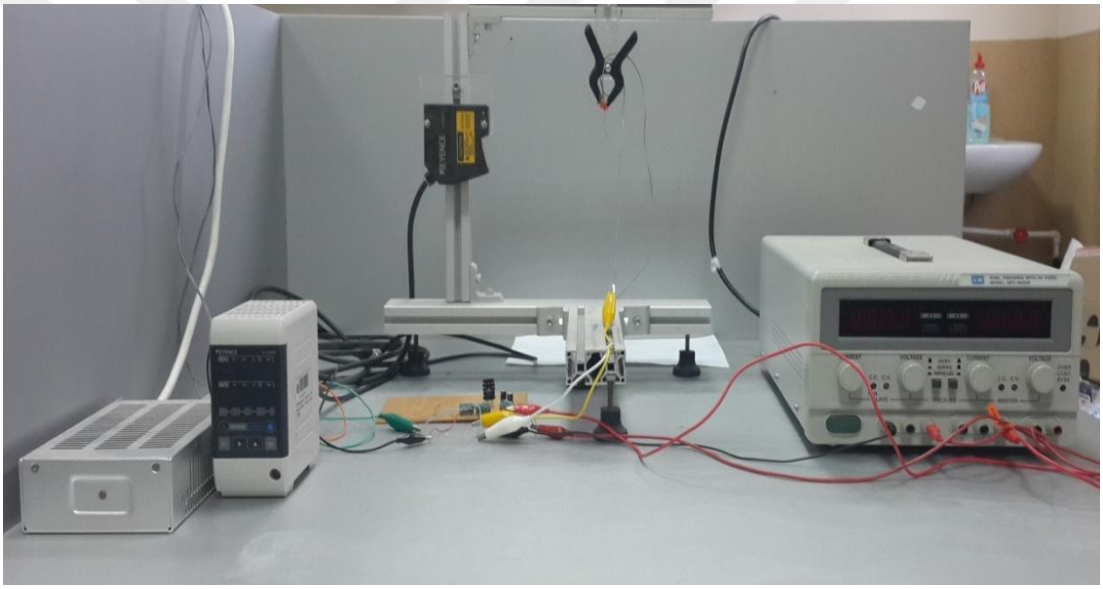

Figure 2.2 Photo of the experimental setup

2.9 Blocking Force Analysis

The blocking force analysis of the actuators was performed precision balance (Precisa 225SM-Dr) as shown in Figure 2.3. The samples size was approximately 5x50x1 mm. The data were logged to a computer by using RS-232 protocol with a sampling frequency of 6 Hz.

Figure 2.3 Precision balance used in experiments

Mechanical and electroactive properties and blocking force analysis of the films and actuators were carried out at ambient temperature (24˚C). The relative humidity level was measured as 45 % during the experiments.

In order to increase the accuracy of the test results, each test was repeated at least three times. Average values were calculated and used in order to interpret the test results.

2.10 Finite Element Analysis (FEA)

The finite element analyses (FEA) were conducted via ANSYS 14.5 packet program in order to determine the maximum tip displacement and blocking force values of actuators.

CHAPTER THREE
RESULTS AND DISCUSSION

3.1 FTIR Analyses

3.1.1 CMC-based Films with Different PEG Loadings

The FTIR spectra of the CMC, CMC-Br (without PEG), CMC-Br-1PEG, CMC-Br-1.5PEG and CMC-Br-2PEG samples are given in Figure 3.1a-e. A broad characteristic band around 3400 cm^{-1} represents the stretching frequency of the hydroxyl group (–OH). The band around 2950 cm^{-1} is owing to asymmetric $–CH_2$ stretching. The absorption bands at 1620 cm^{-1} and around 1080 cm^{-1} validate the carboxyl group (–COO) and $>CH–O–CH_2$ group of sodium carboxymethyl cellulose, respectively. Similar absorption bands were also reported by (Biswal & Singh, 2004; Akar, Altınışık, & Seki, 2012; Chai & Isa, 2013; Habibi, 2014; Ozdemir et al., 2015a).

The absorption bands at 3145 cm^{-1} and 3090 cm^{-1} shows the imidazole ring (C–H) of BMIMBr ionic liquid. The specific bands of BMIMBr are appeared at 2959 cm^{-1} and 2873 cm^{-1} (aliphatic C–H), 1613 cm^{-1} (O–H bending), 1573 cm^{-1} and 1563 cm^{-1} (imidazole ring), 1167 cm^{-1} (imidazole H–C–C and H–C–N bending), 839 cm^{-1} (in-plane imidazole ring bending), 752 cm^{-1} (out-of-plane C–H bending of imidazole ring) (Rajkumar & Ranga Roa, 2008; Rango Rao, Rajkumar, & Varghese, 2009). Besides, the strong absorption band at around 1106 cm^{-1} is related to the stretching of ether groups in PEG (Sahlin & Peppas, 1997; Roberts, Bentley, & Harris, 2002; Singh & Bhat, 2003; Mansur, H. S., Orefice, & Mansur, A. A., 2004; Ozdemir et al., 2015a).

When the FTIR spectra of CMC and CMC-Br are compared, new bands at 1573 cm^{-1} (imidazole ring) and 1167 cm^{-1} (imidazole H–C–C and H–C–N bending) were seen. PEG addition shifted the band from 1573 cm^{-1} to 1571 cm^{-1}. Apart from this, there is no important effect of amount of PEG loading on the FTIR spectra of the

samples. It can also be said that the band at 1106 cm^{-1} confirms the stretching of ether groups in PEG (Ozdemir et al., 2015a).

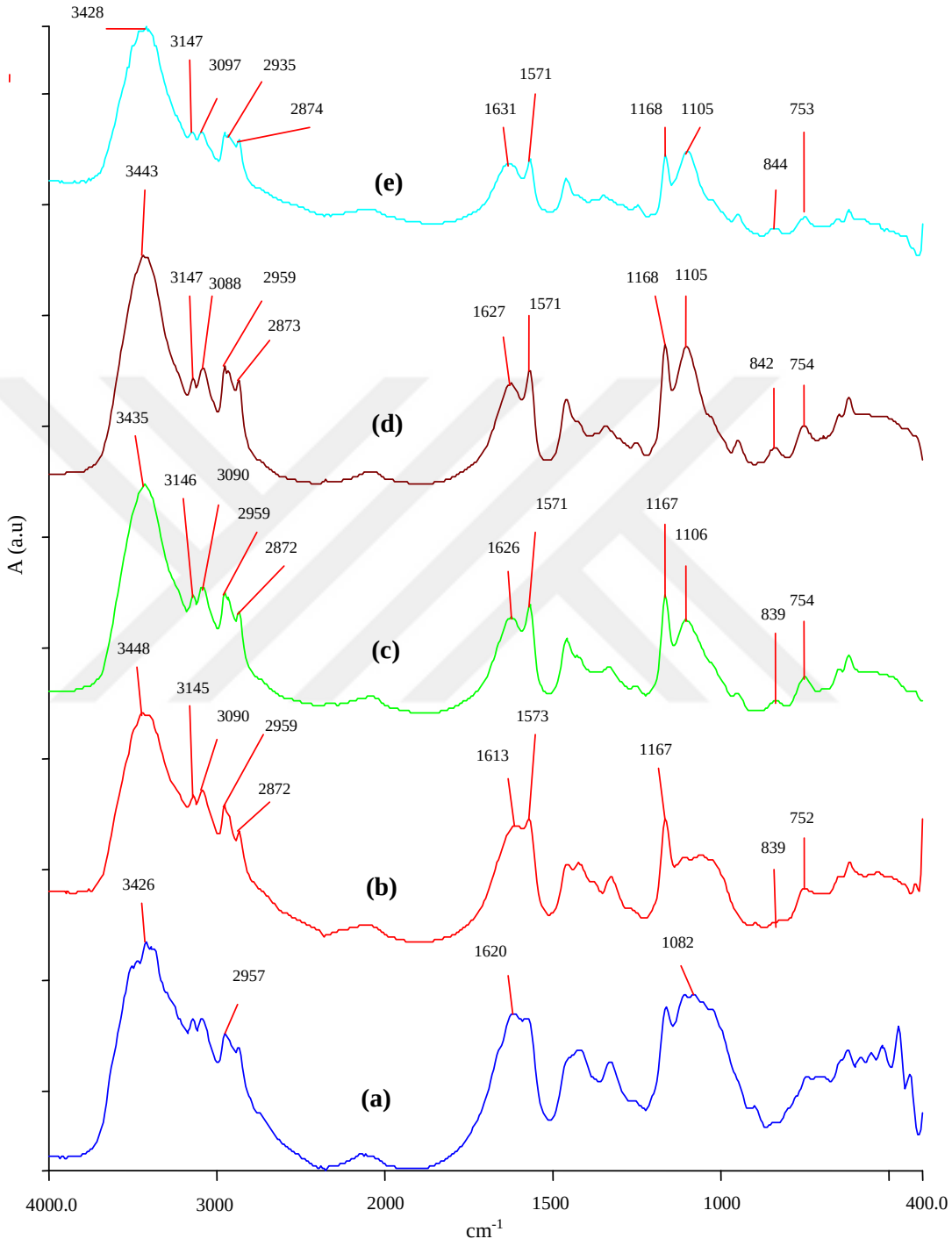

Figure 3.1 FTIR spectrum of **(a)** CMC, **(b)** CMC-Br**, (c)** CMC-Br-1PEG, **(d)** CMC-Br-1.5PEG and **(e)** CMC-Br-2PEG films

3.1.2 CMC-based Films with Different Gr Loadings

The FTIR spectra of CMC-Br (without PEG), CMC-Br (with 1.5 g PEG), CMC-Br-0.1Gr, CMC-Br-0.2Gr, and CMC-Br-0.3Gr samples are shown in Figure 3.2a-e.

Similar bands for the CMC, BMIMBr and PEG were obtained as expected. The bands at around 3400 cm^{-1}, 2960 cm^{-1}, 1610 cm^{-1} and 1070 cm^{-1} belong to the hydroxyl group (–OH), asymmetric $–CH_2$ stretching, carboxyl group (-COO) and $>CH-O-CH_2$ group of sodium carboxymethyl cellulose, respectively (Biswal & Singh, 2004; Akar, Altınışık, & Seki, 2012; Chai & Isa, 2013; Habibi, 2014; Ozdemir et al., 2015b).

The characteristic bands at around 3145 and 3091 cm^{-1}, 2959 and 2872 cm^{-1}, 1613 cm^{-1}, 1573 cm^{-1}, 1167 cm^{-1} shows the imidazole ring (C-H), aliphatic C-H, O-H bending, imidazole ring, imidazole H-C-C and H-C-N bending of BMIMBr ionic liquid, respectively (Rajkumar & Ranga Roa, 2008; Rango Rao, Rajkumar, & Varghese, 2009; Ozdemir et al., 2015b).

An absorption band at 2873 cm^{-1} is related to the methylene group of PEG. The vibration band at around 1462 cm^{-1} is owing to the binding vibration of the $-CH_2$ group. The absorption bands at about 950 and 842 cm^{-1} are due to the C-C stretching (Polu & Kumar, 2011; Polu, Kumar, Causin, & Neppali, 2011; Ozdemir et al., 2015b).

When the Gr with different fractions was added to CMC-Br-1.5PEG samples, absorption bands shifted from 3443 cm^{-1}, 2959 cm^{-1}, 1627 cm^{-1}, and 1346 cm^{-1} to 3441 cm^{-1}, 2957 cm^{-1}, 1629 cm^{-1}, and 1348 cm^{-1}, respectively (Ozdemir et al., 2015b).

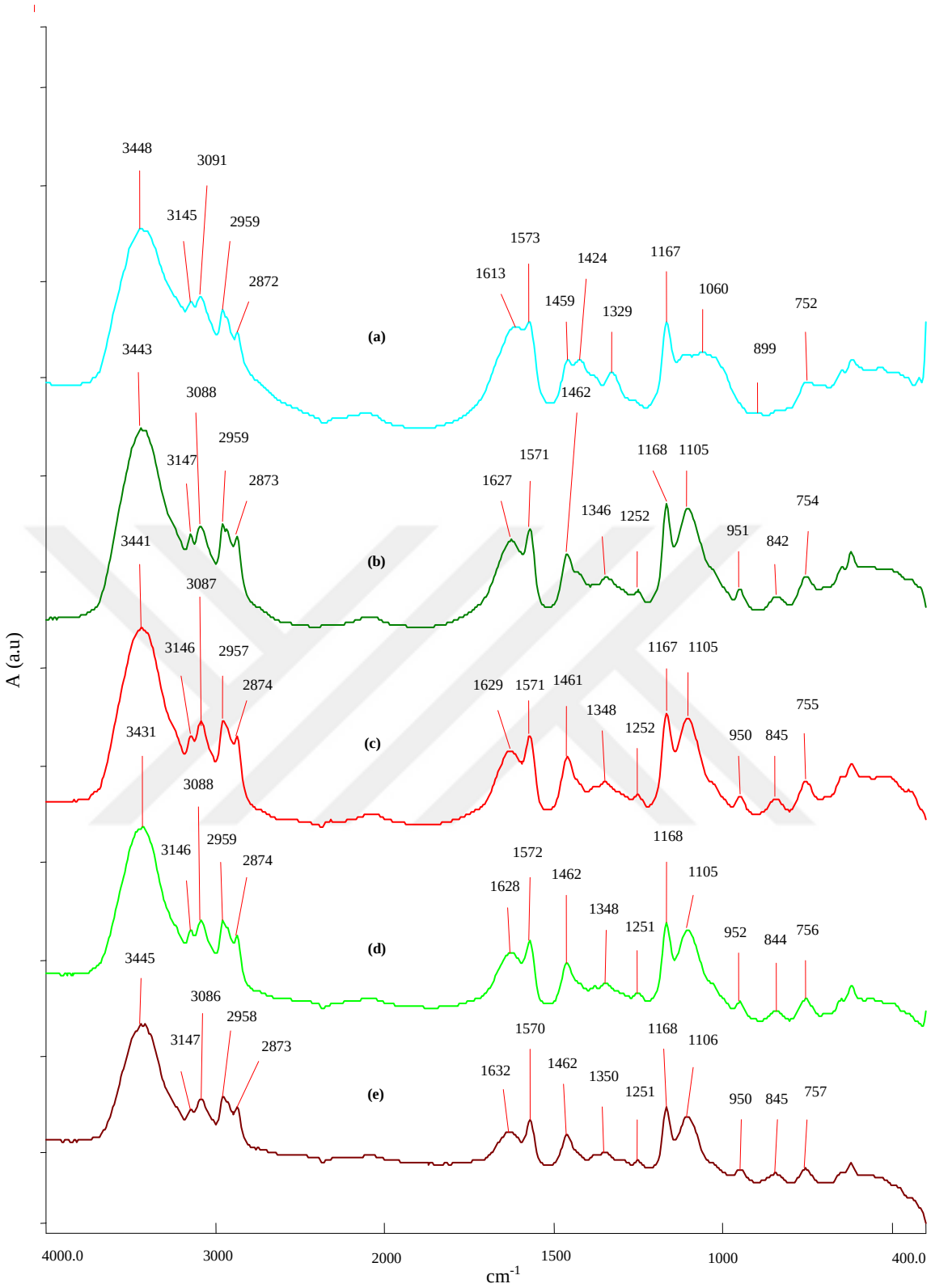

Figure 3.2 FTIR spectrum of **(a)** CMC-Br (without PEG), **(b)** CMC-Br (with 1.5 g PEG)**, (c)** CMC-Br-0.1Gr, **(d)** CMC-Br-0.2Gr and **(e)** CMC-Br-0.3Gr films

3.2 TG Analyses

3.2.1 CMC-based Films with Different PEG Loadings

The effect of PEG loading on thermal stability of samples was determined by TG analyses. TGA profiles for CMC-Br (without PEG), CMC-Br-1PEG, CMC-Br-1.5PEG and CMC-Br-2PEG samples are depicted in Figure 3.3-3.6. Also, the related TGA data were given in Table 3.1. According to Table 3.1, the initial, maximum and final temperatures of the CMC are obtained to be 230 ˚C, 284 ˚C and 321 ˚C, respectively. For the samples of CMC-Br, the initial decomposition temperature of CMC decreased compared to CMC-Br samples. On the other hand, it is observed that final and maximum decomposition temperature of CMC increased. Additionally, after different PEG amount had been added into the CMC-Br, the initial and final decomposition temperature of CMC-Br increased, but the maximum decomposition temperature decreased (Ozdemir et al., 2015a).

According to Figure 3.3-3.6 and Table 3.1, the thermal degradation of the samples is divided into the two main stages. The mass loss for the first stage is owing to the evaporation of water. This stage lasts from approximately 25 ˚C to 110 ˚C. The mass loss for the second stage (from approximately 200 ˚C to 400 ˚C) is due to the decomposition (nonvolatile carbonaceous material) of CMC, BMIMBr and PEG (Ozdemir et al., 2015a).

The total mass losses were calculated in the temperature range of 25 – 600 ˚C and determined as 51.2%, 85.4%, 90.4%, and 84.7% for the samples of CMC, CMC-Br, CMC-Br-1PEG, CMC-Br-1.5PEG, and CMC-Br-2PEG, respectively. It is clearly seen that since BMIMBr ionic liquid has relatively low thermal stability, the total mass loss increases (Ozdemir et al., 2015a).

Besides, the mass losses up to the maximum decomposition temperature were found as 23.8%, 68.4%, 57.5%, 56.4%, and 53.5% for the samples of CMC, CMC-Br, CMC-Br-1PEG, CMC-Br-1.5PEG, and CMC-Br-2PEG, respectively. Therefore,

it can be inferred that adding BMIMBr into the CMC increases the mass loss up to the maximum decomposition temperature and loading PEG into the CMC-Br decreases the mass loss up to the maximum decomposition temperature (Ozdemir et al., 2015a).

Table 3.1 TGA data for the PEG loaded CMC-based samples

Sample name	*Mass Loss (25-110^{o}C) (%)*	*Mass Loss (25-600^{o}C) (%)*	*Mass Loss (up to T_{max}) (%)*	$T_{initial}$ (^{o}C)	T_{max} (^{o}C)	T_{final} (^{o}C)
CMC	4.2	51.2	23.8	230	284	321
CMC-Br	12.4	85.4	68.4	200	300	342
CMC-Br-1PEG	10.2	86.8	57.5	207	293	365
CMC-Br-1.5PEG	8.5	90.4	56.4	206	296	371
CMC-Br-2PEG	17.7	84.7	53.5	203	286	388

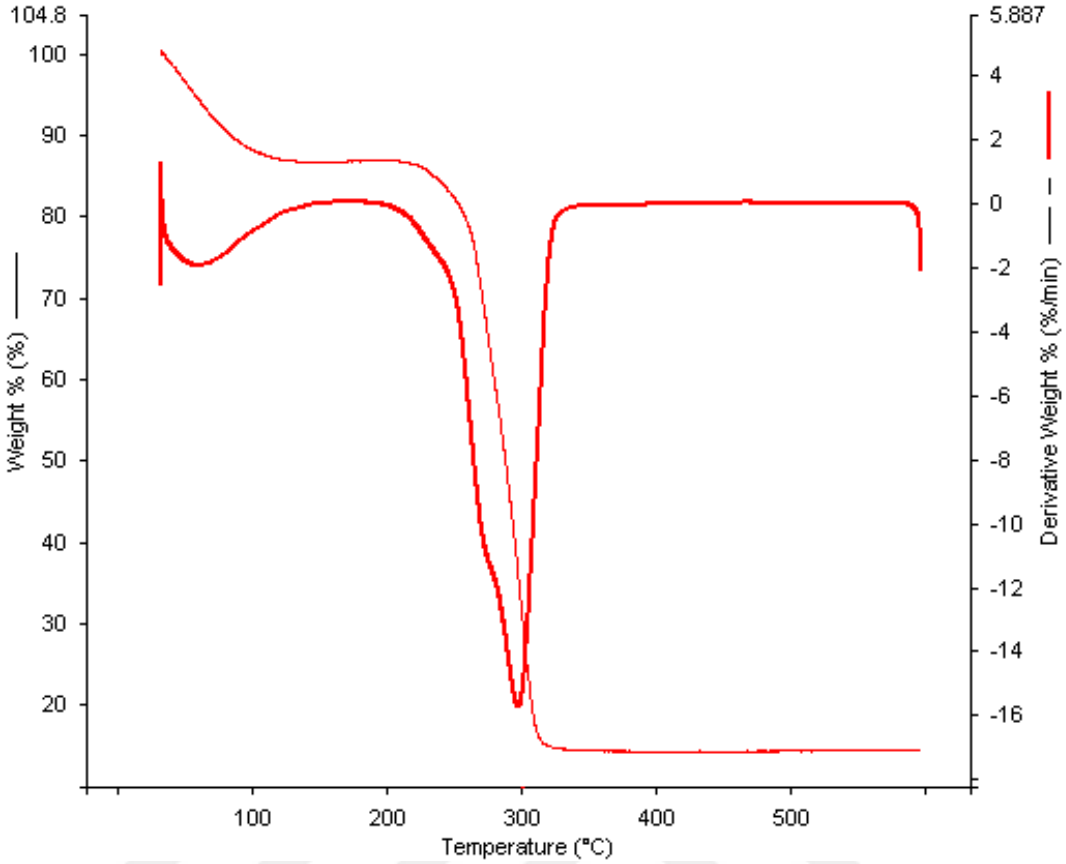

Figure 3.3 TGA curve of CMC-Br film

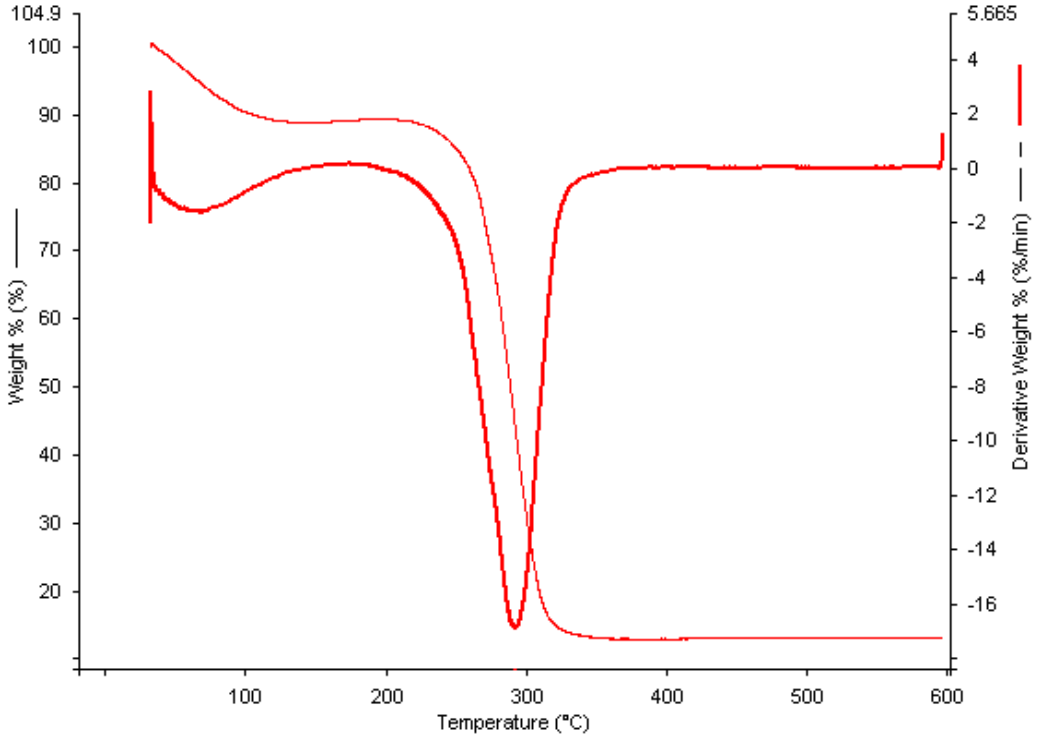

Figure 3.4 TGA curve of CMC-Br-1PEG film

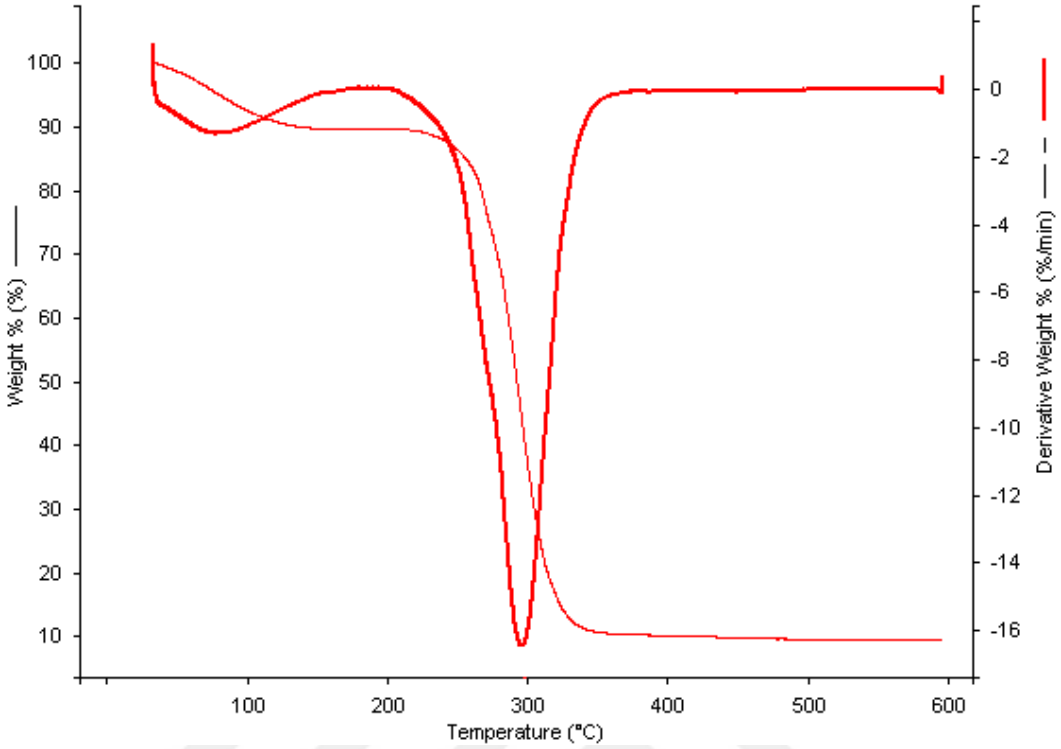

Figure 3.5 TGA curve of CMC-Br-1.5PEG film

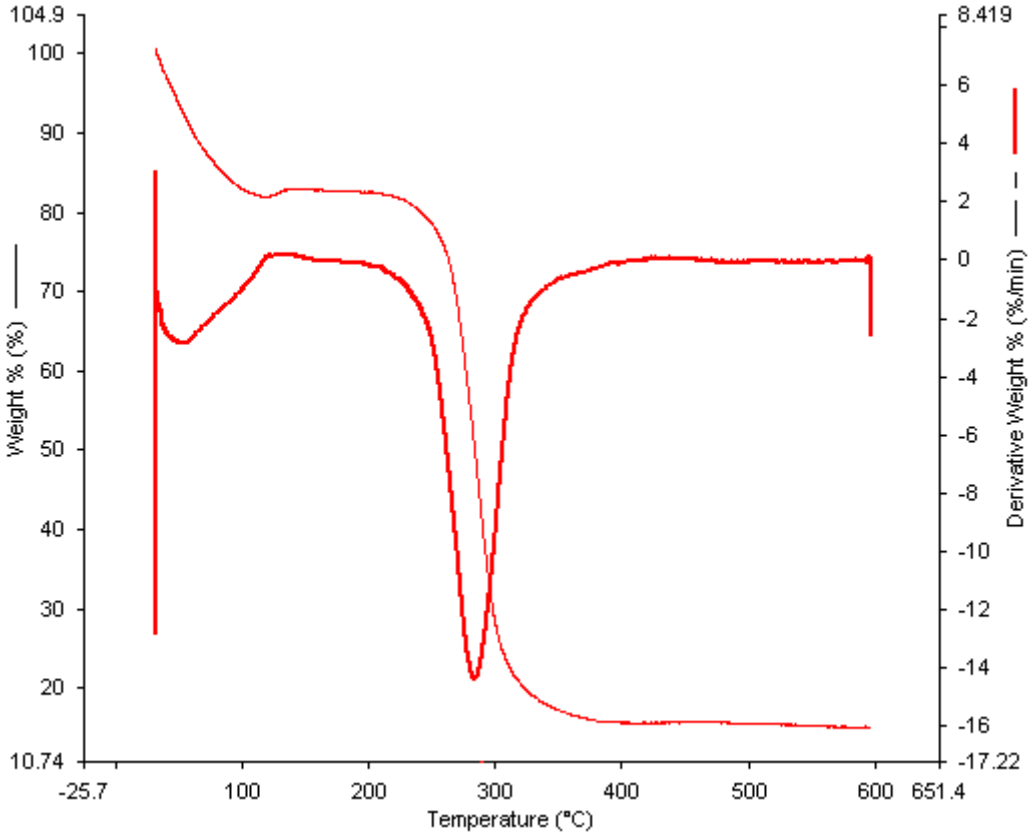

Figure 3.6 TGA curve of CMC-Br-2PEG film

3.2.2 CMC-based Films with Different Gr Loadings

TGA curves of CMC-Br (with 1.5 g PEG), CMC-Br-0.1 Gr, CMC-Br-0.2Gr, and CMC-Br-0.3Gr samples are given in Figure 3.7-3.9. The mass loss up to 110 ˚C, initial decomposition temperature ($T_{initial}$), final decomposition temperature (T_{final}), maximum decomposition temperature (T_{max}), mass loss up to T_{max}, and mass loss up to 600 ˚C are presented in Table 3.2. The decomposition of the all samples takes place in two steps. For the first and second decomposition steps, a small mass loss (8.5 – 12.5%) and more distinct mass loss (56.4 – 58%) were observed (Ozdemir et al., 2015b).

The mass loss for the first step was probably owing to evaporation of bound water. After Gr loading, it is clearly seen that the value of the mass loss up to 110 ˚C increased. The mass loss for the second decomposition step is ascribed to the degradation of side chain and loss of CO_2 of CMC (El-Sayed, Mahmoud, Fatah & Hassen, 2011). Increasing the Gr loading from 0.1 to 0.3 wt.% did not lead to any variation in the maximum decomposition temperature. It is seen from Table 3.2, Gr loadings of 0.1 and 0.2 wt.% increased the initial decomposition temperature while Gr loading of 0.3 wt.% decreased. On the other hand, mass loss up to 600 ˚C of Gr loaded samples decreased considerably. Hence, it can be noted that Gr loading into the CMC-Br films increased the thermal decomposition residues which are observed because of the nonvolatile carbonaceous material (Ozdemir et al., 2015b).

Table 3.2 TGA data for the Gr loaded CMC-based samples

Sample name	*Mass loss up to 110°C (%)*	$T_{initial}$ *(°C)*	T_{max} *(°C)*	T_{final} *(°C)*	*Mass loss up to* T_{max} *(%)*	*Mass loss up to 600°C (%)*
CMC-Br	8.5	206	296	373	56.4	90.4
CMC-Br-0.1Gr	10.3	212	292	366	55.8	88.7
CMC-Br-0.2Gr	12.3	212	292	370	56.7	84.2
CMC-Br-0.3Gr	12.5	202	292	353	58.0	86.9

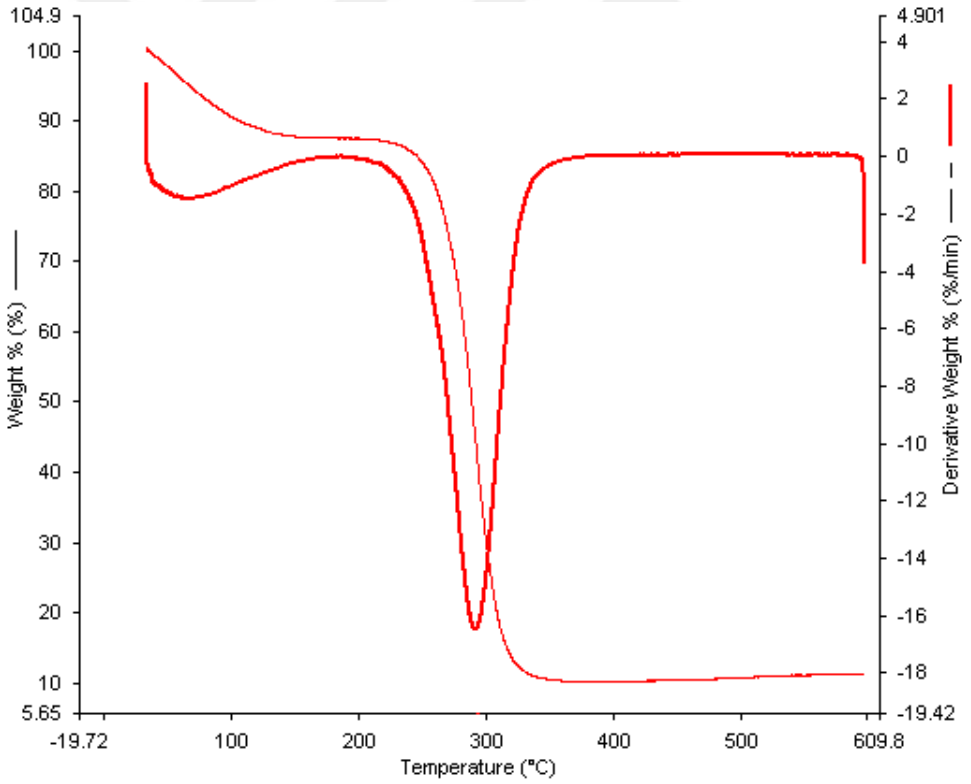

Figure 3.7 TGA curve of CMC-Br-0.1Gr film

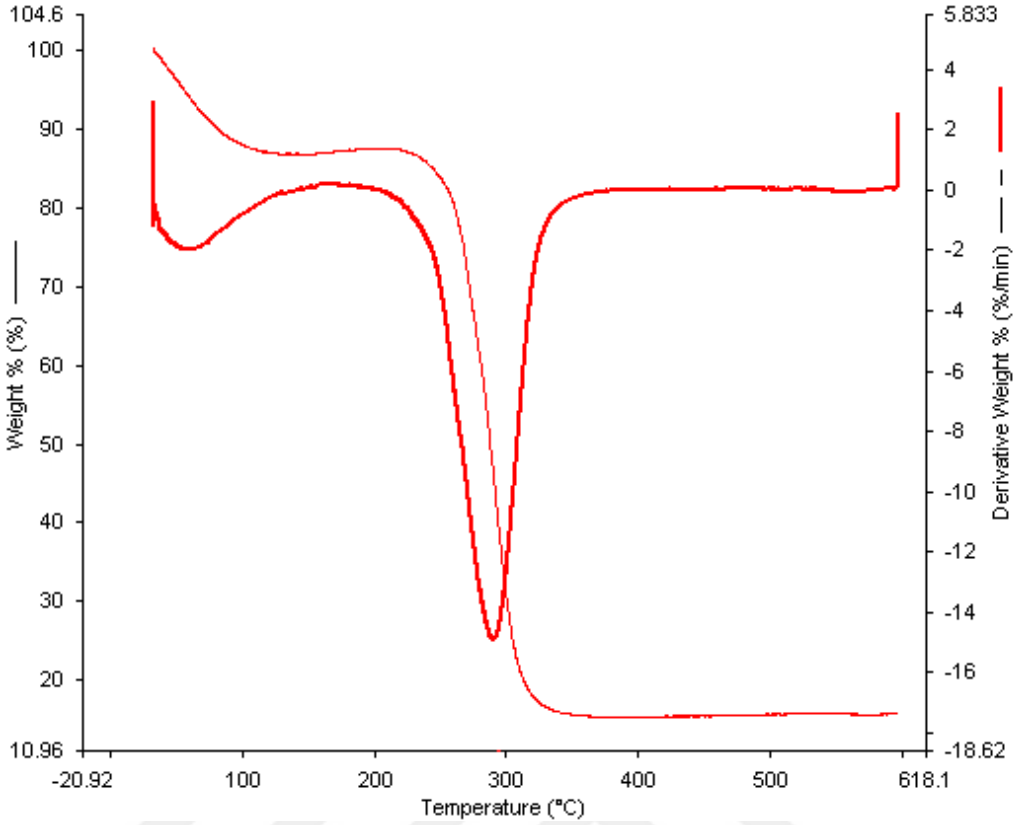

Figure 3.8 TGA curve of CMC-Br-0.2Gr film

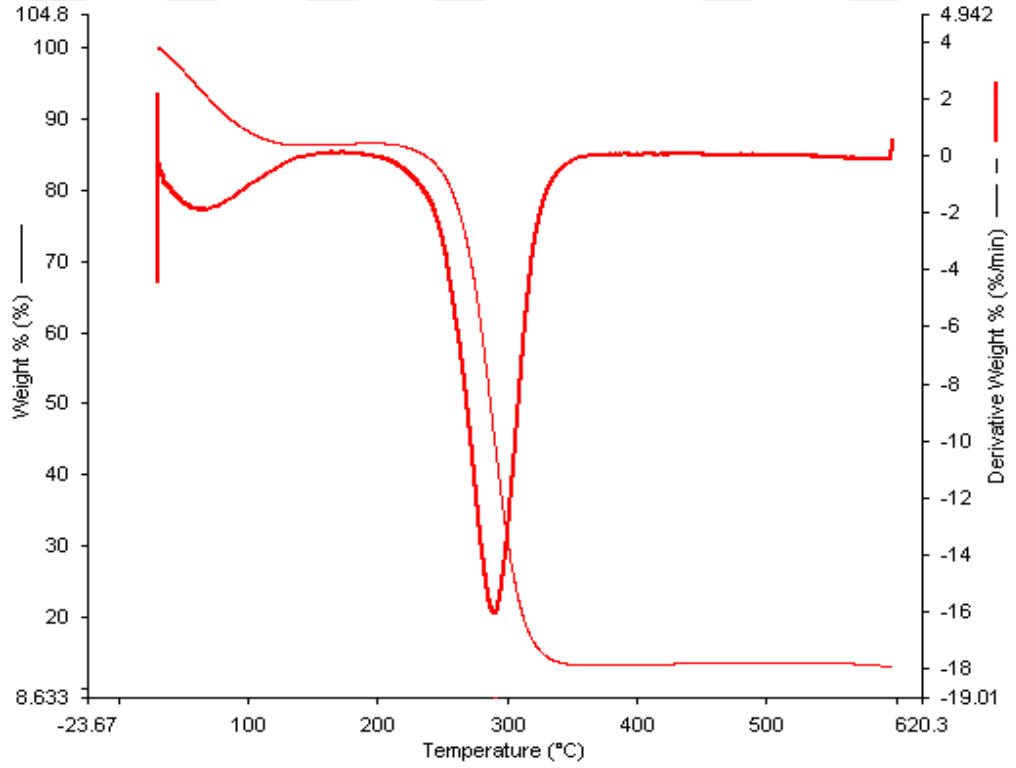

Figure 3.9 TGA curve of CMC-Br-0.3Gr film

3.3 XRD Analyses

3.3.1 CMC-based Films with Different PEG Loadings

X-ray diffraction patterns of CMC, CMC-Br, CMC-Br-1PEG, CMC-Br-1.5PEG, and CMC-Br-2PEG films are given in Figure 3.10-3.14. When these curves were analyzed, one diffraction peak in the region of 2θ=15 – 30˚ was observed.

For the CMC, the characteristic diffraction peak occurs at 2θ=19.82˚ as shown in Figure 3.10. (Ravikiran, Kotresh, Vijayakumari, & Thomas, 2014) found a broad peak at 2θ=20˚ pointing out the amorphous nature of CMC. The characteristic diffraction peak shifted to 2θ=22.70˚ for the samples of CMC-Br (Ozdemir et al., 2015a) (Figure 3.11).

The characteristic diffraction of CMC-Br-1PEG, CMC-Br-1.5PEG and CMC-Br-2PEG is observed at approximately 2θ=23.20˚ (Figure 3.12-3.14). (Bell, Geehanjali, & Subhashini, 2014) found that the XRD pattern of PEG contains two different peaks at 2θ=19.20˚ and 2θ=23.40˚. Besides, when the amount of PEG loading increased from 1 g to 2 g, the intensity of the diffraction peak becomes weaker. (Guleria, Kaith, & Singh, 2012) indicated that as the amount of PEG increased in the solid dispersion, relative reduction in diffraction intensity of samples was obtained. This relative reduction in the intensity of the CMC may be owing to destruction of the crystallinity of CMC structure with PEG loading (Ozdemir et al., 2015a).

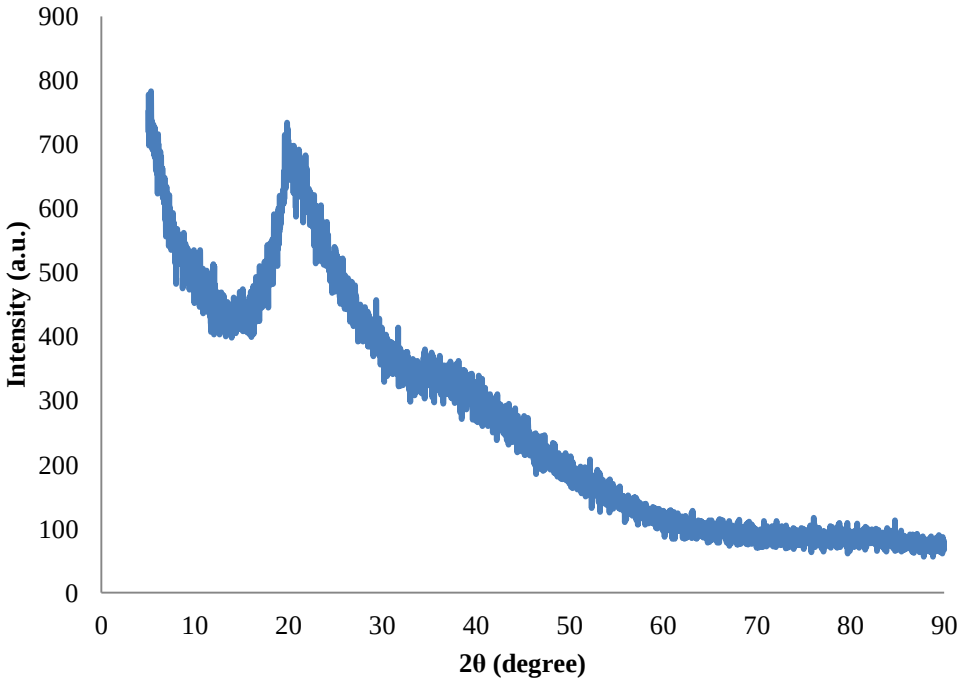

Figure 3.10 X-ray diffraction pattern of CMC

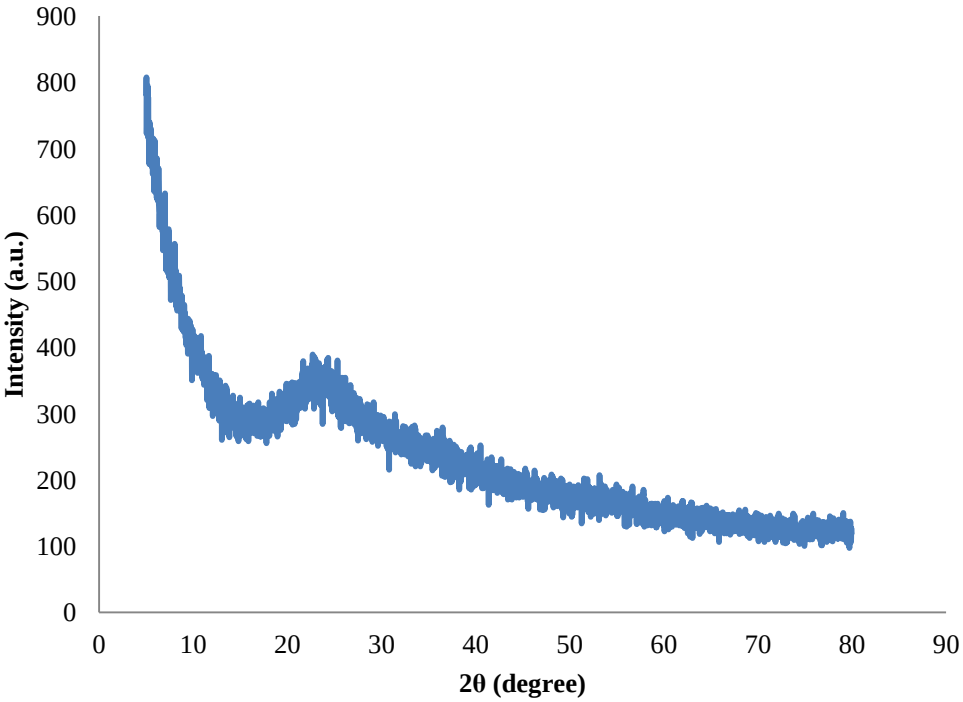

Figure 3.11 X-ray diffraction pattern of CMC-Br film

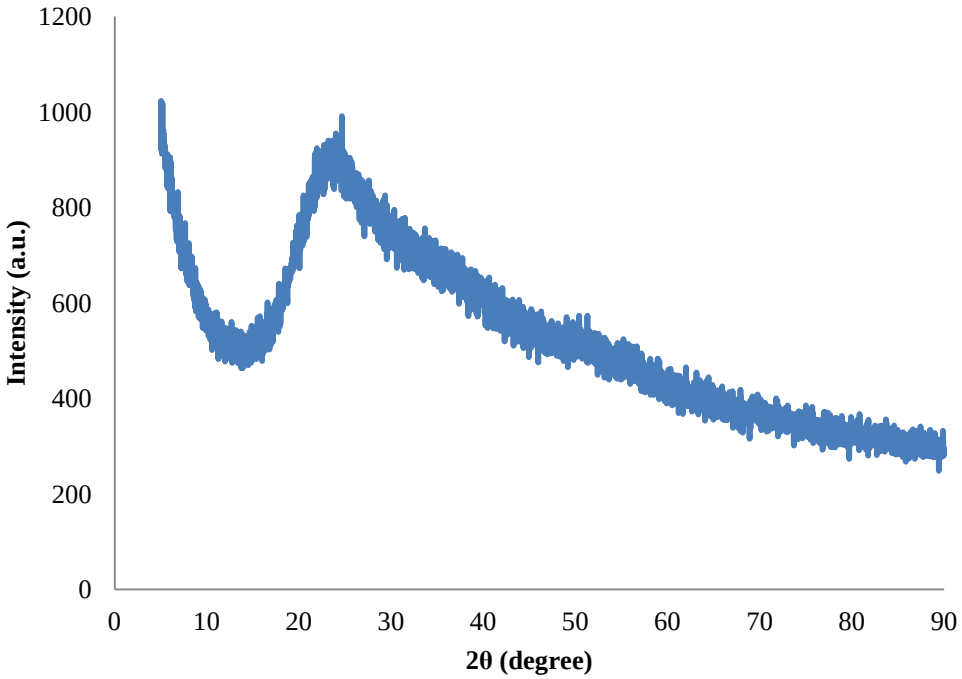

Figure 3.12 X-ray diffraction pattern of CMC-Br-1PEG film

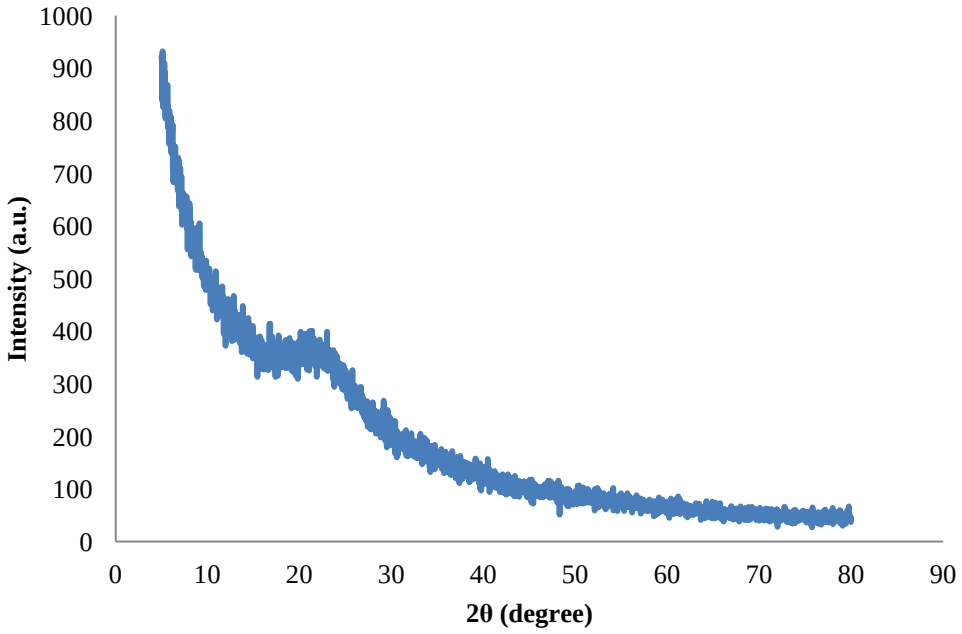

Figure 3.13 X-ray diffraction pattern of CMC-Br-1.5PEG film

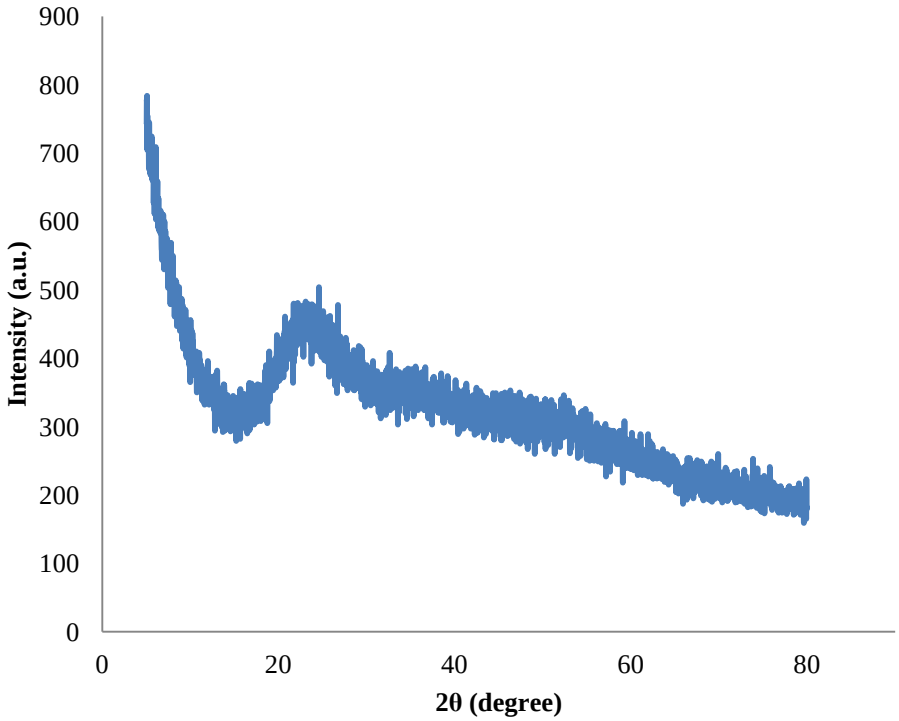

Figure 3.14 X-ray diffraction pattern of CMC-Br-2PEG film

3.3.2 CMC-based Films with Different Gr Loadings

XRD diffraction curves of the CMC-Br-0.1Gr, CMC-Br-0.2Gr and CMC-Br-0.3Gr films are shown in Figure 3.15-3.17.

According to Wojtoniszak et al. (2012), the main characteristic peak of graphite was found as 2θ=26.475º. After graphene nanoplatelets were loaded into the CMC-Br-1.5PEG samples, the main characteristic peak of Gr did not appear distinctly in the patterns of the samples. Also, there is not seen any peak regarding Gr in this range. This is may be related to well dispersion of Gr in CMC-Br. In other words, matrix effect still is dominant in the Gr loaded samples (Ozdemir et al., 2015b).

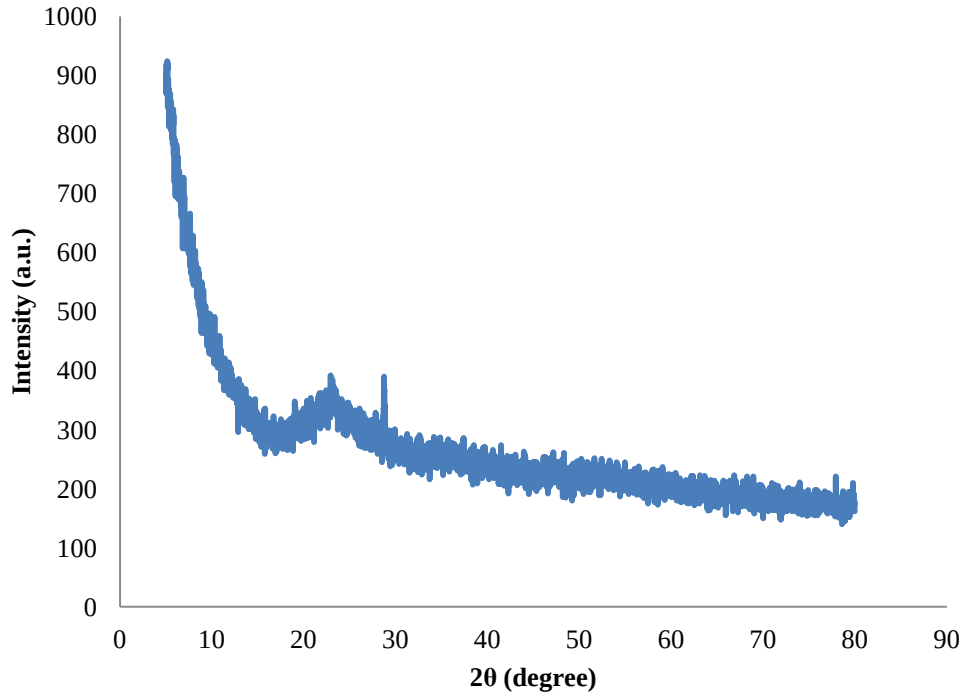

Figure 3.15 X-ray diffraction pattern of CMC-Br-0.1Gr film

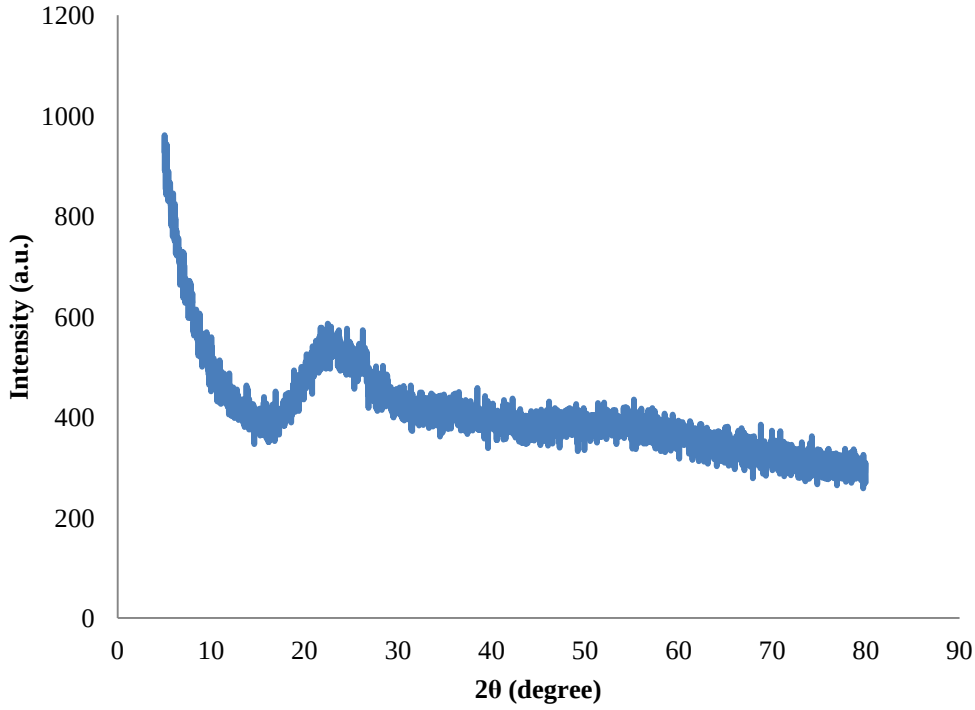

Figure 3.16 X-ray diffraction pattern of CMC-Br-0.2Gr film

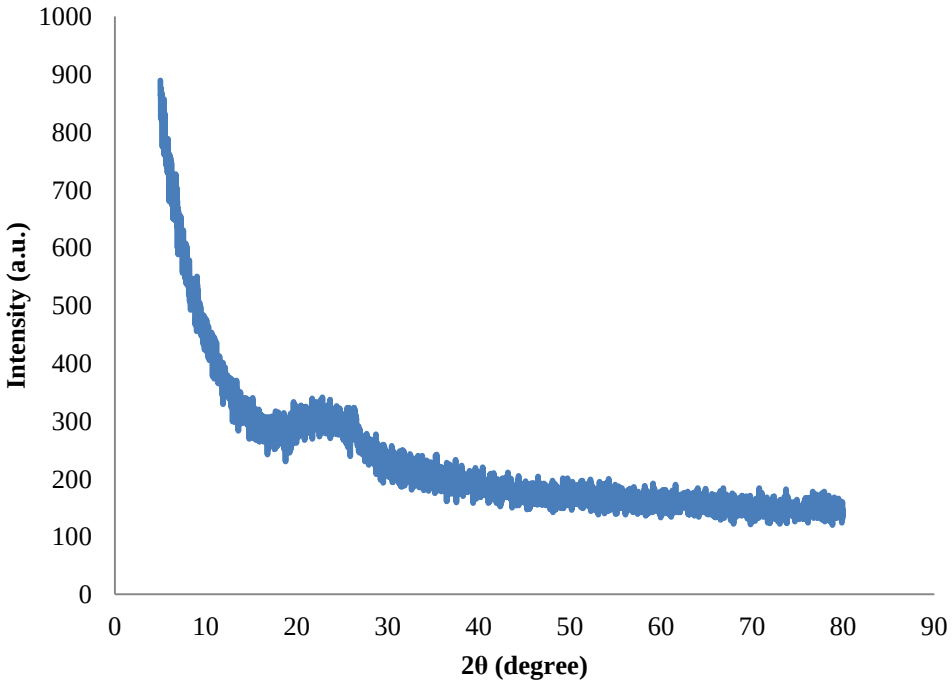

Figure 3.17 X-ray diffraction pattern of CMC-Br-0.3Gr film

3.4 SEM Analyses

3.4.1 CMC-based Films with Different PEG Loadings

SEM images of CMC-Br, CMC-Br-1PEG, CMC-Br-1.5PEG and CMC-Br-2PEG films at different magnifications are given in Figure 3.18-3.21. According to these images, adding PEG with different amounts altered significantly the surface structure of CMC-Br film. In the ionic liquid matrix, the distribution of particles such as PEG is observed in nano-scale and micro-scale (Ozdemir et al., 2015a).

The surface of CMC-Br film, as shown in Figure 3.18, appeared to have fairly uneven and dense irregular structure and CMC particles were randomly dispersed.

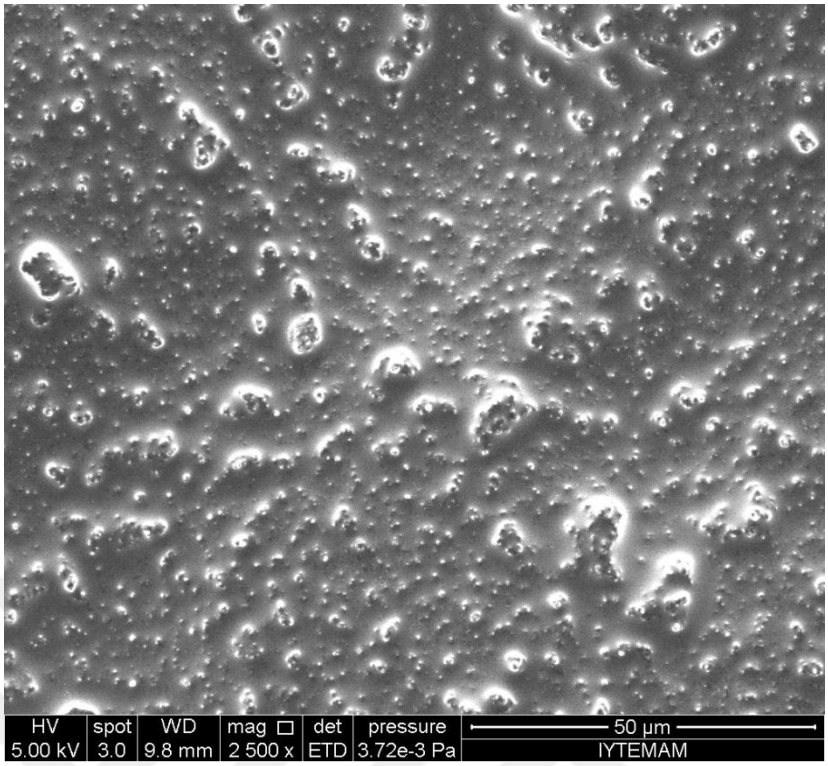

(a)

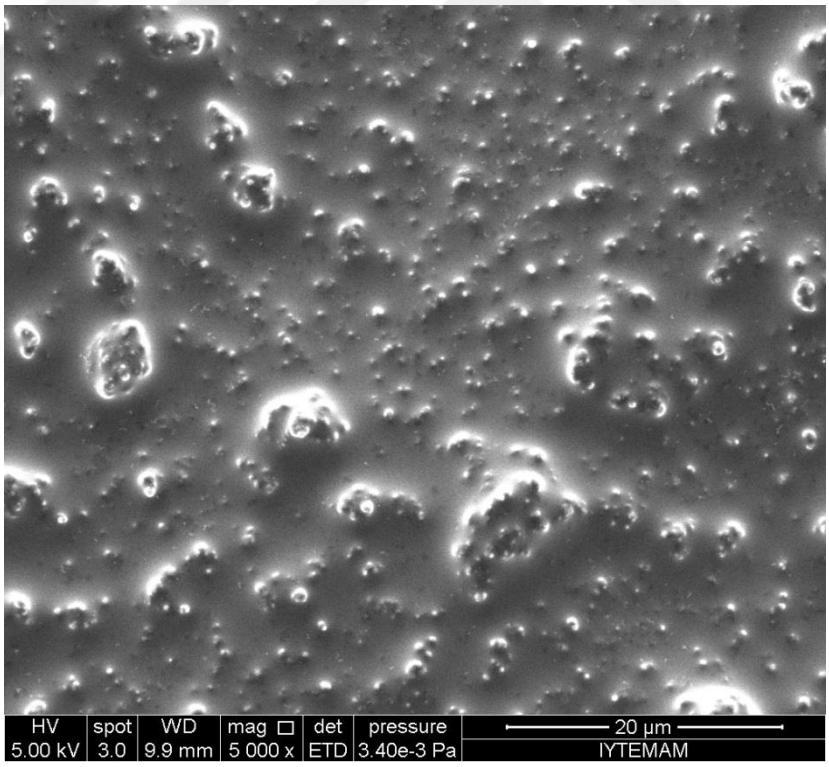

(b)

Figure 3.18 SEM images of CMC-Br film at magnifications of **(a)** 2500x and **(b)** 5000x

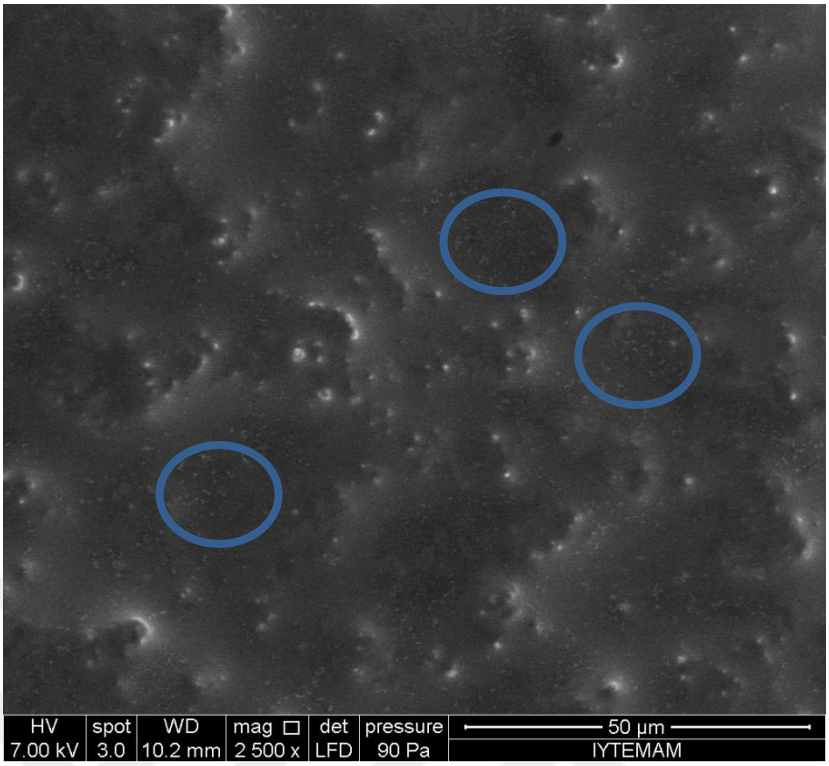

(a)

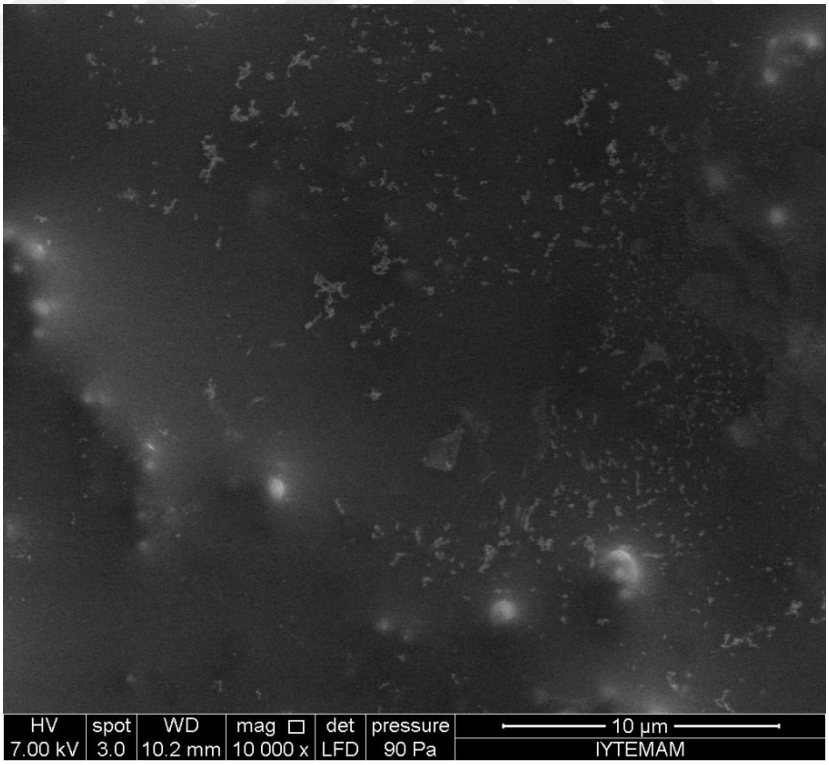

(b)

Figure 3.19 SEM images of CMC-Br-1PEG film at magnifications of **(a)** 2500x and **(b)** 10000x

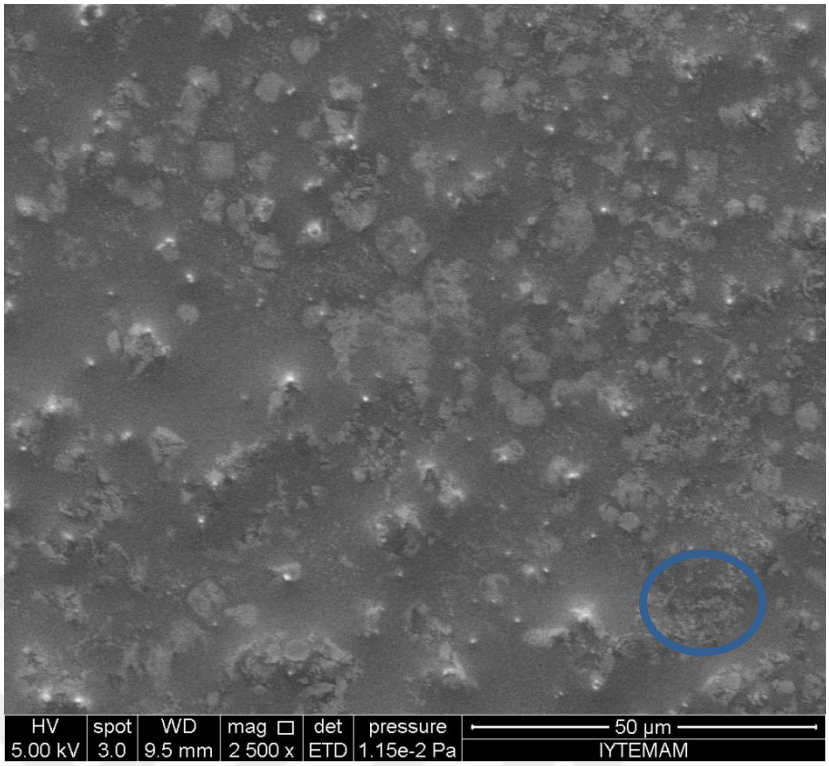

(a)

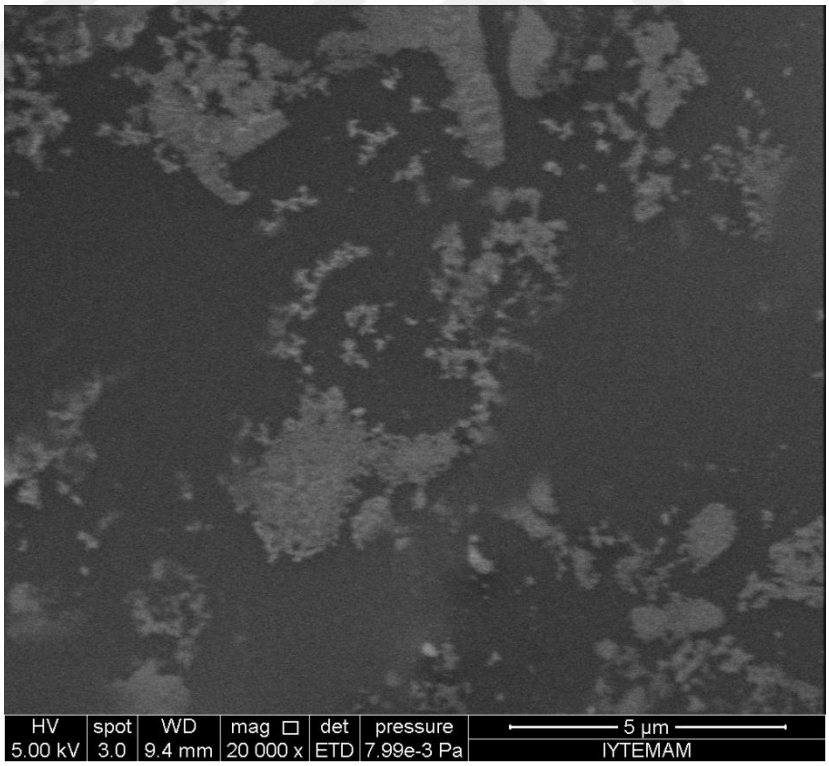

(b)

Figure 3.20 SEM images of CMC-Br-1.5PEG film at magnifications of **(a)** 2500x and **(b)** 20000x

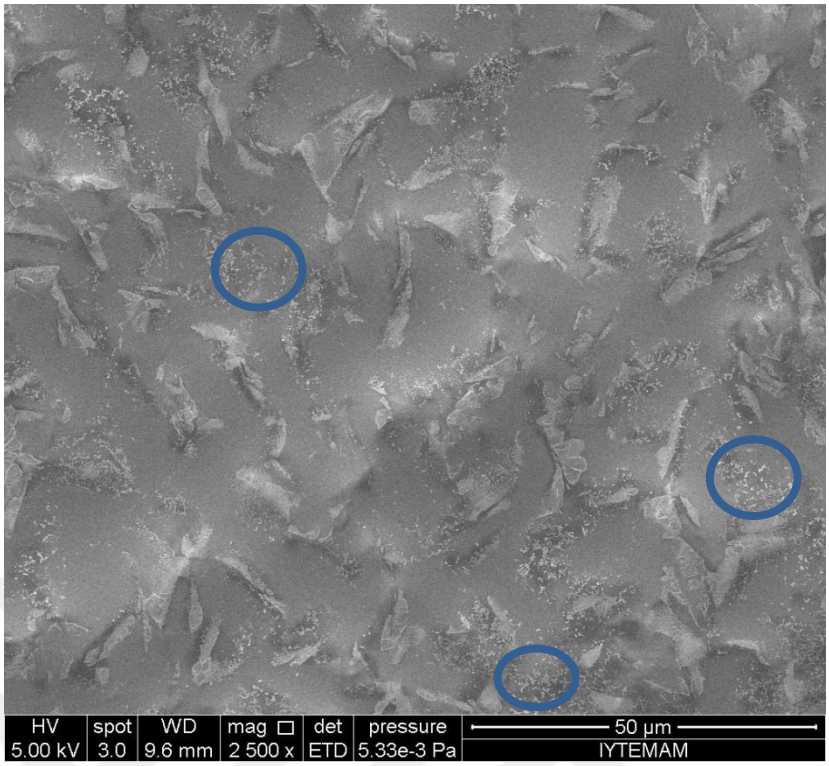

(a)

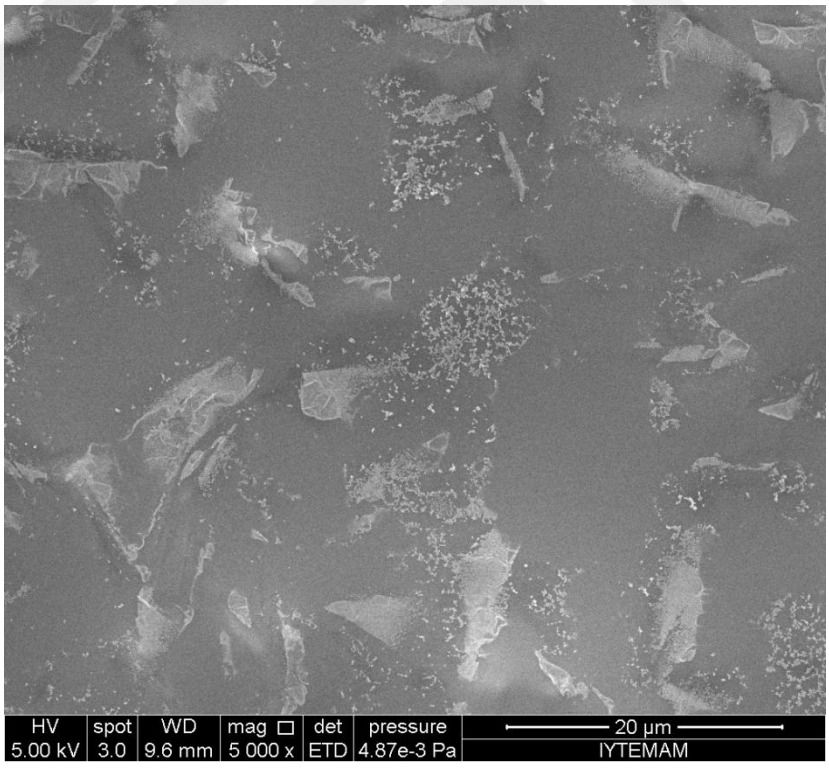

(b)

Figure 3.21 SEM images of CMC-Br-2PEG film at magnifications of **(a)** 2500x and **(b)** 5000x

Besides, it is seen that CMC particles corresponding to bright clusters were embedded in the BMIMBr ionic liquid matrix. These bright clusters were not observed in CMC-Br-2PEG film (Figure 3.21). PEG particles were demonstrated with blue circles in Figure 3.19-3.21. Similar observation was found by Georgiev et al., (2007). Increasing the PEG amount, uneven structure of films decreased. This situation may be probable that PEG reduced the roughness of the surface and heterogeneity (Ozdemir et al., 2015a).

3.4.2 CMC-based Films with Different Gr Loadings

SEM images of CMC-Br-0.1Gr, CMC-Br-0.2Gr and CMC-Br-0.3Gr films at different magnifications are given in Figure 3.22-3.24. From these figures, CMC particles were dispersed in the mixture of BMIMBr, PEG and Gr in nano-scale and micro-scale. CMC particles were seen in the CMC-Br-0.1Gr films while they cannot be seen clearly in the CMC-Br-0.2Gr and CMC-Br-0.3Gr films (Ozdemir et al., 2015b).

It is also seen from the Figure 3.23 and 3.24 that some CMC particles were agglomerated. This is probably related to the amount of Gr. In the higher Gr loadings, the dispersion of CMC particles in the mixture of BMIMBr and PEG decreased. Hence, the surface morphologies of the films including Gr are rougher than CMC-Br films (Ozdemir et al., 2015b).

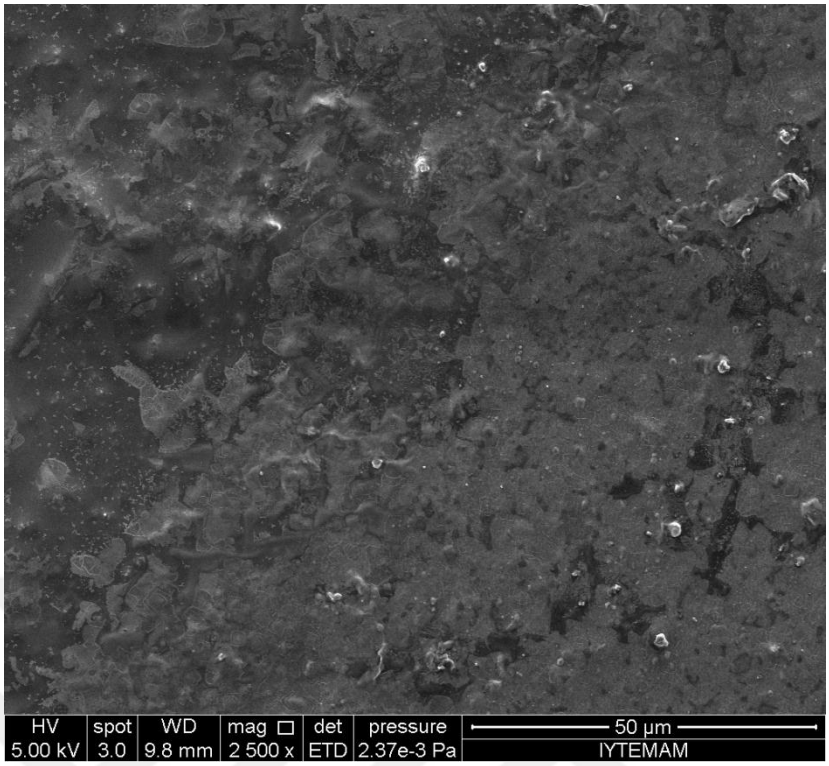

(a)

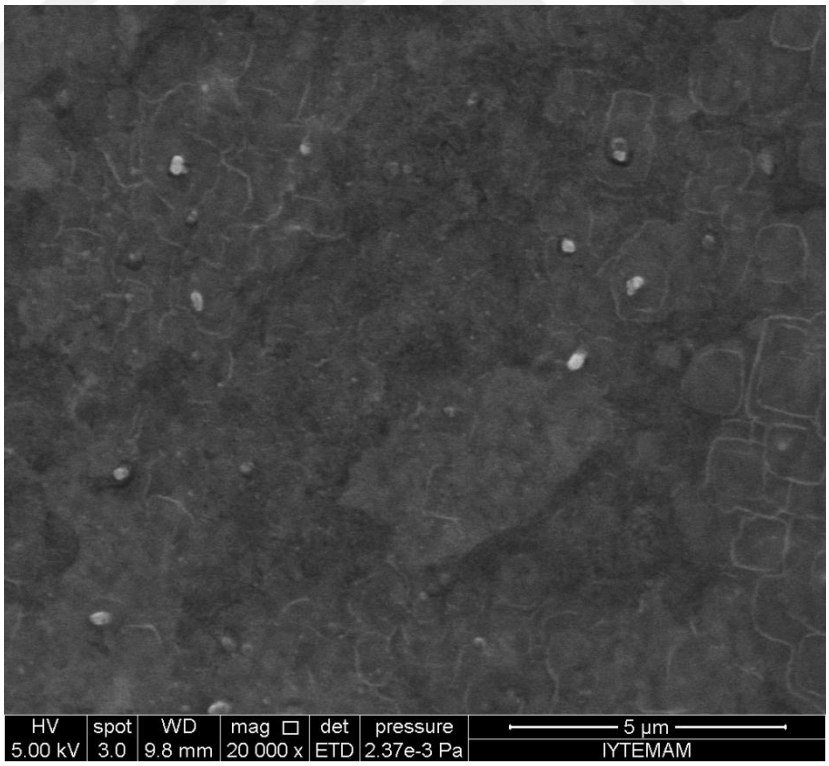

(b)

Figure 3.22 SEM images of CMC-Br-0.1Gr film at magnifications of **(a)** 2500x and **(b)** 20000x

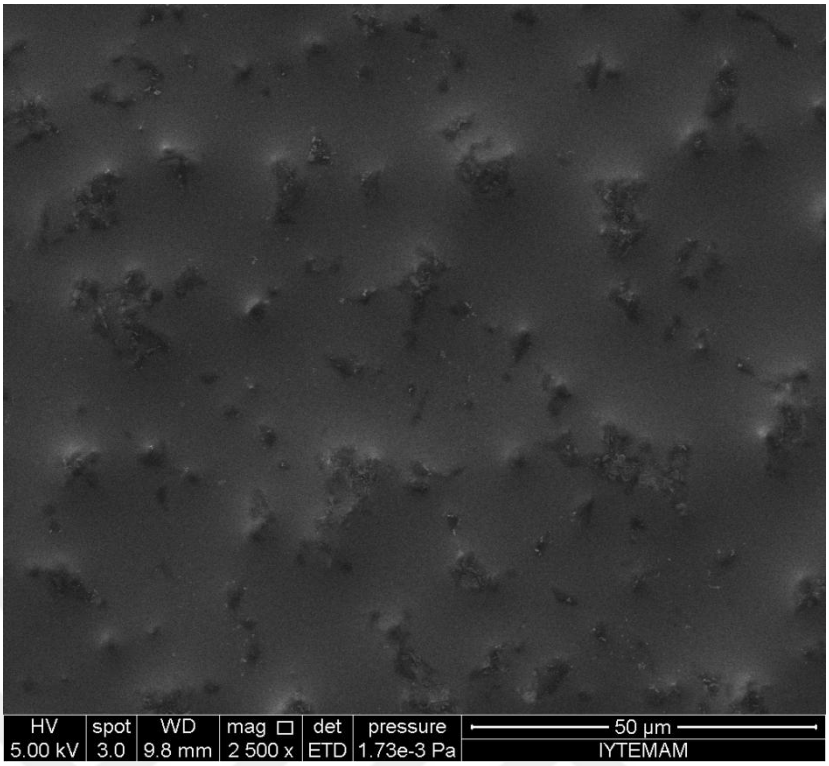

(a)

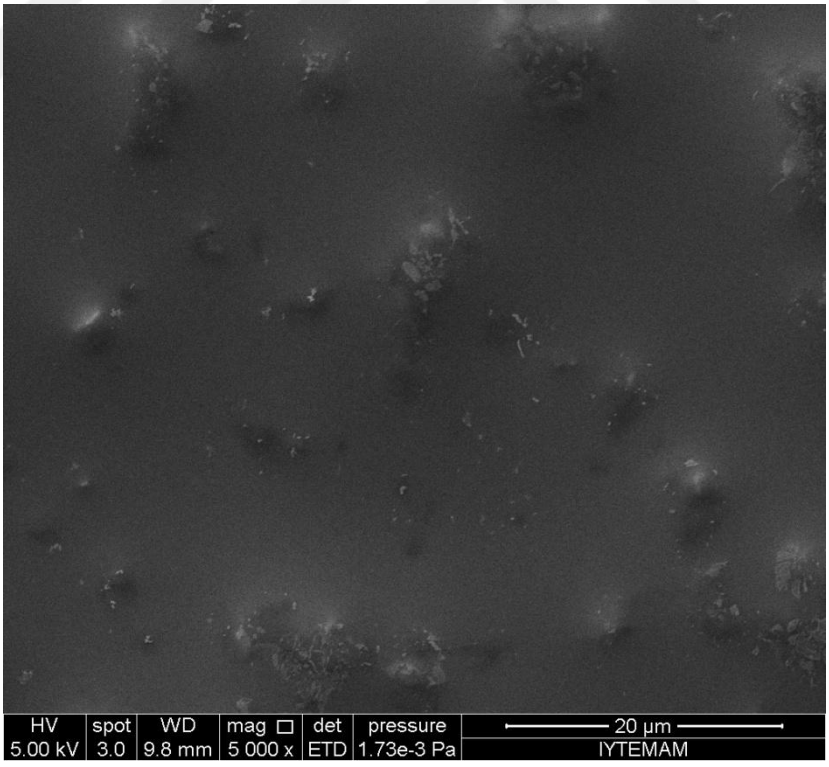

(b)

Figure 3.23 SEM images of CMC-Br-0.2Gr film at magnifications of **(a)** 2500x and **(b)** 5000x

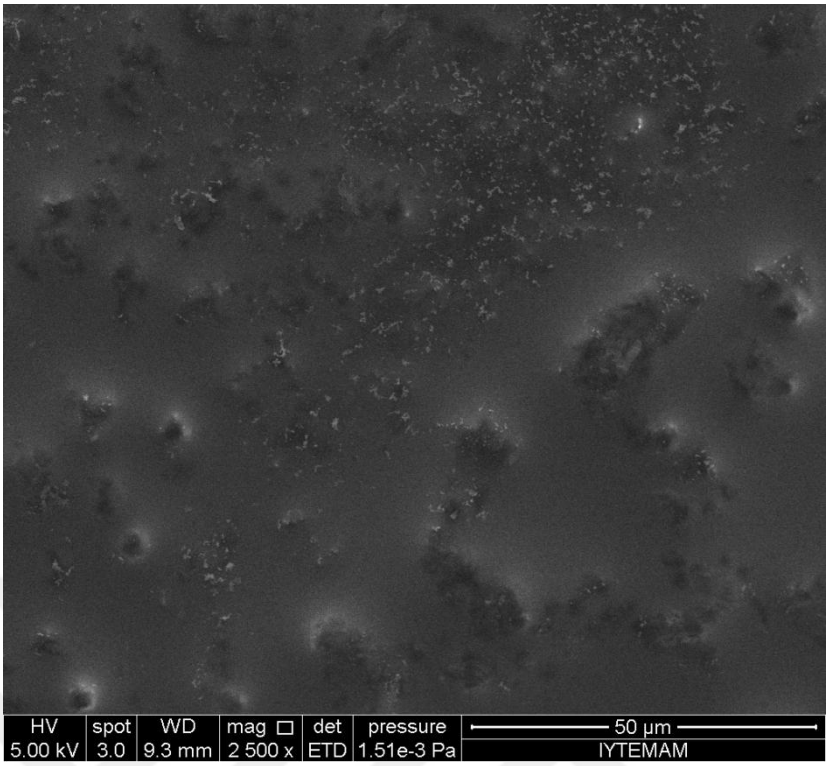

(a)

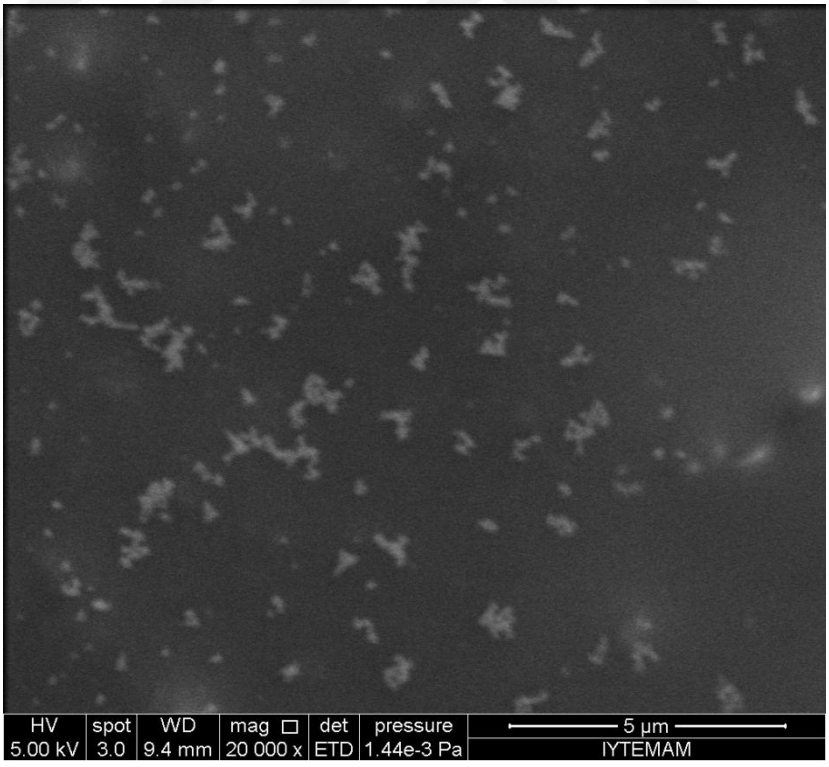

(b)

Figure 3.24 SEM images of CMC-Br-0.3Gr film at magnifications of **(a)** 2500x and **(b)** 20000x

3.5 Mechanical Properties

3.5.1 CMC-based Films with Different PEG Loadings

In this study, polyethylene glycol (PEG) was used as plasticizer. The effects of different amounts of PEG on the mechanical properties such as tensile strength and Young's modulus of CMC-Br, CMC-Br-1PEG, CMC-Br-1.5PEG and CMC-Br-2PEG films and actuators are depicted in Figure 3.25 and 3.26, respectively. Here, Young's modulus or the modulus of elasticity can be identified as the slope of the stress-strain curve in the elastic region.

Tensile strength and Young's modulus of CMC-Br films (without PEG) were obtained to be 12.13 MPa and 0.45 GPa, respectively. After 1 g, 1.5 g and 2 g of PEG were added into the CMC-Br film, tensile strengths of CMC-Br-1PEG, CMC-Br-1.5PEG and CMC-Br-2PEG films increased to 12.25, 12.24 and 12.37 MPa, respectively. According to obtained results, it is seen that PEG loading into the CMC-Br films has not lead to considerable differences in tensile strength of films (Ozdemir et al., 2015a).

However, Young's modulus decreases considerably as the amount of PEG increases. Young's modulus of CMC-Br-1PEG, CMC-Br-1.5PEG and CMC-Br-2PEG were determined to be 0.32, 0.24 and 0.18 GPa, respectively. Yang & Paulson (2000) suggested that the primary role of the plasticizer is to enhance the film flexibility and decrease the brittleness. Also, the addition of plasticizer leads to a decrease in intermolecular forces along polymer chains. Therefore, the flexibility of the films increases (Guilbert, Gontard, & Cuq, 1995; Ozdemir et al., 2015a).

For the CMC-Br, CMC-Br-1PEG, CMC-Br-1.5PEG and CMC-Br-2PEG actuators (gold coated films), tensile strength of the actuators were obtained to be 15.52, 15.55, 15.79 and 16.08 MPa, respectively. It is seen that tensile strength of the actuators increased by 28%, 27%, 29% and %30, respectively, when compared to CMC-Br films.

For the CMC-Br, CMC-Br-1PEG, CMC-Br-1.5PEG and CMC-Br-2PEG actuators, Young's modulus were determined to be 0.50, 0.43, 0.32 and 0.26 GPa, respectively.

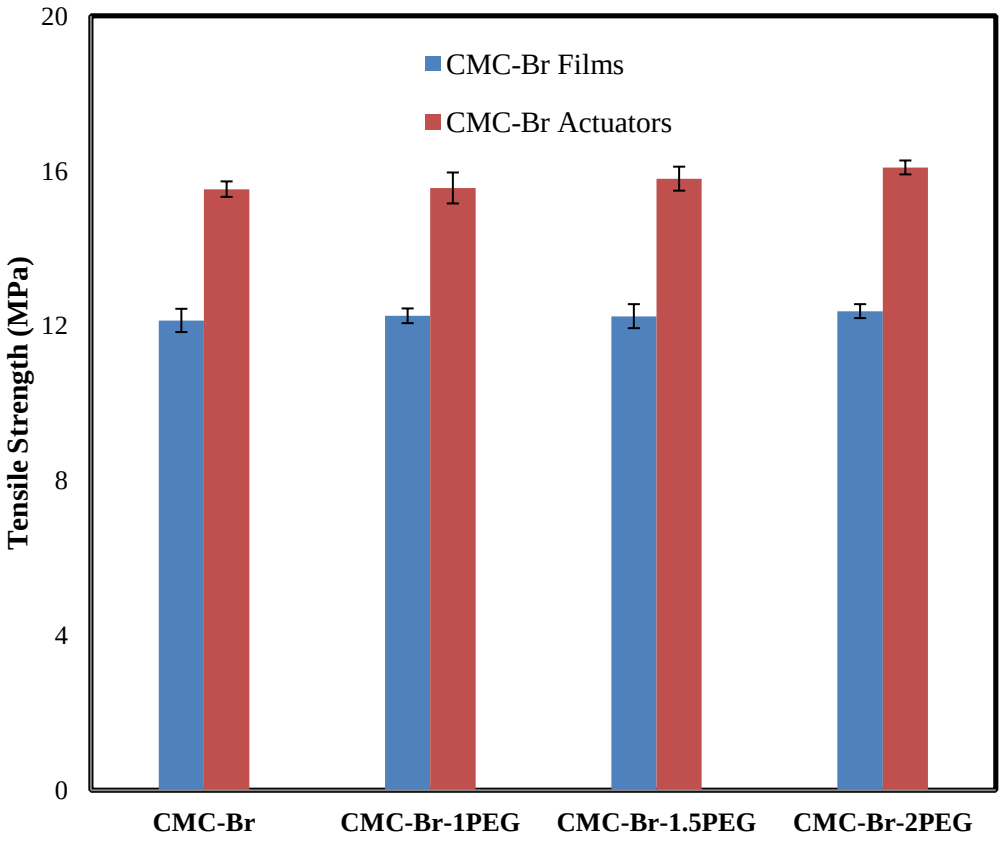

Figure 3.25 Tensile Strength of PEG loaded CMC-Br films and actuators

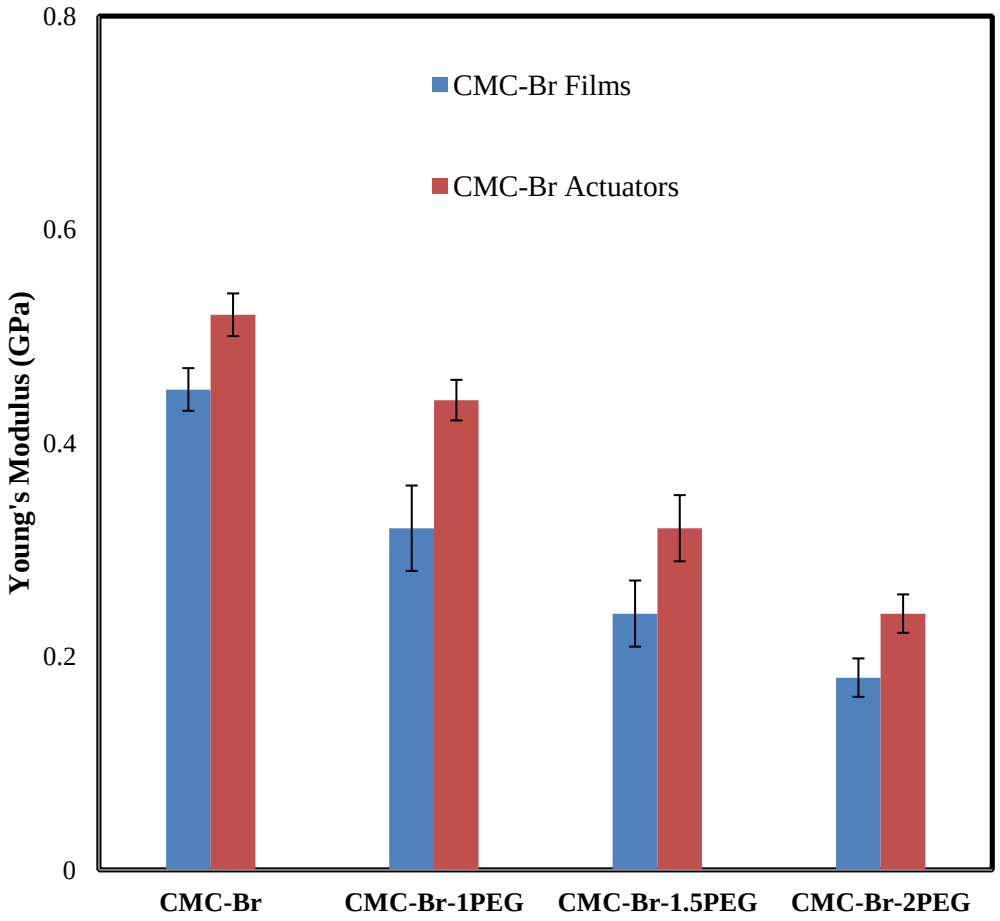

Figure 3.26 Young's Modulus of PEG loaded CMC-Br films and actuators

3.5.2 CMC-based Films with Different Gr Loadings

The weak characteristic of the CMC-based films is a major problem that limits the usage of actuator. In other words, tensile strength of the actuators should be sufficient values. If the actuators are not strong enough, they might be damaged subjected to especially high voltages. (Jung, Jeon, Vadahanambi, & Oh, 2011; Ozdemir et al., 2015b) suggested that the addition of graphene to the polymer may alter the static micro-phase morphology of them.

Tensile strengths of the CMC-Br (with 1.5 PEG), CMC-Br-0.1Gr, CMC-Br-0.2Gr and CMC-Br-0.3Gr films and actuators are shown in Figure 3.27. Tensile strengths of the CMC-Br, CMC-Br-0.1Gr, CMC-Br-0.2Gr and CMC-Br-0.3Gr films were

determined to be 12.24, 15.68, 18.45, and 21.15 MPa, respectively. It is clearly seen that tensile strengths of the all Gr loaded samples were higher than the CMC-Br films. Besides, tensile strengths of the all Gr loaded films increased with increasing the Gr content from 0.1 %wt. to 0.3 wt%. The highest tensile strength was found for CMC-Br-0.3Gr films as 21.15 MPa. Tensile strengths of the CMC-Br, CMC-Br-0.1Gr, CMC-Br-0.2Gr and CMC-Br-0.3Gr actuators were higher than CMC-Br, CMC-Br-0.1Gr, CMC-Br-0.2Gr and CMC-Br-0.3Gr films by about 28, 17, 15 and 18%, respectively (Ozdemir et al., 2015b).

Young's modulus values of the CMC-Br (with 1.5 PEG), CMC-Br-0.1Gr, CMC-Br-0.2Gr and CMC-Br-0.3Gr films and actuators are given in Figure 3.28. Young's modulus of the CMC-Br, CMC-Br-0.1Gr, CMC-Br-0.2Gr and CMC-Br-0.3Gr were obtained to be 0.24, 0.28, 0.34 and 0.42 GPa, respectively. From this figure, Gr loaded CMC-Br films have higher Young's modulus values than CMC-Br film. Moreover, the Young's modulus for the Gr loaded CMC-Br films increased continuously with increasing Gr content from 0.1 %wt. to 0.3 %wt. For the CMC-Br-0.3Gr film, the increase in the Young's modulus was 75% compared to that of CMC-Br film. This may be owing to the significant mechanical properties of Gr such as high Young's modulus and tensile strength values (Nieto, Lahiri, & Agarwal, 2012). Besides, the large surface area of Gr provides significant improvement in the mechanical properties of nanocomposites (Ahmad, Young, & Kinloch, 2015; Ozdemir et al., 2015b).

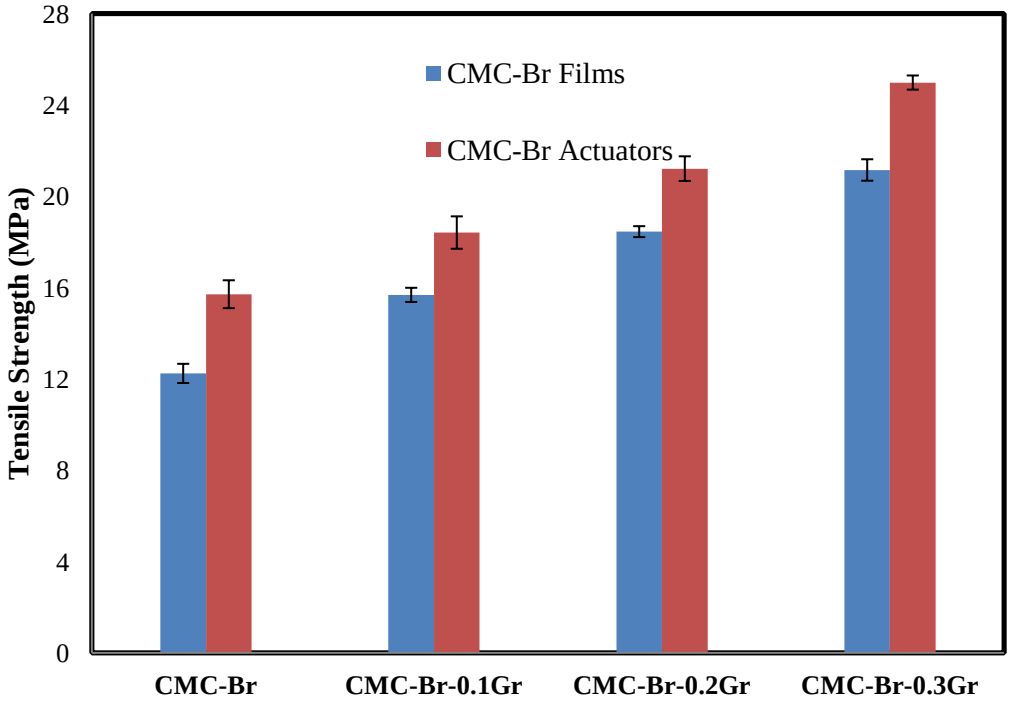

Figure 3.27 Tensile Strength of Gr loaded CMC-Br films and actuators

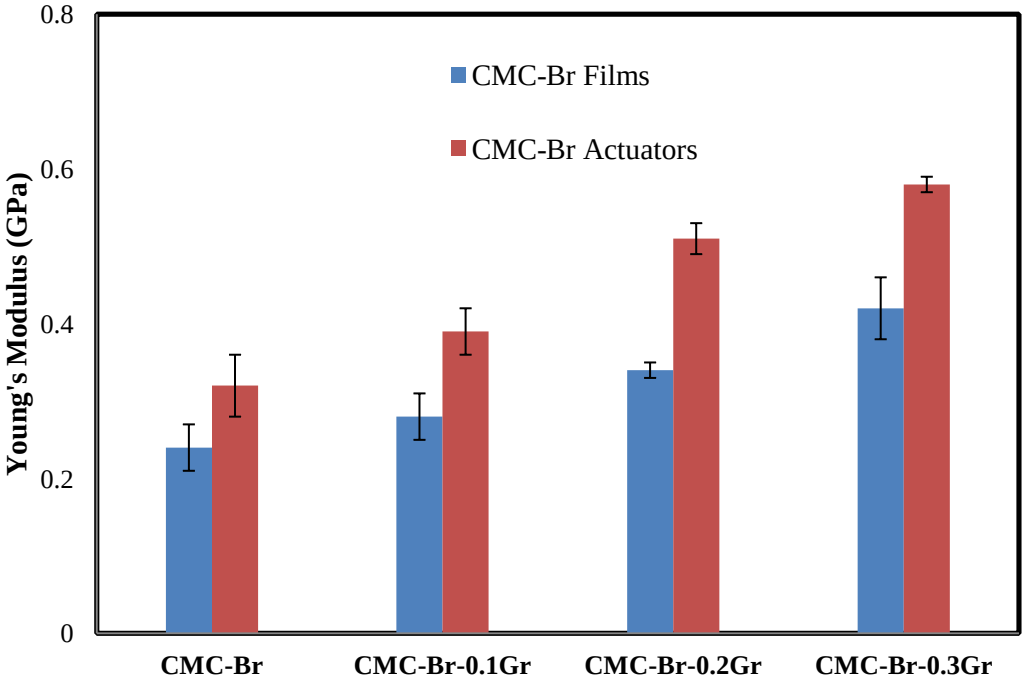

Figure 3.28 Young's Modulus of Gr loaded CMC-Br films and actuators

3.6 Electroactive Properties

3.6.1 CMC-based Actuators with Different PEG Loadings

Time responses of the CMC-Br, CMC-Br-1PEG, CMC-Br-1.5PEG and CMC-Br-2PEG actuators were analyzed in order to investigate the electromechanical performance of the actuators under DC excitation voltages of 1, 3, 5 and 7 V. Tip displacement measurements were performed at a distance of 100 mm from fixed end of cantilever configuration.

When the time responses of actuators were analyzed, it is observed that time evolution of the tip displacements are in an exponential form. And, there is not any back relaxation in contrast to Nafion-based actuators (Figure 3.29-3.38) (Shahinpoor & Kim, 2001; Ozdemir et al., 2015a). Hence, final or steady state values of actuators correspond to maximum tip displacement. Maximum tip displacement values of CMC-Br actuators under DC excitation voltages of 1, 3, 5 and 7 V and CMC-Br-2PEG actuators under DC excitation voltages of 1V and 7V is too small. Therefore, their time responses are not given. According to Figure 3.29-3.38, the experiments were performed 280, 340 and 295 s for the actuator samples of CMC-Br-1PEG, CMC-Br-1.5PEG and CMC-Br-2PEG, respectively.

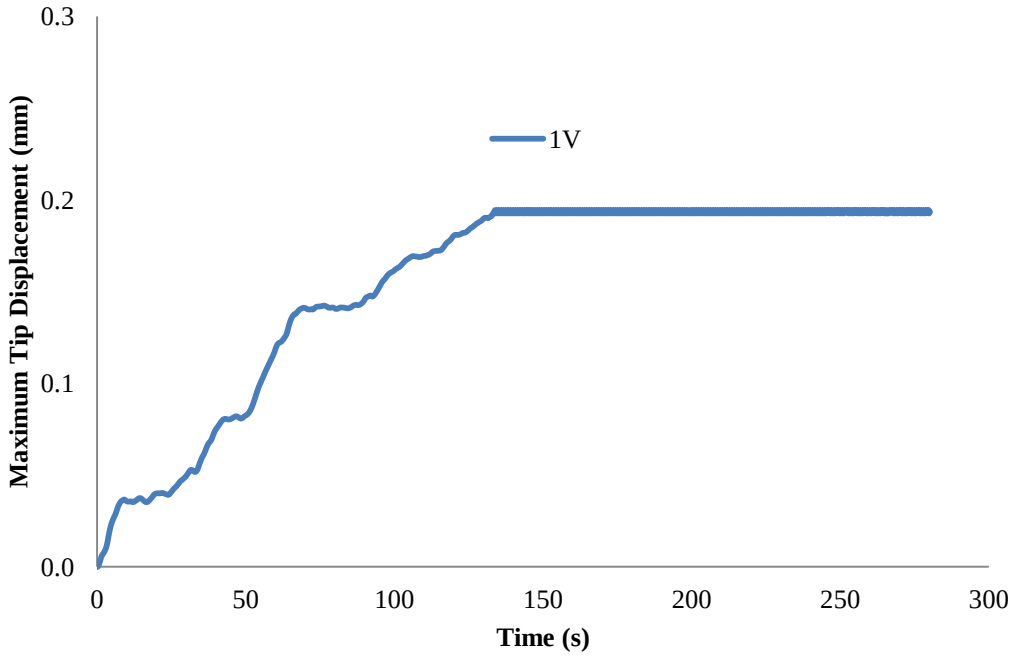

Figure 3.29 The time responses of the tip displacement of CMC-Br-1PEG actuators under DC excitation voltage of 1V

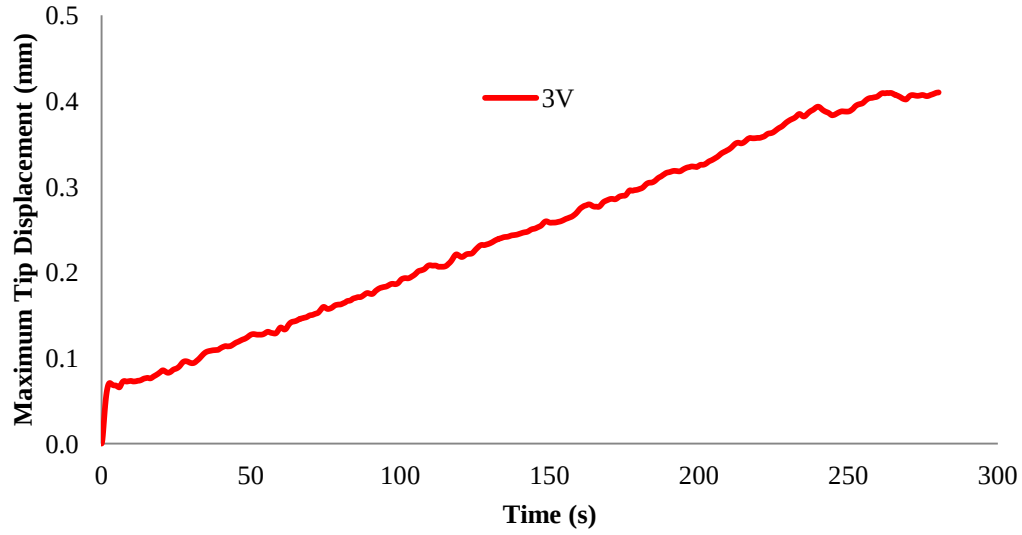

Figure 3.30 The time responses of the tip displacement of CMC-Br-1PEG actuators under DC excitation voltage of 3V

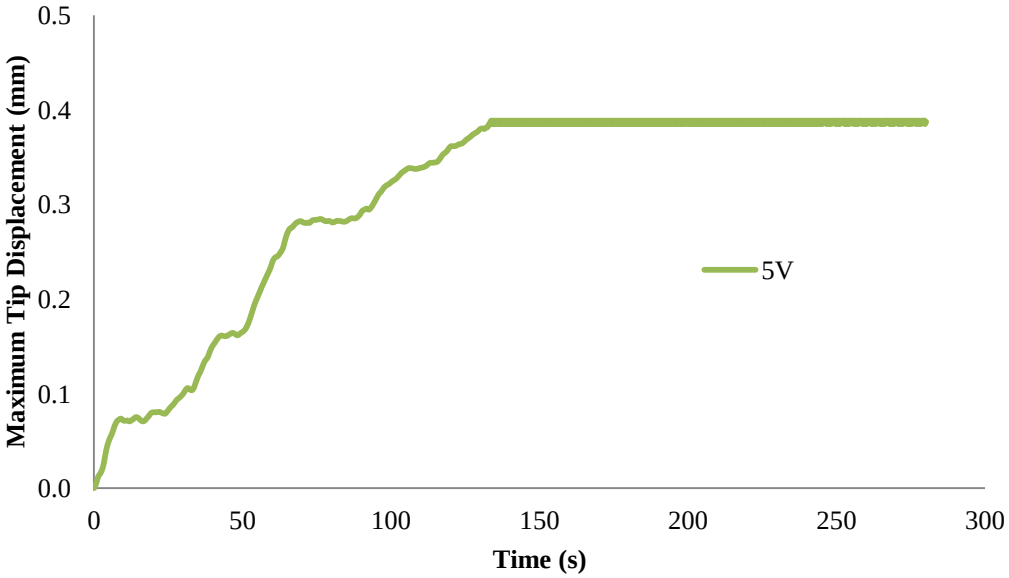

Figure 3.31 The time responses of the tip displacement of CMC-Br-1PEG actuators under DC excitation voltage of 5V

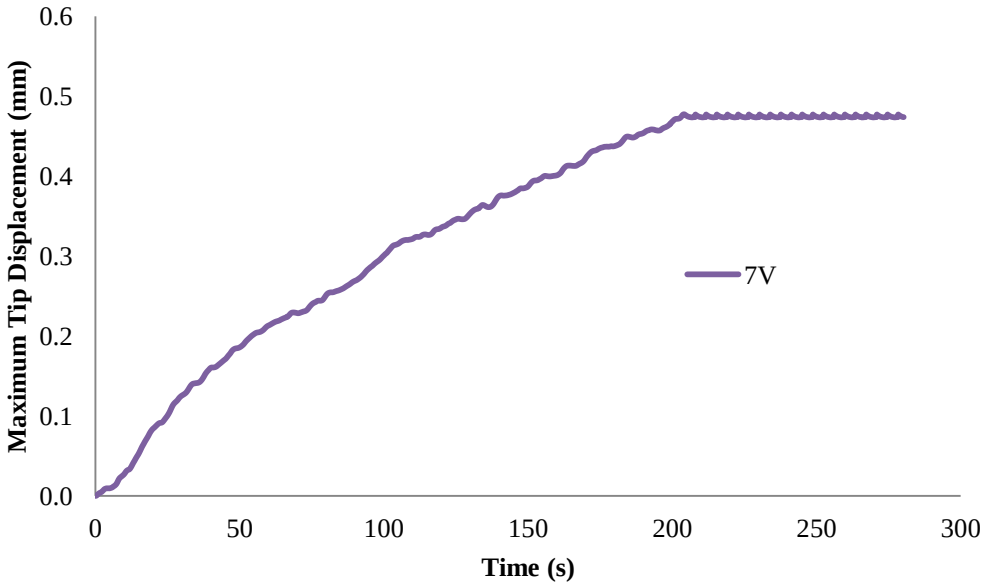

Figure 3.32 The time responses of the tip displacement of CMC-Br-1PEG actuators under DC excitation voltage of 7V

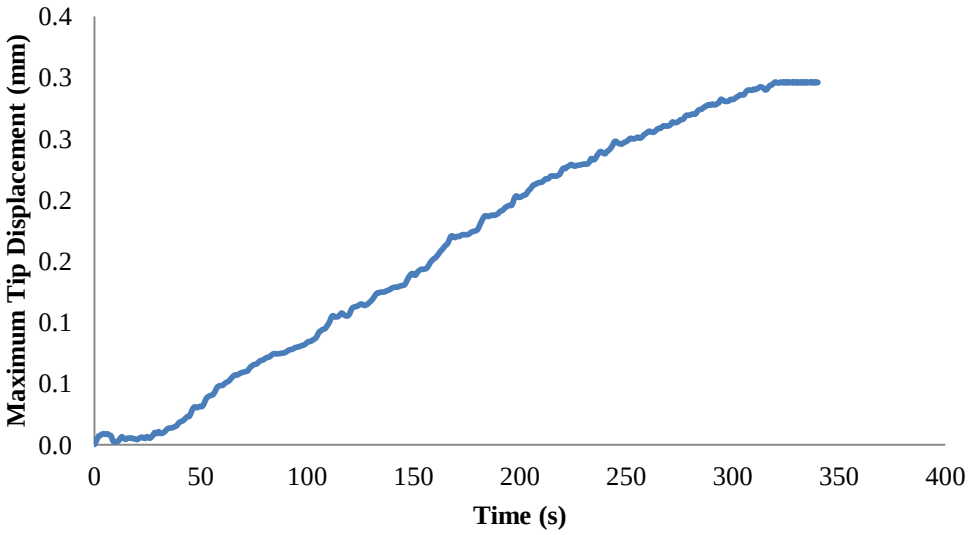

Figure 3.33 The time responses of the tip displacement of CMC-Br-1.5PEG actuators under DC excitation voltage of 1V

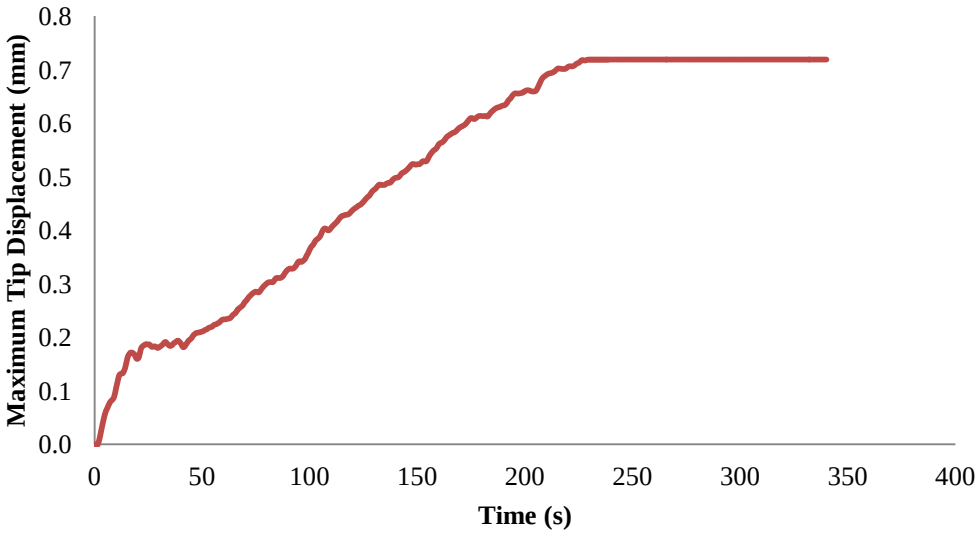

Figure 3.34 The time responses of the tip displacement of CMC-Br-1.5PEG actuators under DC excitation voltage of 3V

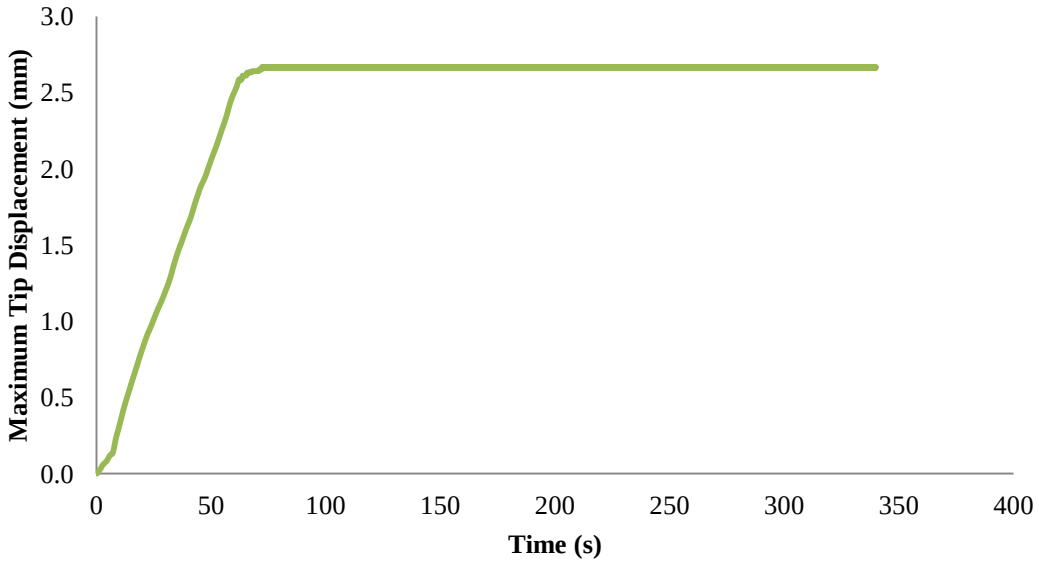

Figure 3.35 The time responses of the tip displacement of CMC-Br-1.5PEG actuators under DC excitation voltage of 5V

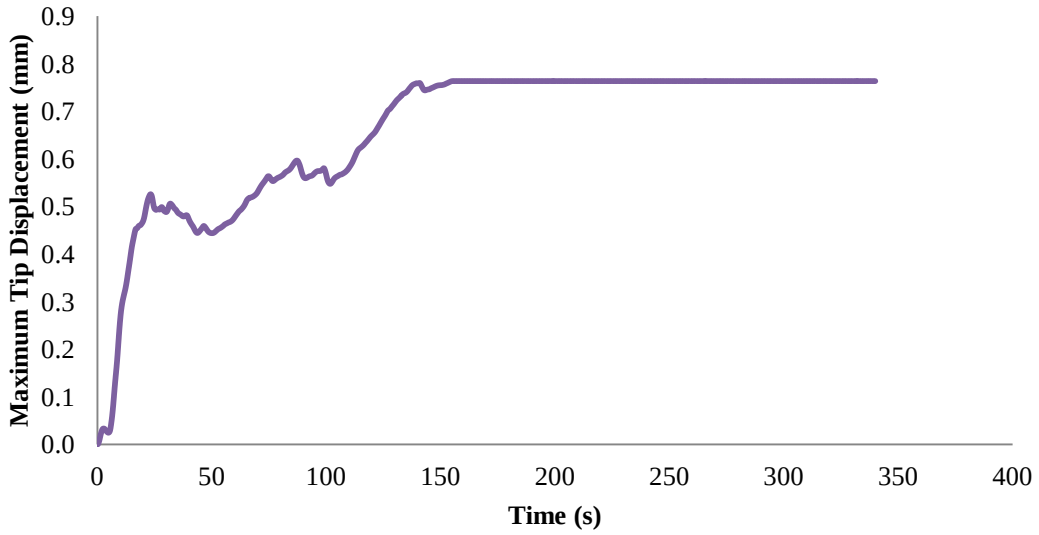

Figure 3.36 The time responses of the tip displacement of CMC-Br-1.5PEG actuators under DC excitation voltage of 7V

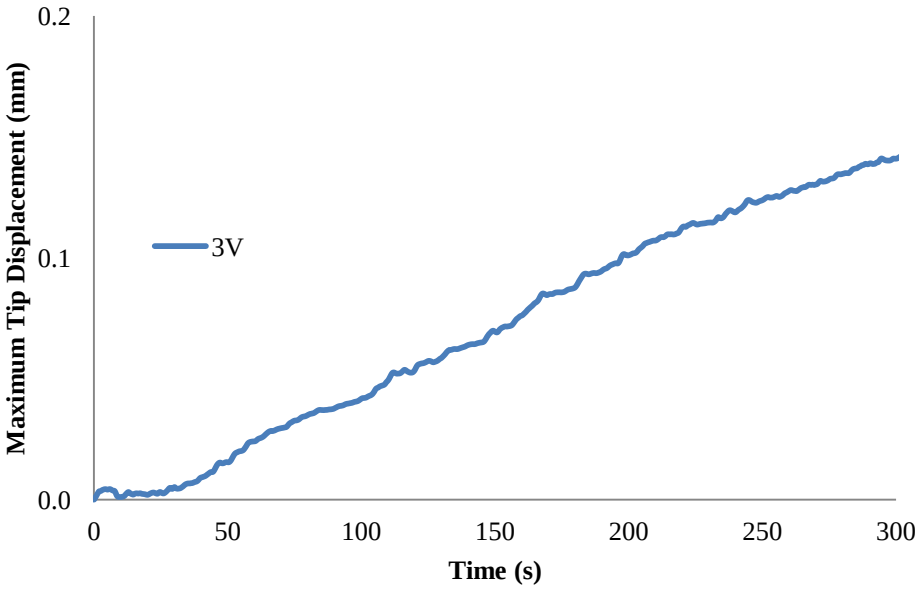

Figure 3.37 The time responses of the tip displacement of CMC-Br-2PEG actuators under DC excitation voltage of 3V

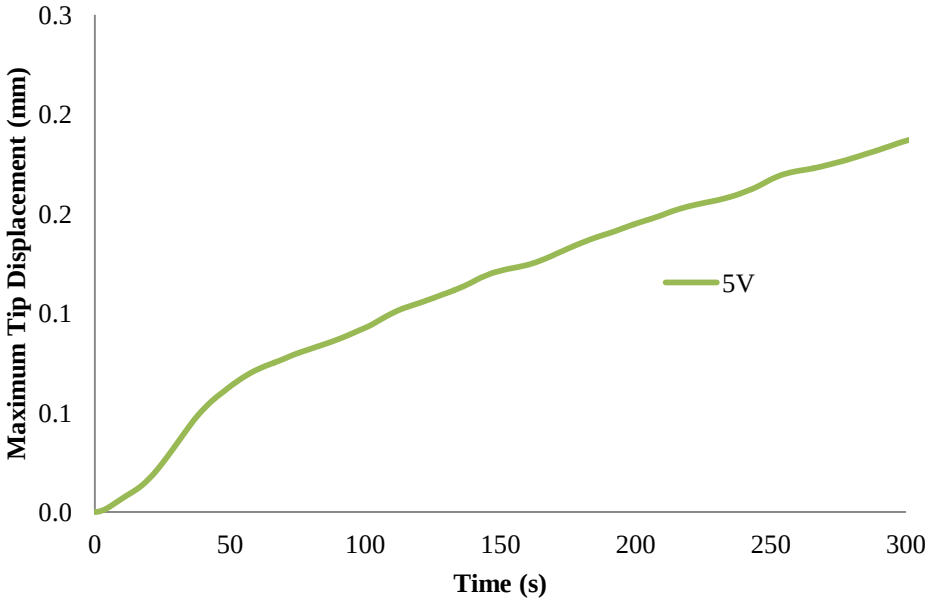

Figure 3.38 The time responses of the tip displacement of CMC-Br-2PEG actuators under DC excitation voltage of 5V

Maximum tip displacement or steady state values of these actuators are shown in Figure 3.39-3.42.

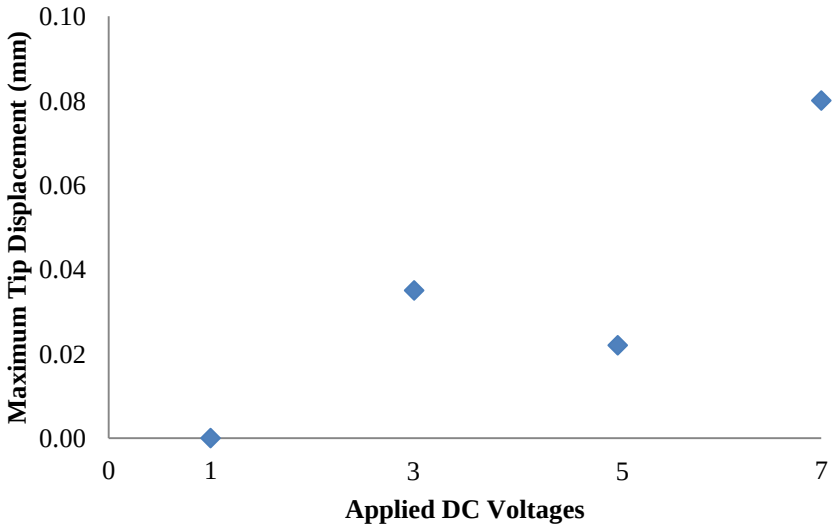

Figure 3.39 Maximum tip displacement of CMC-Br actuators

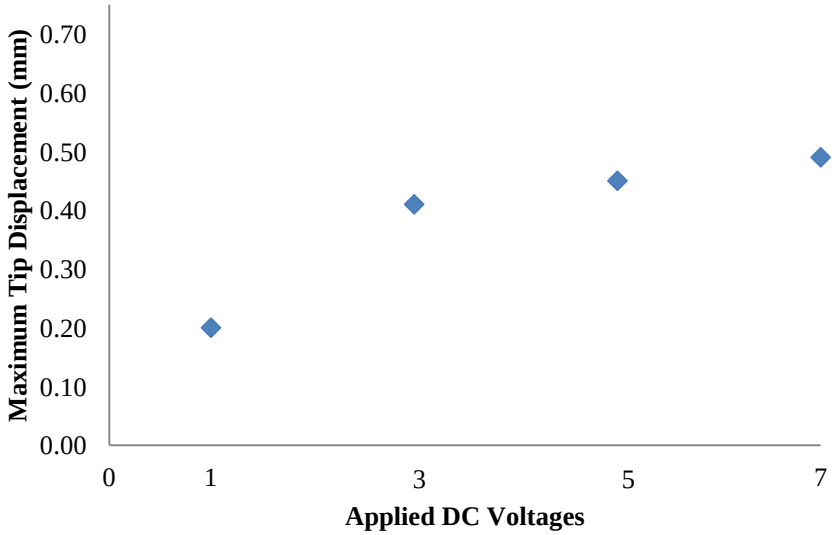

Figure 3.40 Maximum tip displacement of CMC-Br-1PEG actuators

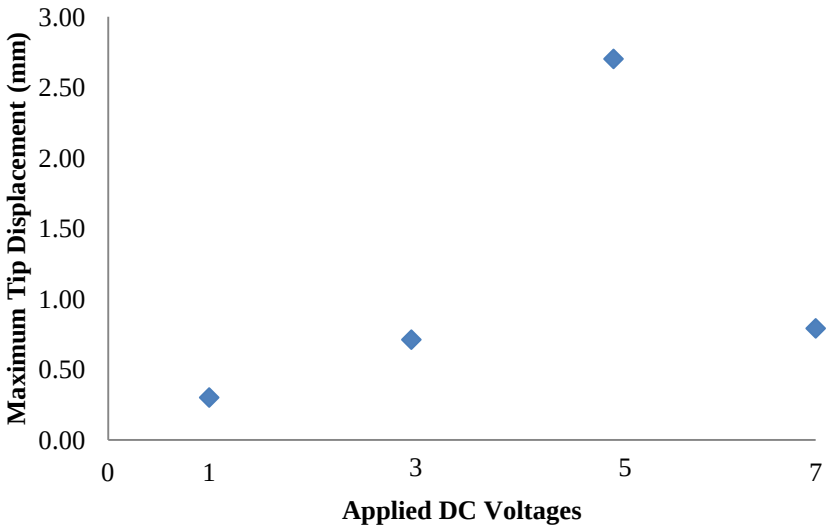

Figure 3.41 Maximum tip displacement of CMC-Br-1.5PEG actuators

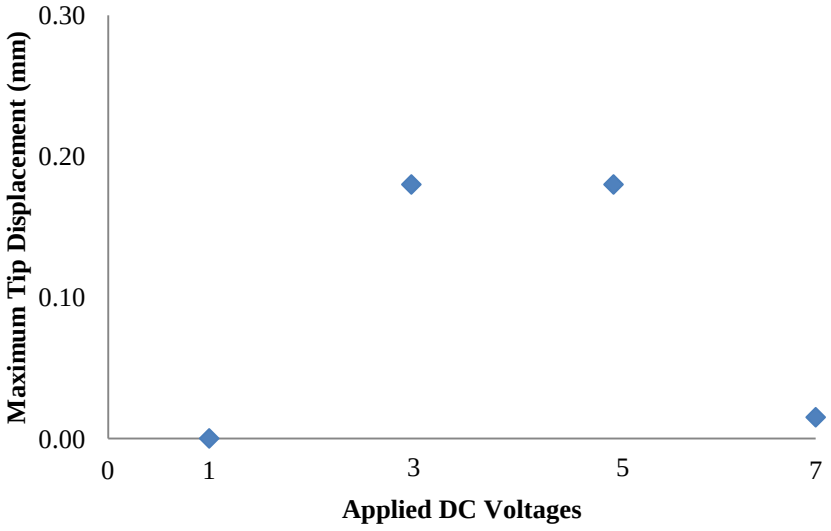

Figure 3.42 Maximum Tip displacement of CMC-Br-2PEG actuators

For better understanding, the maximum tip displacements of the CMC-Br, CMC-Br-1PEG, CMC-Br-1.5PEG and CMC-Br-2PEG are summarized in Table 3.3 (Ozdemir et al., 2015a).

Table 3.3 Maximum tip displacement (mm) values of PEG loaded CMC-based actuators

Sample name	*1V*	*3V*	*5V*	*7V*
CMC-Br	0	0.04	0.02	0.08
CMC-Br-1PEG	0.20	0.41	0.45	0.49
CMC-Br-1.5PEG	0.30	0.71	2.70	0.79
CMC-Br-2PEG	0	0.18	0.18	0.02

For the CMC-Br (without PEG) and CMC-Br-2PEG actuators, maximum tip displacement values are small and these actuators did not move for the excitation voltage of 1V as shown in Figure 3.39 and Figure 3.42, respectively. Besides, the increase in the excitation voltage does not have a consistent effect on maximum tip displacements for all voltages. For the CMC-Br-1PEG and CMC-Br-1.5PEG actuators, maximum tip displacements change with all excitation voltages (Figure 3.40 and 3.41). It can be seen that PEG amount especially in the smaller amounts improved the actuation behavior. But, this positive effect disappeared when 2 g PEG are added to CMC-Br actuators. For this reason, optimal PEG amount has to be determined (Ozdemir et al., 2015a).

Maximum tip displacement of CMC-Br-1PEG actuators increases with increasing the excitation voltage (Figure 3.40). For the CMC-Br-1.5PEG actuators, the increase in excitation voltage lasts from 1 to 5V. After 5V, maximum tip displacement value decreased.

It can be seen from Figure 3.41 and Table 3.3, CMC-Br-1.5PEG actuators exhibits largest maximum tip displacement compared to those of other actuators for all excitation voltage. Maximum tip displacement of CMC-Br-1.5PEG actuators was obtained to be 0.30, 0.71, 2.70 and 0.79 mm for the excitation voltages of 1, 3, 5 and

7V, respectively. According to obtained results, the operating voltage of the PEG loaded CMC-based actuators can be defined as 5V. Because, the maximum tip displacement was obtained in this excitation voltage (Ozdemir et al., 2015a).

3.6.2 CMC-based Actuators with Different Gr Loadings

Electromechanical performances of CMC-Br-0.1Gr, CMC-Br-0.2Gr and CMC-Br-0.3Gr actuators were carried out under DC excitation voltages of 1, 3, 5 and 7V. Tip displacement measurements were performed with laser displacement sensor at a distance of 110 mm from fixed end of cantilever configuration.

For the Gr loaded CMC-based actuators, similar time responses curves with PEG loaded CMC-based actuators were obtained. Time responses curves are in exponential form and have no back relaxation (Figure 3.43-3.54). Hence, final tip displacement values of these actuators were used as maximum tip displacement.

According Figure 3.43-3.45, the experiments were performed 20, 90 and 19 s for the actuator samples of CMC-Br-0.1Gr, CMC-Br-0.2Gr and CMC-Br-0.3Gr, respectively.

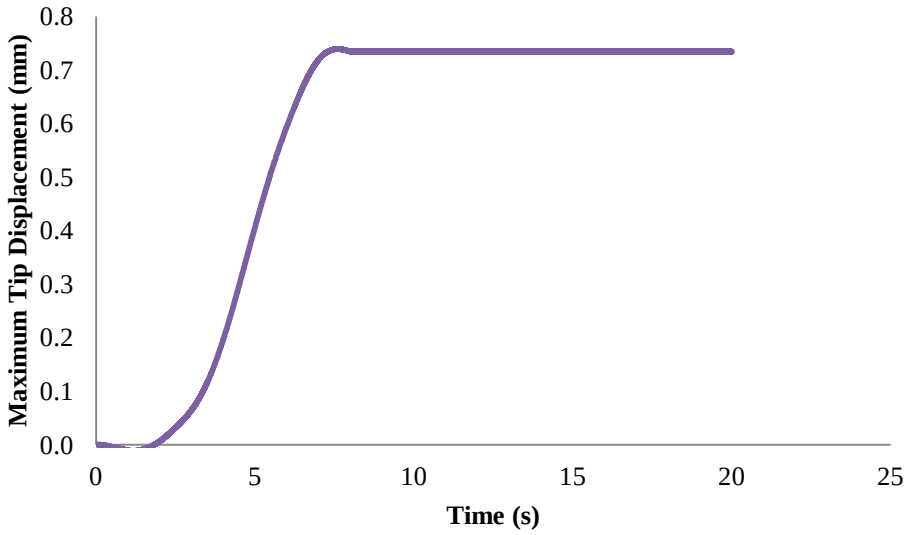

Figure 3.43 The time responses of the tip displacement of CMC-Br-0.1Gr actuators under DC excitation voltage of 1V

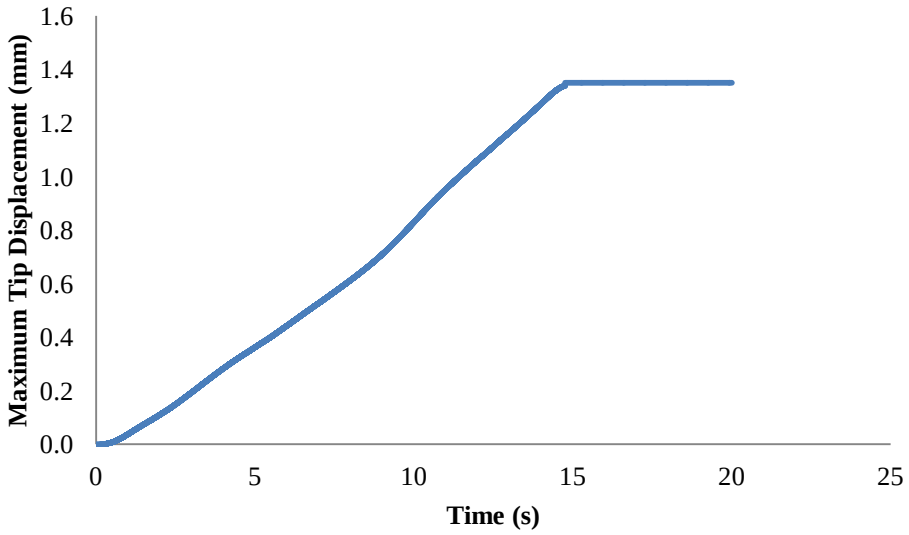

Figure 3.44 The time responses of the tip displacement of CMC-Br-0.1Gr actuators under DC excitation voltage of 3V

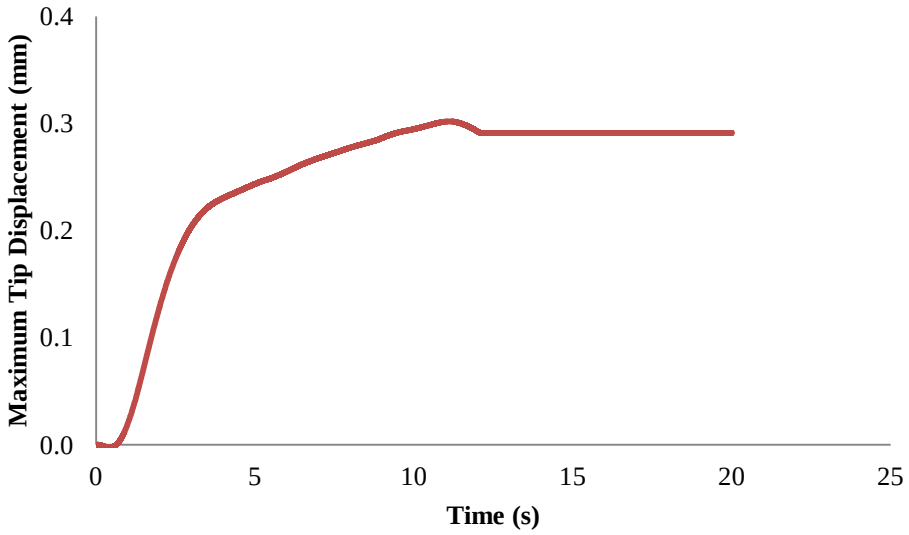

Figure 3.45 The time responses of the tip displacement of CMC-Br-0.1Gr actuators under DC excitation voltage of 5V

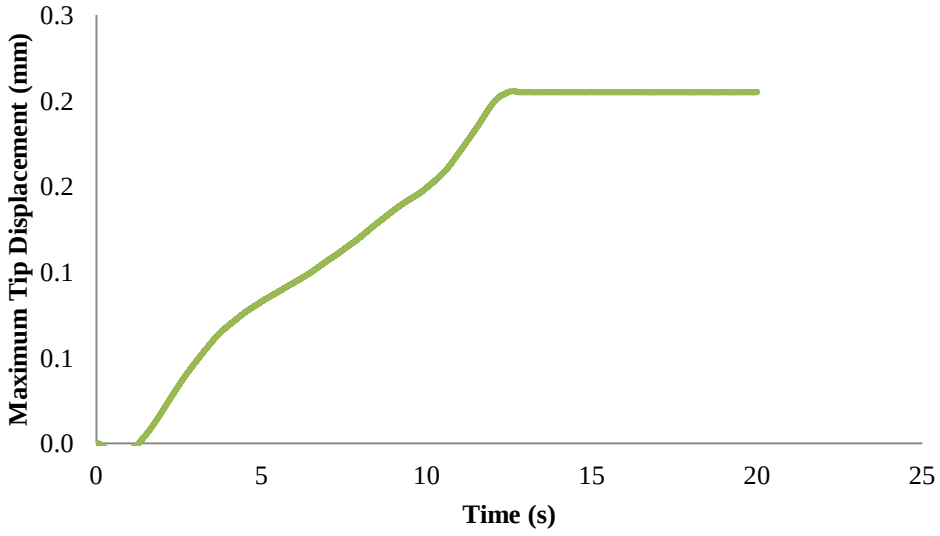

Figure 3.46 The time responses of the tip displacement of CMC-Br-0.1Gr actuators under DC excitation voltage of 7V

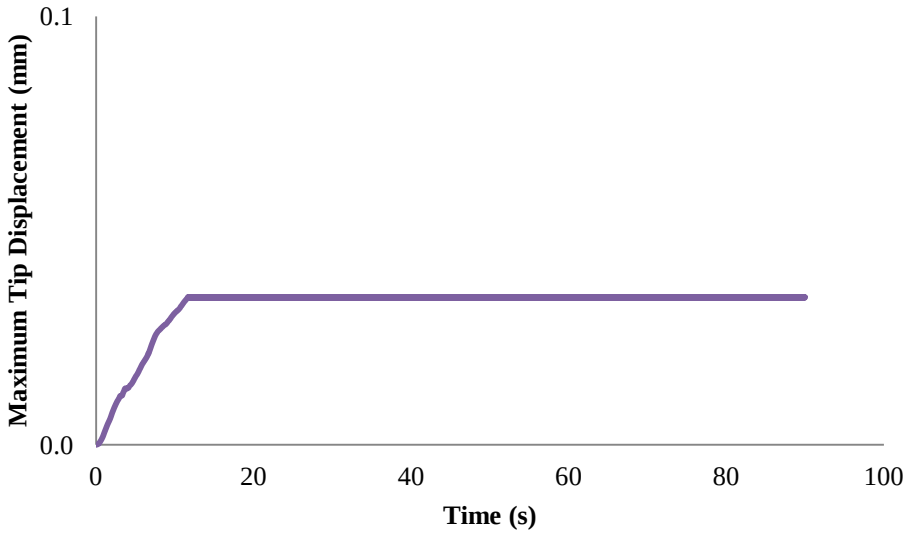

Figure 3.47 The time responses of the tip displacement of CMC-Br-0.2Gr actuators under DC excitation voltage of 1V

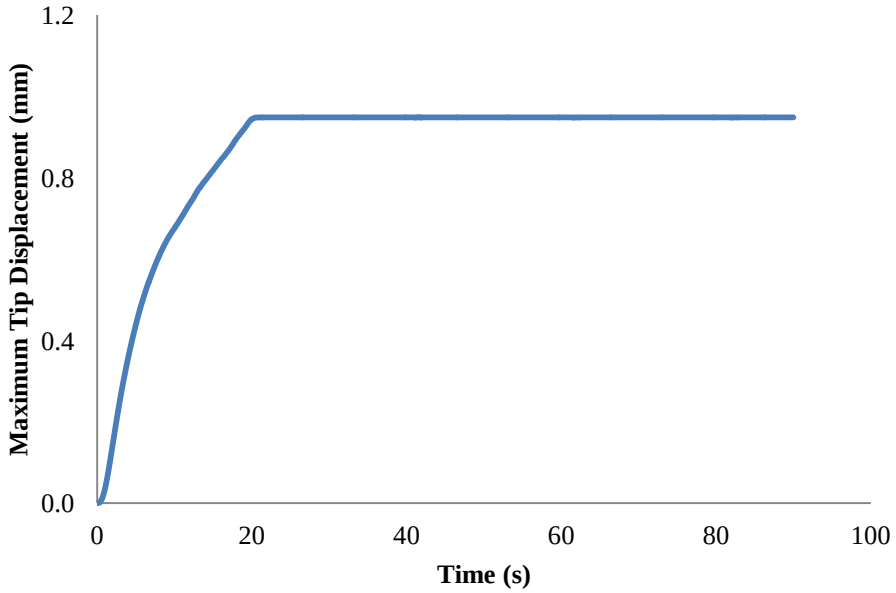

Figure 3.48 The time responses of the tip displacement of CMC-Br-0.2Gr actuators under DC excitation voltage of 3V

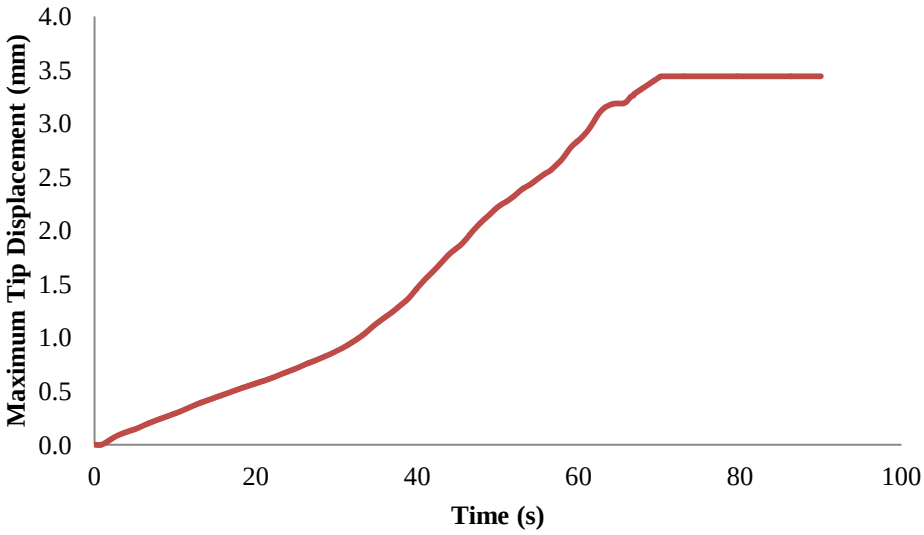

Figure 3.49 The time responses of the tip displacement of CMC-Br-0.2Gr actuators under DC excitation voltage of 5V

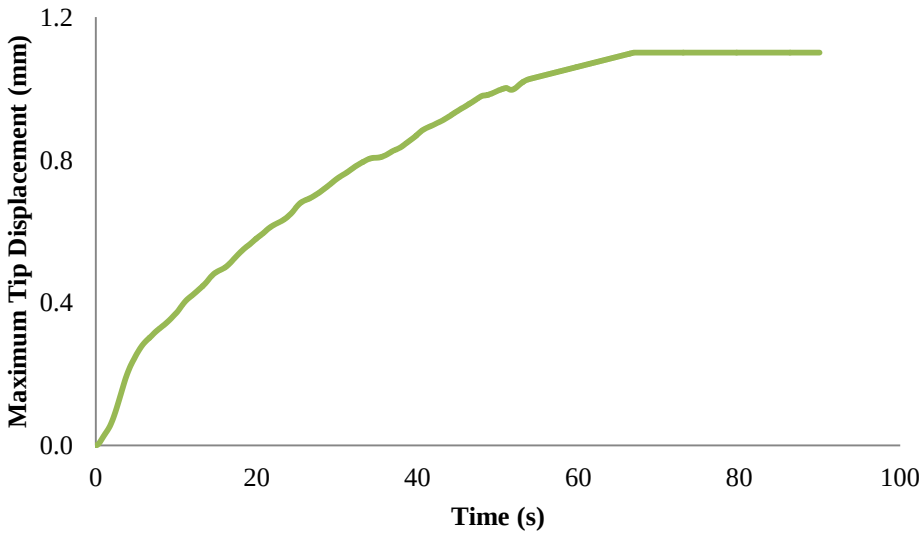

Figure 3.50 The time responses of the tip displacement of CMC-Br-0.2Gr actuators under DC excitation voltage of 7V

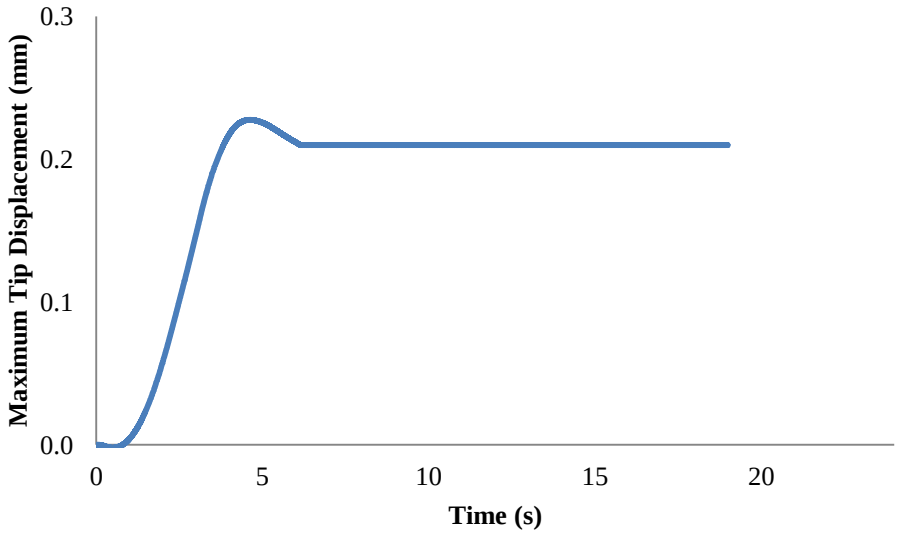

Figure 3.51 The time responses of the tip displacement of CMC-Br-0.3Gr actuators under DC excitation voltage of 1V

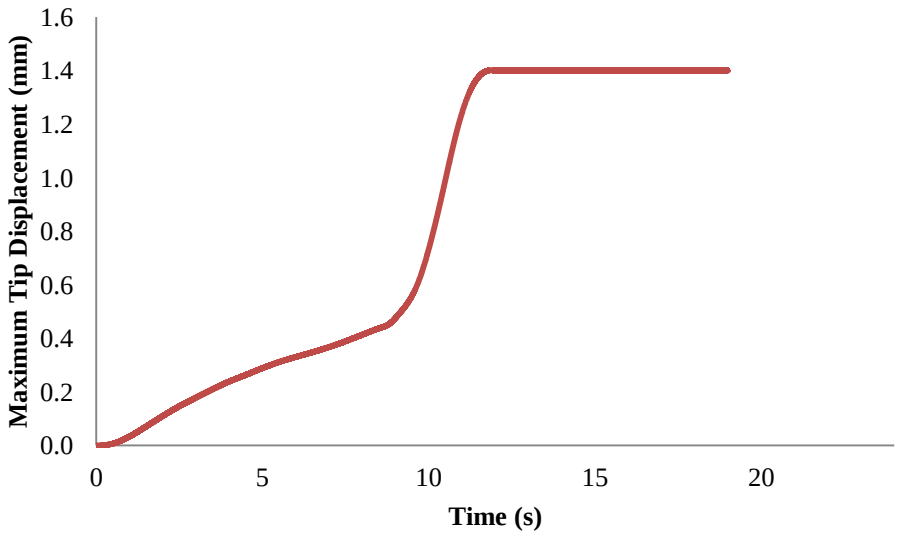

Figure 3.52 The time responses of the tip displacement of CMC-Br-0.3Gr actuators under DC excitation voltage of 3V

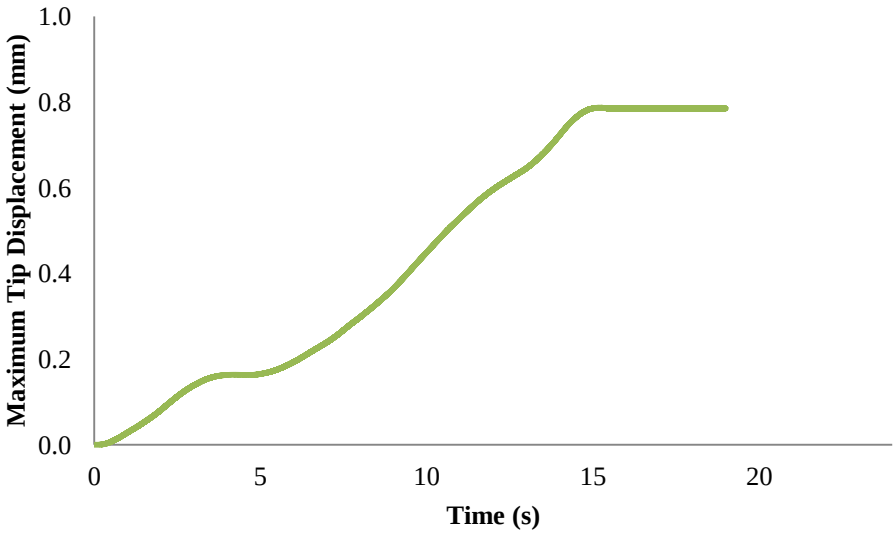

Figure 3.53 The time responses of the tip displacement of CMC-Br-0.3Gr actuators under DC excitation voltage of 5V

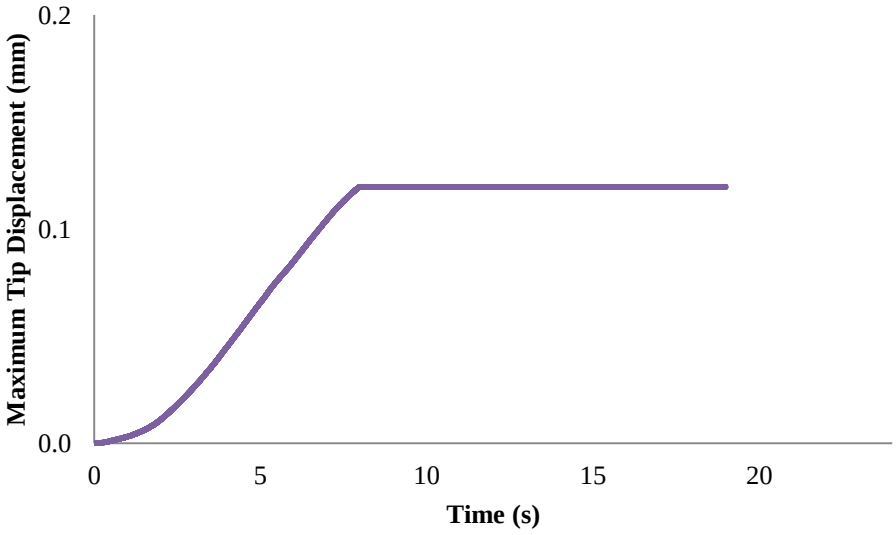

Figure 3.54 The time responses of the tip displacement of CMC-Br-0.3Gr actuators under DC excitation voltage of 7V

Maximum tip displacement or steady state values of these actuators are shown in Figure 3.55-3.57.

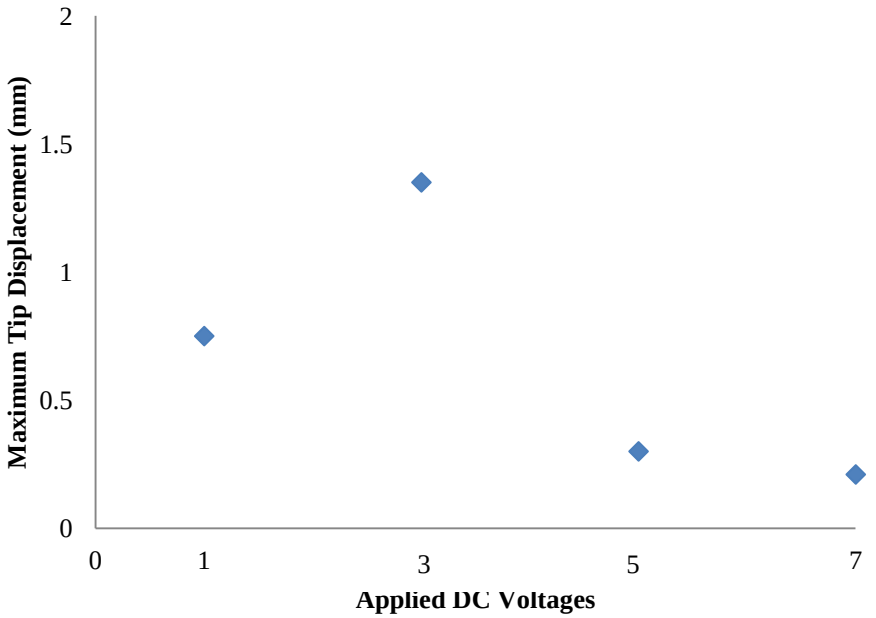

Figure 3.55 Maximum tip displacement of CMC-Br-0.1Gr actuators

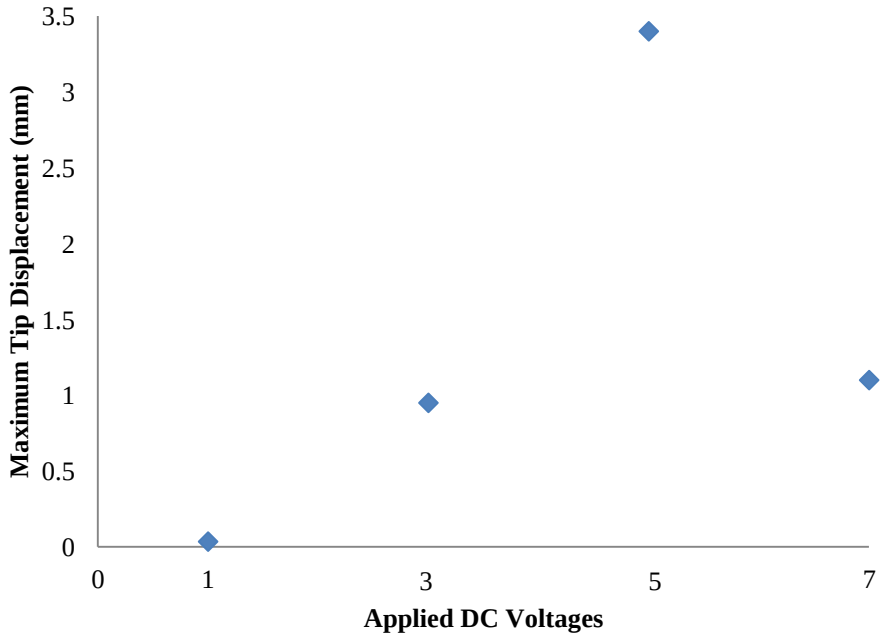

Figure 3.56 Maximum tip displacement of CMC-Br-0.2Gr actuators

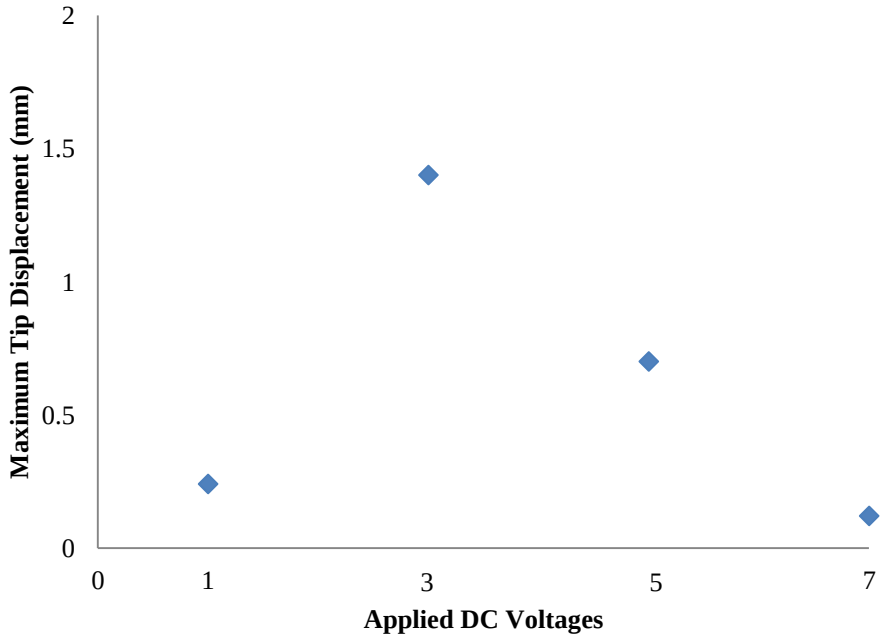

Figure 3.57 Maximum tip displacement of CMC-Br-0.3Gr actuators

For better understanding, the maximum tip displacements of the CMC-Br-0.1Gr, CMC-Br-0.2Gr and CMC-Br-0.3Gr actuators are given in Table 3.4 (Ozdemir et al., 2015b).

Table 3.4 Maximum tip displacement (mm) values of Gr loaded CMC-based actuators

Sample name	*1V*	*3V*	*5V*	*7V*
CMC-Br-0.1Gr	0.75	1.35	0.30	0.21
CMC-Br-0.2Gr	0.04	0.95	3.40	1.10
CMC-Br-0.3Gr	0.24	1.40	0.80	0.12

According to Table 3.4, it can be observed that all Gr loaded CMC-based samples move with the all excitation voltages. Besides, Gr loading has increased the maximum tip displacement of actuators compared to CMC-Br actuators. For the

CMC-Br-1.5PEG (Figure 3.41) and CMC-Br-0.2Gr (Figure 3.34) actuators, the maximum tip displacements have similar characteristics. In other words, maximum tip displacement of these actuators increased when the excitation voltage increased from 1 to 5V, however, decreased when excitation voltage increased from 5 to 7V. Moreover, significant tip motions were obtained for these two actuators under DC excitation voltage of 7V (Ozdemir et al., 2015b).

The maximum tip displacement of CMC-Br-0.2Gr actuators obtained to be 3.40 mm at excitation voltage of 5V. When the actuators were excited with 3V, it is observed that maximum tip displacement of CMC-Br-0.1Gr and CMC-Br-0.3Gr obtained to be 1.35 and 1.40 mm, respectively. From these results, it can be said that Gr loading into CMC-based actuators improved the actuator performance (Ozdemir et al., 2015b).

3.7 Blocking Force Analysis

Huynh, Alici & Spinks (2006), described a method in order to determine the blocking force values of actuators. In this study, blocking force analyses of CMC-based actuators with different PEG loadings and CMC-based actuators with different Gr loadings were conducted using their method. In other words, when DC excitation voltages are applied to the electrodes of IPMC actuators, bending moment occurs. If the tip of the actuators in zero position is contacted on load cell (precision balance), force of the actuators is transferred to load cell under applied voltages. During the experiments, data of the precision balance were simultaneously recorded. Therefore, force output of the actuators under DC excitation voltages was obtained. Blocking force results of the CMC-based actuators were given in next subchapters.

3.7.1 CMC-based Actuators with Different PEG Loadings

Blocking force values of CMC-Br-1PEG, CMC-Br-1.5PEG and CMC-Br-2PEG actuators were measured under DC excitation voltages of 1, 3, 5 and 7V and were given in Table 3.5. It is also noted that CMC-Br (without PEG) and CMC-Br-2PEG

actuators under DC excitation voltages of 1V did not generate any significant force since these actuators did not move under DC excitation voltage.

Table 3.5 Blocking force values (gf) of PEG loaded CMC-based actuators

Sample name	*1V*	*3V*	*5V*	*7V*
CMC-Br	0	0.06	0.02	0.13
CMC-Br-1PEG	0.42	0.79	0.85	0.86
CMC-Br-1.5PEG	0.48	1.12	2.83	1.21
CMC-Br-2PEG	0	0.20	0.20	0.02

When the blocking force values of PEG loaded CMC-based actuators are analyzed, it is observed that blocking force values of CMC-Br-1PEG actuators increase with increasing the excitation voltages. On the other hand, the increase in excitation voltages lasts from 1 to 5V for the CMC-Br-1.5PEG actuators. The maximum blocking force value was obtained to be 2.83 gf for the CMC-Br-1.5PEG actuators under DC excitation voltage of 5V. These results are compatible with the maximum tip displacement of CMC-based actuators with different PEG loadings.

3.7.2 CMC-based Actuators with Different Gr Loadings

Blocking force values of CMC-based actuators with different Gr loadings (0.1, 0.2 and 0.3 wt.%) were measured under DC excitation voltages of 1, 3, 5 and 7V. The results were given in Table 3.6. It is seen from the Table 3.6 that all actuators generate significant blocking force when the DC excitation voltages of 1, 3, 5 and 7V are applied.

Table 3.6 Blocking force values (gf) of Gr loaded CMC-based actuators

Sample name	*1V*	*3V*	*5V*	*7V*
CMC-Br-0.1Gr	1.48	2.51	0.78	0.48
CMC-Br-0.2Gr	0.07	1.62	3.84	1.84
CMC-Br-0.3Gr	0.51	2.59	1.24	0.19

When the blocking force values of Gr loaded CMC-based actuators are analyzed, it is seen that blocking force values of CMC-Br-0.2Gr actuators increase with increasing the DC excitation voltages until 5V, then, decreased under DC excitation voltage of 7V. The maximum blocking force value obtained to be 3.84 gf at excitation voltage 5V for the CMC-Br-0.2Gr actuators. Besides, it is observed that Gr loading has increased the blocking force values compared to CMC-Br actuators.

3.8 Finite Element Analysis (FEA)

In this section, finite element analyses were performed via Ansys 14.5 packet program in order to determine the blocking force values and maximum tip displacement of IPMC actuators. Obtained results from finite element analyses were compared to experimental results.

3.8.1 Blocking Force Values of CMC-based Actuators with Different PEG Loadings

Experimental blocking force values of CMC-based actuators with different PEG loadings were introduced in Section 3.7.1. In this subchapter, blocking force values were obtained via finite element analyses. Blocking force values of IPMC via FEA were determined by Lughmani, Jho, Lee & Rhee (2009). Similar analyses were conducted with their study.

In order to determine the blocking force or actuation force (reaction force) at the tip of the CMC-based actuators, the contact element was used. All CMC-based actuators with different PEG loadings were modeled 5x50x1 mm as shown in Figure 3.58.

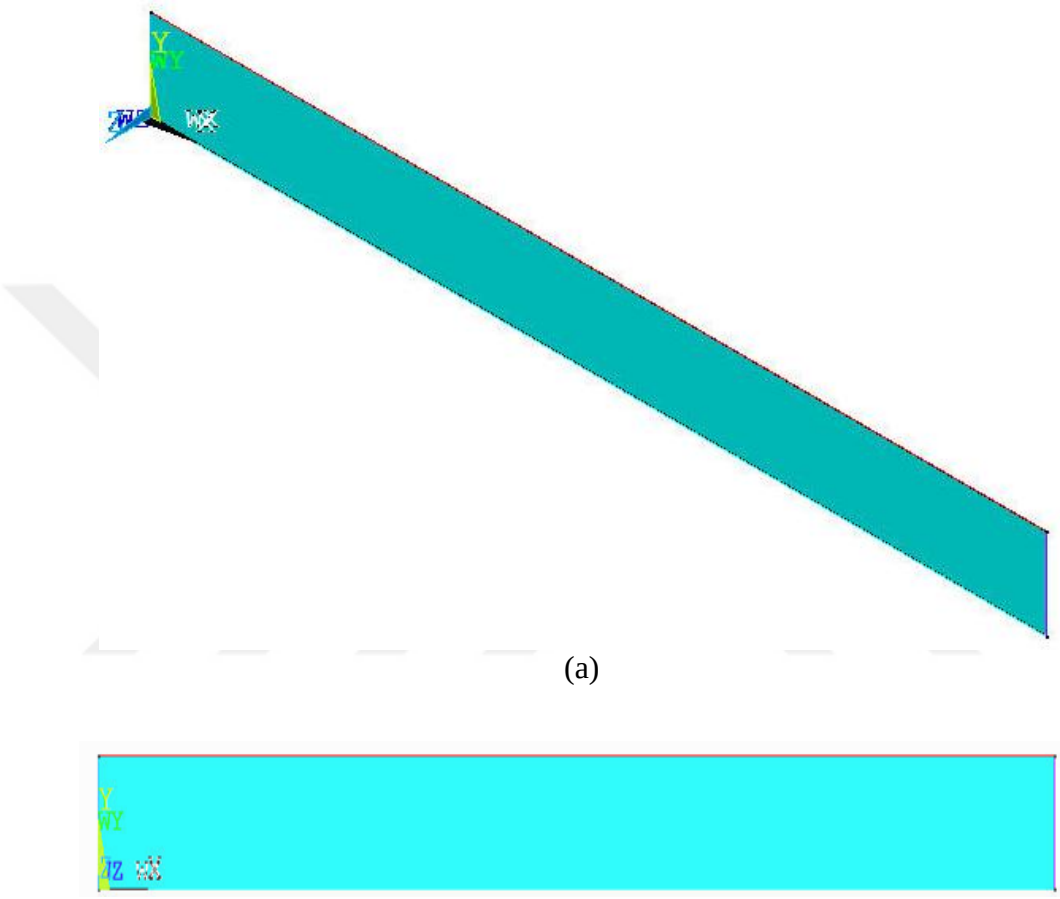

(a)

(b)

Figure 3.58 Simulated IPMC model (a) iso view and (b) top view

After, the constraints at the clamped edges of the CMC-based actuators were applied as fixed support to the clamped edges. The maximum tip displacement values obtained from the laser displacement sensor (Table 3.3) were applied in the z-direction. An example of visual simulation of blocking force in z-direction of CMC-Br-1.5PEG actuators under DC excitation voltage of 5V was given in Figure 3.59. From this figure, the reaction force in the z-direction was obtained to be approximately 0.029 N (2.99 gf) at clamped edges.

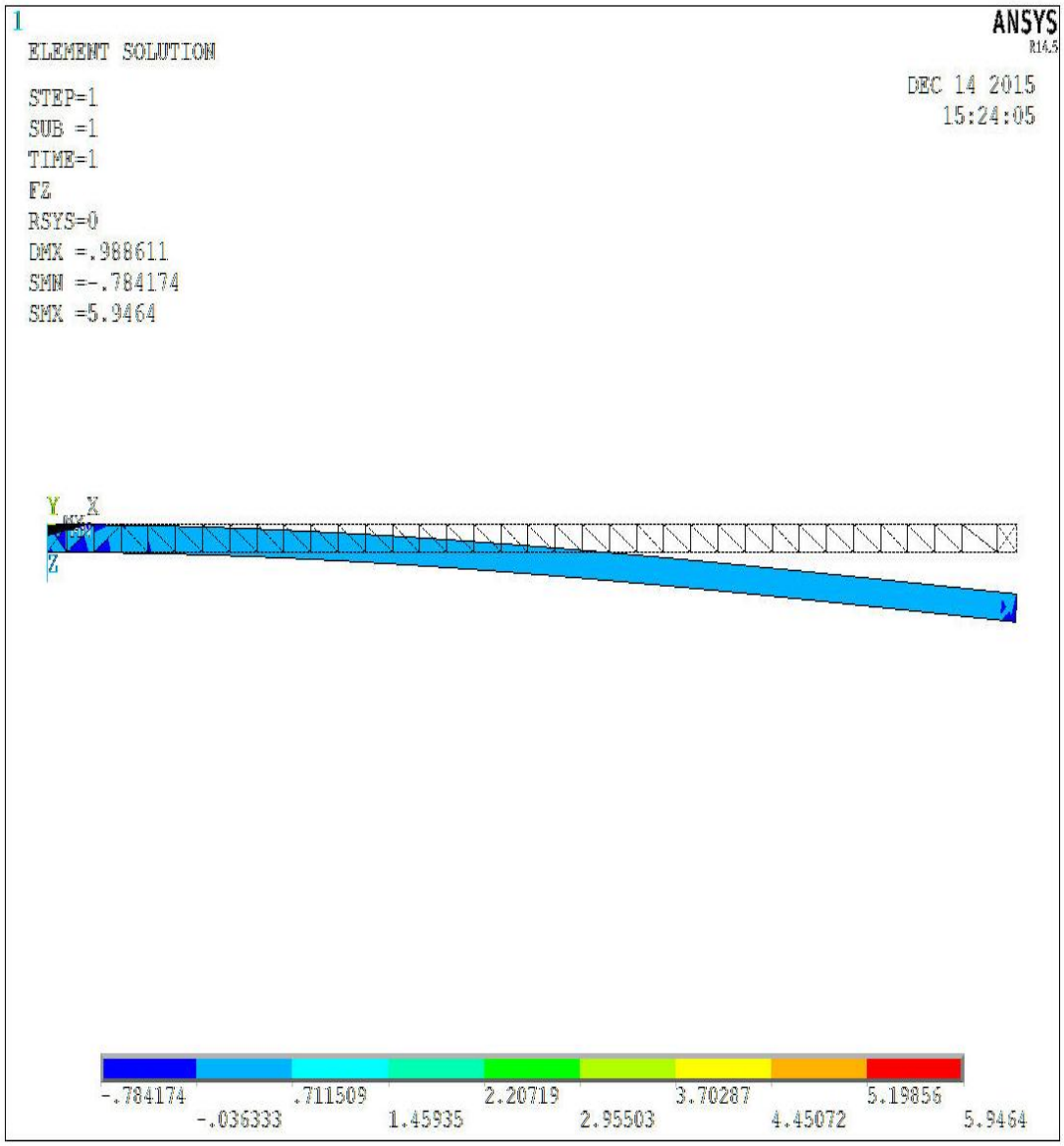

Figure 3.59 Simulated blocking force of CMC-Br-1.5PEG actuator under DC excitation voltage of 5V

The reaction force values in other words simulated and experimental blocking force values of other CMC-based actuators with different PEG loadings were summarized in Table 3.7.

Table 3.7 Simulated and experimental blocking force values (gf) of PEG loaded CMC-based actuators

Sample name		*1V*	*3V*	*5V*	*7V*
CMC-Br	*Simulated*	0	0.09	0.05	0.24
	Experimental	0	0.06	0.02	0.13
CMC-Br-1PEG	*Simulated*	0.46	0.91	0.99	1.02
	Experimental	0.42	0.79	0.85	0.86
CMC-Br-1.5PEG	*Simulated*	0.56	1.24	2.99	1.37
	Experimental	0.48	1.12	2.83	1.21
CMC-Br-2PEG	*Simulated*	0	0.31	0.31	0.05
	Experimental	0	0.20	0.20	0.02

When the blocking force values of CMC-based actuators with different PEG loadings obtained from both experimental (Table 3.5) and finite element analysis are compared together (Table 3.7), it is clearly seen that simulated blocking force values agree well with experimental results. It can be also said that simulated blocking force values of CMC-Br-1PEG actuators increase with increasing the DC excitation voltages. For the CMC-Br-1.5PEG actuators, simulated blocking force values increase with increasing the DC excitation voltages until 5V.

3.8.2 Blocking Force Values of CMC-based Actuators with Different Gr Loadings

Similar method and analysis in Section 3.8.1 was conducted in order to determine the blocking force values of CMC-based actuators with different Gr loadings. Experimental blocking force values of CMC-based actuators with different Gr loadings were introduced in Section 3.7.2. In this subchapter, simulated blocking force values of CMC-Br-0.1Gr, CMC-Br-0.2Gr and CMC-Br-0.3Gr actuators were determined. An example of visual simulation of blocking force in z-direction of

CMC-Br-0.2Gr actuators under DC excitation voltage of 5V was given in Figure 3.60. From this figure, the reaction force in the z-direction was obtained to be approximately 0.041 N (4.14 gf) at clamped edges.

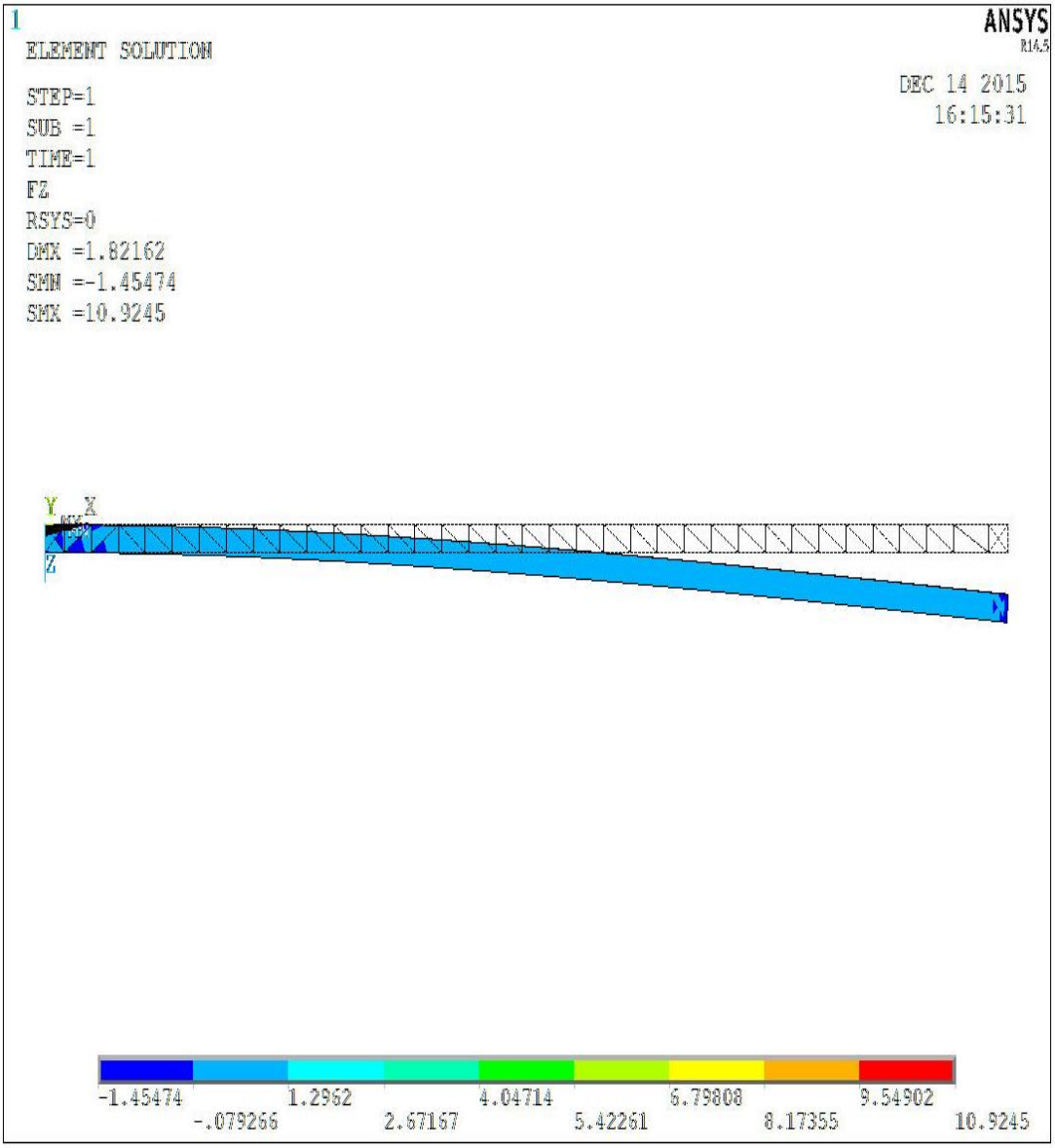

Figure 3.60 Simulated blocking force of CMC-Br-0.2Gr actuator under DC excitation voltage of 5V

The reaction force values in other words simulated and experimental blocking force values of other CMC-based actuators with different Gr loadings were summarized in Table 3.8.

Table 3.8 Simulated and experimental blocking force values (gf) of Gr loaded CMC-based actuators

Sample name		*1V*	*3V*	*5V*	*7V*
CMC-Br-0.1Gr	*Simulated*	1.52	2.71	0.90	0.51
	Experimental	1.48	2.51	0.78	0.48
CMC-Br-0.2Gr	*Simulated*	0.12	1.71	4.14	1.99
	Experimental	0.07	1.62	3.84	1.84
CMC-Br-0.3Gr	*Simulated*	0.62	2.73	1.43	0.29
	Experimental	0.51	2.59	1.24	0.19

When the blocking force values of CMC-based actuators with different Gr loadings obtained from both experimental (Table 3.6) and finite element analysis are compared together (Table 3.8), good agreement was observed between simulated blocking force values and experimental results. Besides, the maximum simulated blocking force value was obtained to be approximately (0.0406) 4.14 gf in CMC-Br-0.2Gr actuators under DC excitation voltage of 5V.

3.8.3 Maximum Tip Displacement of CMC-based Actuators with Different PEG Loadings

Experimental maximum tip displacements of CMC-based actuators with different PEG loadings were determined in Section 3.6.1. In this subchapter, simulated maximum tip displacement values were obtained with finite element analyses. Maximum tip displacements of IPMC with finite element analyses were investigated by Nam & Kwan (2012). Similar finite element analyses were conducted with their study.

In order to determine the maximum tip displacement of the CMC-based actuators with different PEG loadings, actuators were modeled 5x50x1 mm as shown in Figure 3.58. The induced stress as the deformation mechanism is added to finite element analyses by using the "INISTATE" command. The constraints at the clamped edges were applied as fixed support to the clamped edges. The Young's moduli (Elastic modulus) of the CMC-based actuators with different PEG loadings are 0.52, 0.44, 0.32 and 0.24 GPa for CMC-Br, CMC-Br-1PEG and CMC-Br-1.5PEG, respectively (Figure 3.26). Poisson's ratio of the all actuators is 0.487 (Nam & Kwan, 2012). Diaphragm radius of the all actuators is approximately 4.75 mm.

After above mechanical properties were entered to ANSYS packet program, DC excitation voltages of 1, 3, 5 and 7V were applied. An example of visual simulation of maximum tip displacement in z-direction of CMC-Br-1.5PEG actuators under DC excitation voltage of 5V was given in Figure 3.61. It can be seen that the maximum tip displacement in the z-direction was obtained to be approximately 2.78 mm at free edges.

The simulated and experimental maximum tip displacements of other CMC-based actuators with different PEG loadings were summarized in Table 3.9.

Table 3.9 Simulated and experimental maximum tip displacement (mm) values of PEG loaded CMC-based actuators

Sample name		*1V*	*3V*	*5V*	*7V*
CMC-Br	*Simulated*	0.02	0.07	0.04	0.10
	Experimental	0	0.04	0.02	0.08
CMC-Br-1PEG	*Simulated*	0.24	0.47	0.49	0.53
	Experimental	0.20	0.41	0.45	0.49
CMC-Br-1.5PEG	*Simulated*	0.36	0.81	2.78	0.84
	Experimental	0.30	0.71	2.70	0.79
CMC-Br-2PEG	*Simulated*	0.02	0.25	0.24	0.04
	Experimental	0	0.18	0.18	0.02

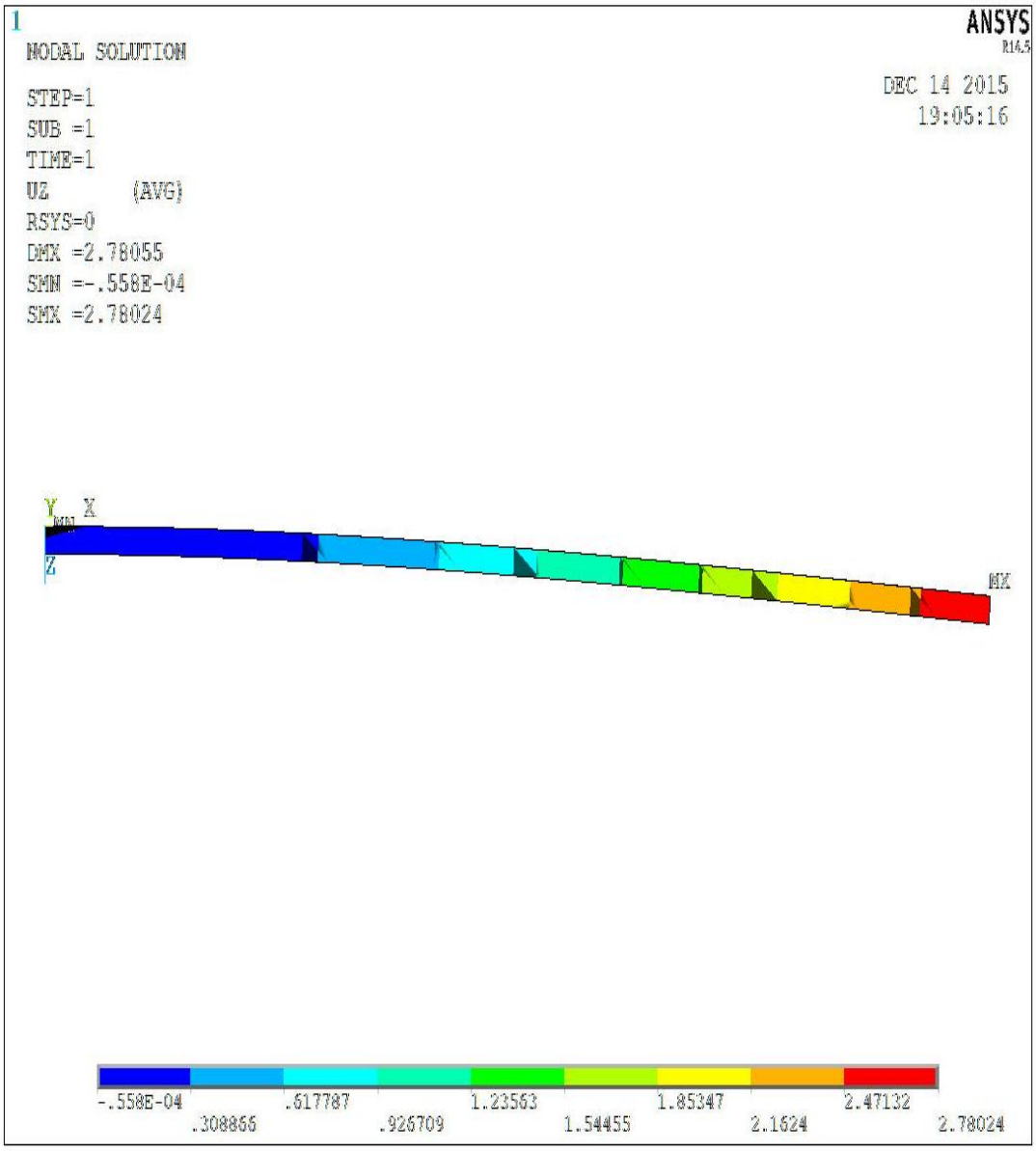

Figure 3.61 Simulated maximum tip displacement of CMC-Br-1.5PEG actuator under DC excitation voltage of 5V

When the maximum tip displacement values of CMC-based actuators with different PEG loadings obtained from both experimental (Table 3.3) and finite element analysis (Table 3.9) are compared, very close results was obtained. The simulated maximum blocking force values is 2.78 mm. It is also noted that the maximum tip displacement of CMC-Br and CMC-Br-2PEG actuators under DC excitation voltage of 1V is 0.02 mm in contrast to experimental result of those actuators.

3.8.4 Maximum Tip Displacement of CMC-based Actuators with Different Gr Loadings

Similar method and analysis in Section 3.8.3 was conducted in order to determine the maximum tip displacement values of CMC-based actuators with different Gr loadings. Experimental blocking force values of CMC-based actuators with different Gr loadings were introduced in Section 3.6.2. In this subchapter, simulated maximum tip displacement of CMC-Br-0.1Gr, CMC-Br-0.2Gr and CMC-Br-0.3Gr actuators were determined. The Young's moduli (Elastic modulus) of the CMC-based actuators with different Gr loadings are 0.39, 0.51 and 0.58 GPa for CMC-Br-0.1Gr, CMC-Br-0.2Gr and CMC-Br-0.3Gr, respectively (Figure 3.28). Poisson's ratio of the all actuators is 0.487 (Nam & Kwan, 2012). Diaphragm radius of the all actuators is approximately 4.75 mm. An example of visual simulation of maximum tip displacement in z-direction of CMC-Br-0.2Gr actuators under DC excitation voltage of 5V was given in Figure 3.62. From this figure, the maximum tip displacement in the z-direction was obtained to be approximately 3.51 mm at free edges.

The simulated and experimental maximum tip displacements of other CMC-based actuators with different Gr loadings were summarized in Table 3.10.

Table 3.10 Simulated and experimental maximum tip displacement (mm) values of Gr loaded CMC-based actuators

Sample name		*1V*	*3V*	*5V*	*7V*
CMC-Br-0.1Gr	*Simulated*	0.81	1.42	0.34	0.29
	Experimental	0.75	1.35	0.30	0.21
CMC-Br-0.2Gr	*Simulated*	0.07	1.02	3.51	1.18
	Experimental	0.04	0.95	3.40	1.10
CMC-Br-0.3Gr	*Simulated*	0.31	1.47	0.86	0.19
	Experimental	0.24	1.40	0.80	0.12

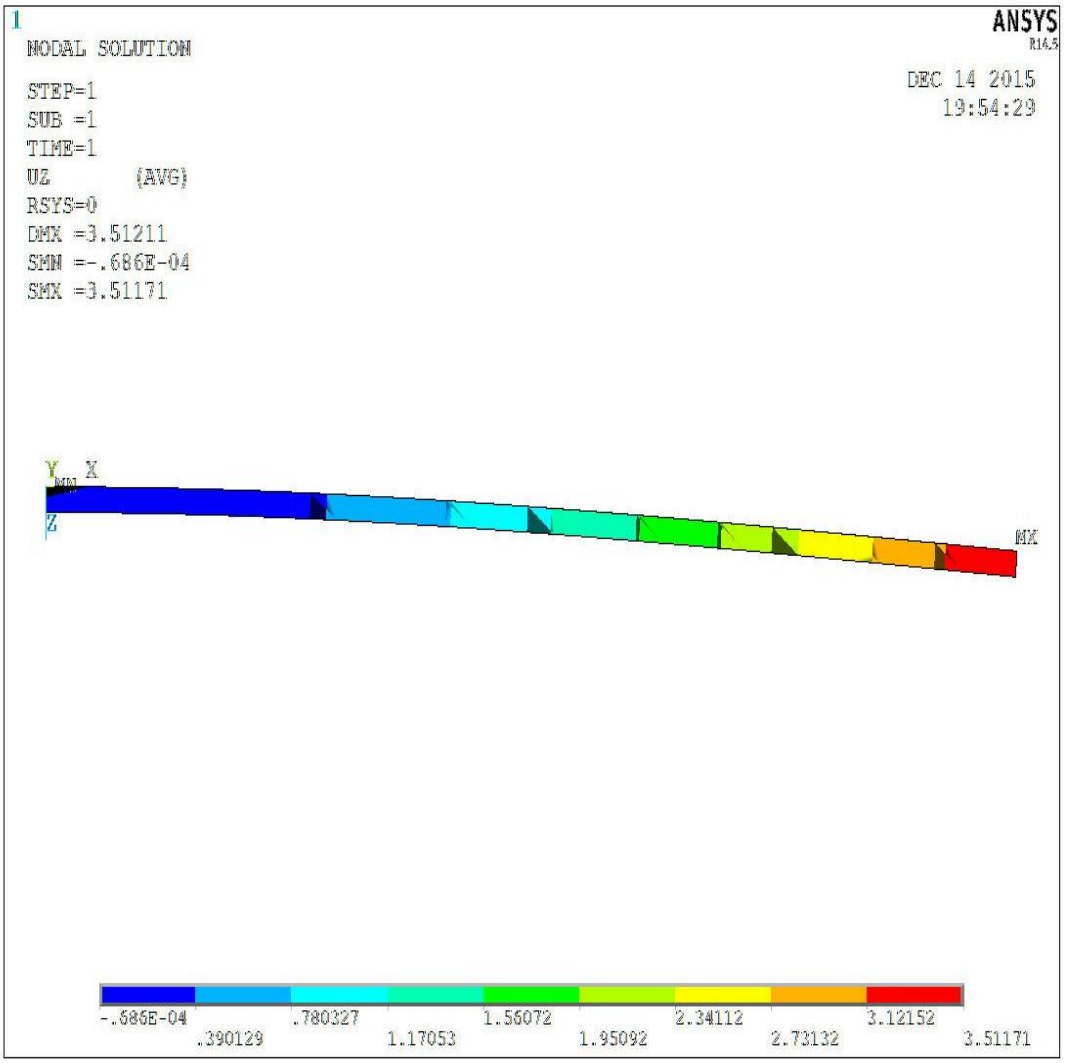

Figure 3.62 Simulated maximum tip displacement of CMC-Br-0.2Gr actuator under DC excitation voltage of 5V

When the maximum tip displacement values of CMC-based actuators with different Gr loadings obtained from both experimental (Table 3.4) and finite element analysis (Table 3.10) are compared, good agreement was obtained. The simulated maximum blocking force values is 3.51 mm. Besides, Gr loading into CMC-based actuators has increased the simulated maximum tip displacement values compared to CMC-Br actuators.

CHAPTER FOUR
CONCLUSIONS

In the present study, experimental investigations were carried out to obtain the electroactive performance of carboxymethylcellulose (CMC)-based actuators. In order to fabricate the CMC-based films, 1-butyl-3-methylimidazolium bromide (BMIMBr) and polyethylene glycol (PEG) were used as ionic liquid and plasticizer, respectively. Characterization of films was performed by way of Fourier transform infrared spectroscopy (FTIR), X-ray diffraction (XRD), thermogravimetric (TG), and scanning electron microscopy (SEM) analyses. Mechanical properties of films were determined by tensile tests. Both surfaces of these films were then coated with gold-leaf to fabricate the CMC-based ionic polymer metal composite (IPMC) actuator.

In the first part of the study, CMC-based films were produced to improve the both mechanical and electromechanical performances with three different PEG loadings (1, 1.5 and 2 g). After the optimal amount of PEG in terms of the maximum tip displacement was found as 1.5 g, graphene nanoplatelets (Gr) at different ratios (0.1, 0.2 and 0.3 wt.%) were added so as to improve the electromechanical behavior. Blocking force values of these actuators were determined both experimental and finite element analyses. Besides, maximum tip displacements of these actuators were found via finite element analyses. The following conclusions can be drawn in the view of such experimental results:

- ✓ From the FTIR analyses, new chemical functional groups occurred with adding the BMIMBr, PEG and Gr into the CMC. As the PEG amount increases, the FTIR spectra of the PEG loaded CMC-based films does not change significantly. Similar observations can be also seen in Gr loaded CMC-based films. Very small shifts are observed due to weak secondary attractive forces between PEG, Gr and other components.

- ✓ Adding BMIMBr into the CMC, total mass losses (25 – 600 ˚C) increases because of the low thermal stability of BMIMBr. On the other hand, it is not

seen any considerable effect of PEG amount on the total mass loss (25 – 600 ˚C). It can be also observed that Gr loading into the CMC-Br-1.5PEG film increases the thermal decomposition residues owing to nonvolatile carbonaceous material.

- ✓ When the PEG amount increases, it is observed that relative reduction in diffraction intensity of CMC-based films obtained because of the destruction of the crystallinity of CMC structure. For the Gr-loaded CMC-based films, the main characteristic peak of Gr is not seen distinctly. It is probable that Gr was good dispersed in the CMC matrix.

- ✓ From the SEM images of films, the surface of the CMC-Br film is fairly uneven while uneven structure of the CMC-Br film decreases as the PEG amount increases from 1 g to 2 g. On the other hand, it is observed that some CMC particles were agglomerated for the Gr loaded CMC-based films due to dispersion of CMC particles.

- ✓ In order to improve the mechanical properties, PEG is used as plasticizer. Because, the brittle characteristic limits the usage of film as actuator. According to tensile test results, Young's modulus of CMC-Br film decreases significantly with increases the PEG amount. Hence, the flexibility of the films increases. On the other hand, Young's modulus CMC-Br-1.5PEG film increases with increasing the Gr amount. Besides, both tensile strength and Young's modulus of actuators are higher than those of films. It can be explained with the greater tensile strength of gold-leaf compared to CMC-based film.

- ✓ According to electroactive properties of the PEG loaded CMC-based actuators, it can be seen that PEG loading has positive and negative effect on electroactive performance of actuators. Thus, an optimal PEG loading amount has to be determined. Besides, the maximum tip displacement of the actuators varies with applied excitation voltage. The operating voltage and optimal PEG loading amount of the PEG loaded CMC-based can be defined as 5V and 1.5 g. For the

Gr loaded CMC-based actuators, the maximum tip displacement is observed as 3.40 mm under DC excitation voltage of 5 V in CMC-Br-0.2Gr actuators. When CMC-Br actuators and Gr loaded CMC-based actuators are compared, it can be concluded that Gr loadings into the CMC-Br actuators improve the actuation performance. Also, significant maximum tip displacement values for CMC-Br-1.5PEG and CMC-Br-0.2Gr actuators are obtained when actuators are excited with DC voltage of 7V.

- ✓ Blocking force values of CMC-based actuators with different PEG and Gr loadings increase with increasing the DC excitation voltage 1 to 5V for the CMC-Br-1.5PEG and CMC-Br-0.2Gr actuators. After 5V, the blocking force value decreases. The maximum blocking force values are obtained 2.83 and 3.84 gf at DC excitation voltage of 5V for CMC-Br-1.5PEG and CMC-Br-0.2Gr actuators, respectively.

- ✓ From the finite element analyses (Ansys 14.5 packet program), simulated blocking force values of CMC-based actuators with different PEG and Gr loadings are good agreement with the experimental results. The maximum difference between simulated and experimental decrease when DC excitation voltages increase.

- ✓ When the maximum tip displacements of CMC-based actuators are analyzed, the maximum difference is found as 3% and 4% for the CMC-Br-1.5PEG and CMC-Br-0.2Gr actuators at DC excitation voltage of 5V. As the DC voltage increases, the maximum difference between experimental and simulated results decreases. It can be concluded that proposed finite element analysis can be used in predicting the maximum tip displacement and blocking force of CMC-based actuators with different PEG and Gr loadings.

The following investigations can be carried out in the future:

- The environmental effect such as temperature and humidity effects on the electromechanical performances of CMC-based actuators may be investigated.

- The electromechanical behaviors and blocking force values of CMC-based actuators with different ionic liquids may be tested.

- Thickness and dimension effects on the electromechanical behavior of CMC-based actuators may be performed.

- Different types of electrodes (Pt and Cu) effects on the electromechanical behavior of CMC-based actuators may be investigated.

REFERENCES

Ahmad, S. R., Young, R. J., & Kinloch, I. A. (2015). Raman spectra and mechanical properties of Graphene/Polypropylene nanocomposites. *International Journal of Chemical Engineering and Applications, 6* (1), 1-5.

Akar, E., Altınışık, A., & Seki, Y. (2012). Preparation of pH-and ionic-strength responsive biodegradable fumaric acid crosslinked carboxymethyl cellulose. *Carbohydrate Polymers, 90*, 1634-1641.

Akbari, J., & Heydari, A. (2012). Synthesis of Mn3O4 nanoparticles with controlled morphology using ionic liquid. *Current Nanoscience, 8*, 398-401.

Bar-Cohen, Y. (2001). *Electroactive polymer (Eap) actuators as artificial muscles (reality, potential, and challenges)*. Washington: SPIE Press.

Bar-Cohen, Y. (2012). Electroactive polymer (Eap) as actuators for biomimetic applications. *Proceedings of the Asme International Mechanical Engineering Congress and Exposition (Imece 2010), 9*, 655-660.

Barron, A. R. (2012). *Physical methods in chemistry and nano science*. Connexions: Houston, TX, 365.

Bell, S. S. J., Geethanjali, R., & Subhashini, S. (2014). Synthesis and characterization of PolyEthylene Glycol-g-Arginine and its corrosion - Inhibition behaviour on mild steel. *Journal of Environmental Nanotechnology, 3* (1), 23-29.

Biswal, D. R., & Singh, R.P. (2004). Characterisation of carboxymethyl cellulose and polyacrylamide graft copolymer. *Carbohydrate Polymers, 57*, 379-387.

Cai, Z., & Kim, J. (2010). Bacterial cellulose/poly (ethylene glycol) composite: characterization and first evaluation of biocompatibility. *Cellulose, 17*, 83-91.

Cao, Y., Wu, J., Zhang, J., Li, H. Q., Zhang, Y., & He, J. S. (2009). Room temperature ionic liquids (RTILs): A new and versatile platform for cellulose processing and derivatization. *Chemical Engineering Journal*, *147*, 13-21.

Chai, M. N., & Isa, M. I. N. (2013). The oleic acid composition effect on the carboxymethyl cellulose based biopolymer electrolyte. *Journal of Crystallization Process and Technology*, *3* (1), 1-4.

Chen, Z., Tan, X., & Shahinpoor, M. (2005). Chen, Z., Tan, X., & Shahinpoor, M. (2005, July). Quasi-static positioning of ionic polymer-metal composite (IPMC) actuators. *In Proceedings of the IEEE/ASME International Conference on Advanced Intelligent Mechatronics*, 60-65.

Edgar, K. J., Buchanan, C. M., Debenham, J. S., Rundquist, P. A., Seiler, B. D, Shelton, M. C., et al. (2001). Advances in cellulose ester performance and application. *Progress in Polymer Science*, *26*, 1605-1688.

El-Sayed. S., Mahmoud, K. H., Fatah, A. A., & Hassen, A. (2011). DSC, TGA and dielectric properties of carboxymethyl cellulose/polyvinyl alcohol blends. *Physica B: Condensed Matter*, *406*, 4068-4076.

Fang, B., Lin, C. K., & Ju, M. (2010). Development of sensing/actuating ionic polymer-metal composite (IPMC) for active guide-wire system. *Sensors and Actuators A: Physical*, *158*, 1-9.

Feng, Y. Y., Zhang, X. Q., Shen, Y. T., Yoshino, K., & Feng, W. (2012). A mechanically strong, flexible and conductive film based on bacterial cellulose/graphene nanocomposite. *Carbohydrate Polymers*, *87*, 644-649.

Fleming, M., Hubbard, J., Kim, K. J., & Leang, K. K. (2011). Mitigating IPMC back-relaxation effect through controlled activation of patterned electrodes. *In ASME 2011 Conference on Smart Materials, Adaptive Structures and Intelligent Systems*, 65-72.

Georgiev, G. A., Sarker, D. K., Al-Hanbali, O., Georgiev, G. D., & Lalchev, Z. (2007). Effects of poly (ethylene glycol) chains conformational transition on the properties of mixed DMPC/DMPE-PEG thin liquid films and monolayers. *Colloids and Surface B: Biointerfaces*, *59* (2), 184-193.

Guilbert, S., Gontard, N., & Cuq, B. (1995). Technology and applications of edible protective films. *Packaging Technology and Science. 8*, 339-346.

Guleria, R., Kaith, N. S., & Singh, R. (2012). Peg based solid dispersions of gliclazide: A comparative study. *International Journal of Pharmacy and Pharmaceutical Sciences*, *4*, 507-512.

Gurunathan, K., Murugan, A. V., Marimuthu, R., Mulik, U. P., & Amalnerkar, D. P. (1999). Electrochemically synthesised conducting polymeric materials for applications towards technology in electronics, optoelectronics and energy storage devices. *Materials Chemistry and Physic*, *61*, 173-191.

Habibi, N. (2014). Preparation of biocompatible magnetite-carboxymethyl cellulose nanocomposite: Characterization of nanocomposite by FTIR, XRD, FESEM and TEM. *Spectrochimica Acta Part A: Molecular and Biomolecular Spectroscopy*, *131*, 55-58.

Haldorai, Y., & Shim, J. J. (2014). Chemo-responsive bilayer actuator film: fabrication, characterization and actuator response. *New Journal of Chemistry*, *38*, 2653-2659.

He, Q., Yu, M., Li, Y., Ding, Y., Guo, D., & Dai, Z. (2012). Investigation of ionic polymer metal composite actuators loaded with various tetraethyl orthosilicate contents. *Journal of Bionic Engineering, 9,* 75-83.

Heinämäki, J. T., Iraizoz, C., A., Nordström, A. J., & Yliruusi, J. K. (1994). Comparative evaluation of ammoniated aqueous and organic-solvent-based celluloseester enteric coating systems: a study on free films. *International Journal of Pharmaceutics, 109,* 9-16.

Heinze, T., & Pfeiffer, K. (1999). Studies on the synthesis and characterization of carboxymethylcellulose. *Angewandte Makromolekulare Chemie, 266,* 37-45.

Huang, Y., Liang, J. J., & Chen, Y. S. (2012). The application of graphene based materials for actuators. *Journal of Materials Chemistry, 9,* 3671-3679.

Huynh, N. N., Alici, G., & Spinks, G. M. (2006). Force analysis and characterisation of polymer actuators. *2006 IEEE/RSJ International Conference on Intelligent Robots and Systems,* 5465-5470.

Jung, H. J., Jeon, J. H., Vadahanambi, S., & Oh, I. K. (2011). Electro-active graphene-Nafion actuators. *Carbon, 49,* 1279-1289.

Jung, H. J., Vadahanambi, S., & Oh, I. K. (2010). Electro-active nano-composite actuator based on fullerene-reinforced Nafion. *Composites Science and Technology, 70,* 584-592.

Jung, J. Y., & Oh, I. K. (2007). Novel nanocomposite actuator based on sulfonated poly(styrene-b-ethylene-co-butylene-b-styrene) polymer. *Journal of Nanoscience and Nanotechnology, 7,* 3740-3743.

Kikuchi, K., & Tsuchitani, S. (2009). Nafion (R)-based polymer actuators with ionic liquids as solvent incorporated at room temperature. *Journal of Applied Physics*, doi:10.1063/1.3204961.

Kim, J., Yun, S., & Ounaies, Z. (2006). Discovery of cellulose as a smart material. *Macromolecules*, *39*, 4202-4206.

Kim, K. B., & Kim, J. (2013). Fabrication and characterization of electro-active cellulose films regenerated by using 1-butyl-3-methylimidazolium chloride ionic liquid. *Proceedings of the Institution of Mechanical Engineers Part C Journal of Mechanical Engineering Science*, *203-210*, 1989-1996.

Kim, K. J., & Tadokoro, S. (2007). *Electroactive polymers for robotics applications: artificial muscles and sensors*. Germany: Springer.

Lee, J. W., & Yoo, Y. T. (2009). Anion effects in imidazolium ionic liquids on the performance of IPMCs. *Sensors and Actuators B: Chemical*, *137*, 539-546.

Lu, J., Kim, S. G., Lee, S., & Oh, I. K. (2008). A biomimetic actuator based on an ionic networking membrane of poly (styrene-alt-maleimide)-incorporated poly (vinylidene fluoride). *Advanced Functional Materials*, *18*, 1290-1298.

Lughmani, W. A., Jho, J. Y., Lee, J. Y., & Rhee, K. (2009). Modeling of bending behavior of IPMC beams using concentrated ion boundary layer. *International Journal of Precision Engineering and Manufacturing*, *10*, 131-139.

Mahadeva, S. K., & Kim, J. (2010). Effect of polyethylene oxide–polyethylene glycol content and humidity on performance of electro-active paper actuators based on cellulose/polyethylene oxide–polyethylene glycol microcomposite. *Polymer Engineering & Science*, *50*, 1199-1204.

Mansur, H. S., Orefice, R. L., & Mansur, A. A. (2004). Characterization of poly (vinyl alcohol)/poly (ethylene glycol) hydrogels and PVA-derived hybrids by small-angle X-ray scattering and FTIR spectroscopy. *Polymer*, *45*, 7193-7202.

Murphy, E. B., & Wudl, F. (2010). The world of smart healable materials. *Progress in Polymer Science*, *35*, 223-251.

Muzart, J. (2006). Ionic liquids as solvents for catalyzed oxidations of organic compounds. *Advanced Synthesis & Catalysis*, *348*, 275-295.

Nam, D. N. C., & Kwan, A. K. (2012). Ionic polymer metal composite transducer and self-sensing ability. *Smart Actuation and Sensing Systems – Recent Advances and Future Challenges*, 203-222.

Nieto, A., Lahiri, D., & Agarwal, A. (2012). Synthesis and properties of bulk graphene nanoplatelets consolidated by spark plasma sintering. *Carbon*, *50*, 4068-4077.

Ozdemir, O., Karakuzu, R., Sarikanat, M., Akar, E., Seki, Y., Cetin, L., et al. (2015a). Effects of PEG loading on electromechanical behavior of cellulose-based electroactive composites. *Cellulose*, *22*, 1873-1881.

Ozdemir, O., Karakuzu, R., Sarikanat, M., Seki, Y., Akar, E., Cetin, L., et al. (2015b). Improvement of the electromechanical performance of carboxymethylcellulose-based actuators by graphene nanoplatelet loading. *Cellulose*, *22*, 3251-3260.

Pang, J. H., Liu, X., Zhang, X. M., Wu, Y. Y., & Sun, R. C. (2013). Fabrication of cellulose film with enhanced mechanical properties in Ionic Liquid 1-Allyl-3-methylimidaxolium chloride (AmimCl). *Materials*, *6*, 1270-1284.

Panwar, V., Cha, K., Park, J. O., & Park, S. H. (2012). High actuation response of PVDF/PVP/PSSA based ionic polymer metal composites actuator. *Sensors and Actuators B: Chemical*, *161*, 460-470.

Patil, M. L., & Sasai, H. (2008). Recent developments on chiral ionic liquids: Design, synthesis, and applications. *The Chemical Record*, 8, 98-108.

Plechkova, N. V., & Seddon, K. R. (2008). Applications of ionic liquids in the chemical industry. *Chemical Society Reviews*, *37*, 123-150.

Polu, A. R., & Kumar, R. (2011). Impedance spectroscopy and FTIR studies of PEG - based polymer electrolytes. *E-Journal of Chemistry*, *8*, 347-353.

Polu, A. R., Kumar, R., Causin, V., & Neppalli, R. (2011). Conductivity, XRD, and FTIR studies of New Mg^{2+}-ion-conducting solid polymer electrolytes: [PEG: $Mg(CH_3COO)_2$]. *Journal of the Korean Physical Society*, *59*, 114-118.

Rajkumar, T., & Ranga Rao, G. (2008). Characterization of hybrid molecular material prepared by 1-butyl 3-methyl imidazolium bromide and phosphotungstic acid. *Materials Letters*, *62*, 4134-4136.

Ramenskaya, L. M., Grishina, E. P., Pimenova A. M., & Gruzdev M. S. (2008). The influence of water on the physicochemical characteristics of 1-Butyl-3-methylimidazolium bromide ionic liquid. *Russian Journal of Physical Chemistry A, 82*, 1098-1103.

Ranga Rao, G., Rajkumar, T., & Varghese, B. (2009). Synthesis and characterization of 1-butyl 3-methyl imidazolium phosphomolybdate molecular salt. *Solid State Sciences*, *11* (1), 36-42.

Ravikiran, Y. T., Kotresh, S., Vijayakumari, S. C., & Thomas, S. (2014). Liquid petroleum gas sensing performance of polyaniline-carboxymethyl cellulose composite at room temperature. *Current Applied Physics, 14*, 960-964.

Roberts, M. J., Bentley, M. D, & Harris, J. M. (2002). Chemistry for peptide and protein PEGylation. *Advanced Drug Delivery Reviews, 54*, 459-476.

Sahlin, J. J., & Peppas, N. A. (1997). Near-field FTIR imaging: a technique for enhancing spatial resolution in FTIR microscopy. *Journal of Applied* Polymers, *63*, 103-110.

Shahinpoor, M., & Bar-Cohen, Y., Simpson, J. O., & Smith, J. (1998). Ionic polymer-metal composites (IPMCs) as biomimetic sensors, actuators and artificial muscles-a review. *Smart Materials & Structures, 7*, R15-R30.

Shahinpoor, M., & Kim, K. J. (2001). Ionic polymer-metal composites: I. Fundamentals. *Smart Materials & Structures*, *10*, 819-833.

Shahinpoor, M., & Kim, K. J. (2005). Ionic polymer-metal composites: IV. Industrial and medical applications. *Smart Materials & Structures*, *14*, 197-214.

Shokri, J., & Adibkia, K. (2013). *Application of cellulose and cellulose derivatives in pharmaceutical industries*. Intech, 47-66.

Singh, T. J., & Bhat, S. V. (2003). Morphology and conductivity studies of a new solid polymer electrolyte: $(PEG)_xLiClO_4$. *Bulletin of Materials Science*, *26*, 707-714.

Swatloski, R. P., Spear, S. K., Holbrey, J. D., & Rogers, R. D. (2002). Dissolution of cellose with ionic liquids. *Journal of the American Chemical Society*, *124*, 4974-4975.

Qiu, X. Y., & Hu, S. W. (2013). "Smart" materials based on cellulose: A review of the preparations, properties, and applications. *Materials, 6*, 738-781.

Wei, L., Bingjie, S., & Peiyi, Wu. (2009). Study on hydrogen bonds of carboxymethyl cellulose sodium film with two-dimensional correlation infrared spectroscopy. *Carbohydrate Polymers, 78*, 453-461.

Wojtoniszak, M., Chen, X., Kalenczuk, R. J., Wajda, A., Lapczuk, J., Kurzewski, M., et al. (2012). Synthesis, dispersion, and cytocompatibility of graphene oxide and reduced graphene oxide. *Colloids and Surfaces B: Biointerfaces*, *89*, 79-85.

Yang, L., & Paulson, A. T. (2000). Mechanical and water vapour barrier properties of edible gellan films. *Food Research International, 33*, 563-570.

Yang, W., Choi, H., Choi, S., Jeon, M., & Lee, S. Y. (2012). Carbon nanotube-graphene composite for ionic polymer actuators. *Smart Materials and Structures, 21*, 055012/1-7.

Zhao, Y., Song, L., Zhang, Z. P., & Qu, L. T. (2013). Stimulus-responsive graphene systems towards actuator applications. *Energy & Environmental Science*, *6*, 3520-3536.